PHD

Some optical and electrical properties of ZnSiP2.

Humphreys, Richard George

Award date:
1975

Awarding institution:
University of Bath

SOME OPTICAL AND ELECTRICAL PROPERTIES OF $ZnSiP_2$

submitted by Richard George Humphreys

for the degree of Doctor of Philosophy

of the University of Bath

1975

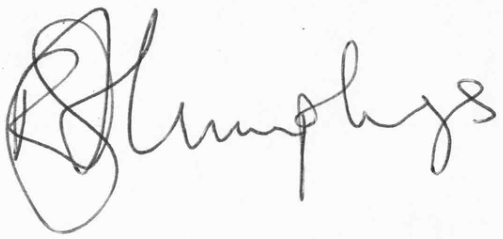

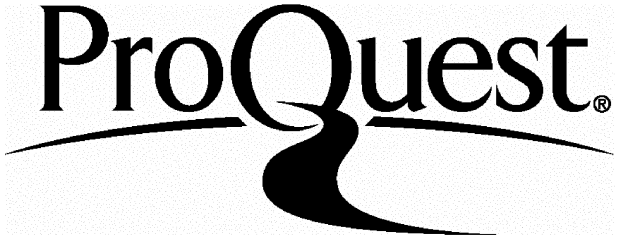

Acknowledgements

It is a pleasure to thank all those who have helped me in doing this work, especially Dr B. R. Pamplin for supervising it, Dr A. Miller and Dr W. C. Clark for many useful discussions and Professor S. H. Ayliffe for providing the facilities. I am also indebted to R. C. J. Draper for help with apparatus, B. Chapman for taking the X-ray photographs, and E. F. Lambson and W. A. Horler for technical assistance.

My thanks are also due to Honeywell Inc., who generously funded not only the whole project, but also a visit to their laboratories in Minneapolis, U.S.A. where the photoconductivity and photovoltaic effect measurements were made. I am grateful to the staff at their laboratories for the hospitality shown to me on this trip, especially to Dr D. Long and Dr R. J. Stokes for organising it and Dr P. W. Kruse and Dr R. G. Schulze for help with the measurements and discussion of the results.

It is also a pleasure to thank Pat Richardson for typing the thesis so efficiently.

Abstract

A variety of optical and electrical properties of $ZnSiP_2$ have been studied. Single crystals of this material were grown from solution in zinc or tin, using an accelerated crucible rotation technique. Its lattice parameters have been measured between room temperature and 1100 C and the anisotropy of the thermal expansion coefficients interpreted in terms of the bonding of the crystal.

The absorption edges of the best crystals showed well defined structure due to pseudodirect transitions between the three crystal field and spin-orbit split valence bands and the lowest conduction band minimum. The lowest band gap, after taking account of the exciton binding energy, was found to be 2.082 eV at room temperature. The valence band splittings and the relative strengths of the transitions were interpreted in terms of the quasicubic model. The absorption due to the two strongest excitons was fitted to a simple model, and the exciton binding energy estimated to be 22 meV. From the magnitude of the absorption coefficient, the matrix element for pseudodirect transitions was estimated to be about a thousand times weaker than that for direct transitions in the III V compounds.

An absorption peak found only in low resistivity n-type material in the near infra-red was attributed to transitions between the Γ_3 and Γ_2 conduction bands ($X_1 - X_3$ in zinc blende) at about 0.7 eV.

The electrical properties of the crystals were measured between liquid nitrogen temperature and 200 C. Crystals grown from Sn, and some of those from Zn were fairly low resistivity n-type (.5 - 20 ohm cm) while others grown from Zn were high resistivity ($\sim 10^8$ ohm cm) p-type. Electron mobilities up to 160 $cm^2\ V^{-1}\ S^{-1}$, and hole mobilities up to 22 $cm^2\ V^{-1}\ S^{-1}$ were measured. The dominant scattering mechanism was probably due to ionised impurities.

Measurements of photoconductivity and photovoltaic effect at a rectifying metal contact had spectral responses substantially in agreement with the absorption measurements, although the structure due to pseudo-direct transitions was not resolved. Strong trapping of excess carriers was observed even in the best optical material.

CONTENTS

LIST OF FIGURES

TABLES

CHAPTER 1

Introduction

1.1 Derivation of the II IV V_2 compounds

Over the past two or three decades a considerable amount of effort has been devoted to the investigation of semiconductors with structures derived from that of diamond. The origin of the semiconducting properties of these materials lies in the covalent tetrahedral bonding of the diamond lattice. This takes the form of two interpenetrating face centred cubic lattices one of which is displaced by $(\frac{1}{4}, \frac{1}{4}, \frac{1}{4})$ of the unit cell dimensions relative to the other. It was found that the semiconducting properties of silicon and germanium were retained, although modified, if these two sublattices are occupied respectively by atoms from the groups III and V of the periodic table, forming the III V compounds with the zinc blende structure. The nitrides form in the closely related wurtzite structure which is favoured by more ionic compounds. The similar II VI compounds have either the wurtzite or the zinc blende structure.

The tetrahedral binding in these materials derives from the formation of covalent bonds with sp^3 hybridised orbitals. These bonds are strong and highly directional, with an angle between the bonds of 109.47°. In a perfect lattice, there are exactly the same number of valence electrons as are required to fill these bonds completely.

The III V and II VI semiconductors derive from the group IV elements with the diamond structure according to the Grimm-Somerfeld (1926) rule, which states that a related structure may exist if the average number of valence electrons per atom is the same as for the parent. By a similar process (Pamplin (1964)) other groups of materials can be derived from the III V and II VI compounds, such as the II IV V_2 and I III VI_2 compounds by substitution for the cations in the parent

materials. The first materials of these types synthesised were I III VI_2 compounds made by Hahn et al (1953) which were found to have the chalcopyrite structure, Fig 1.1. Austin et al. (1956) predicted the existence of II IV V_2 compounds and the first samples were prepared by Goodman (1957). Some twenty three II IV V_2 compounds have now been prepared.

The literature on these materials is now fairly extensive. Review articles have been written by Borshchevskii et al (1967), Goryunova et al. (1970), Sileika (1973) and Kaufman and Schneider (1974). Bibliographies have been produced by Pamplin (1965), Ray (1967) and Draper et al. (1973). A recent book by Shay and Wernick (1975) gives a more extensive review.

1.2 Crystal Structure

Most II IV V_2 compounds normally crystallise in the chalcopyrite structure (Chalcopyrite is the mineral $CuFeS_2$, but the term will be used throughout this work to denote the structure). This is similar to the zinc blende structure taken up by the III V compounds, but the cation sublattice now accommodates two different atomic species. These are ordered so that each group V atom is surrounded by two group II and two group IV atoms. This ordering reduces the crystal symmetry and the conventional chalcopyrite unit cell resembles two zinc blende unit cells stacked one on top of the other. Denoting a general II IV V_2 compound as $A^{II}B^{IV}C^{V}_2$, the BC bond length is usually smaller than the AC. This means that the group V atom at $(\frac{1}{4}, \frac{1}{4}, \frac{1}{8})$ in the 'ideal' chalcopyrite structure is shifted to $(x, \frac{1}{4}, \frac{1}{8})$ where x is greater than $\frac{1}{4}$ (conventionally the group II atoms are taken to be at the corners of the unit cell). The effect of this on the structure is shown in Fig. 1.2. Each cation is tetrahedrally bonded to four anions, and the BC_4 tetrahedra are rotated slightly with respect to the crystallographic axes and in the opposite sense to the AC_4 tetrahedra.

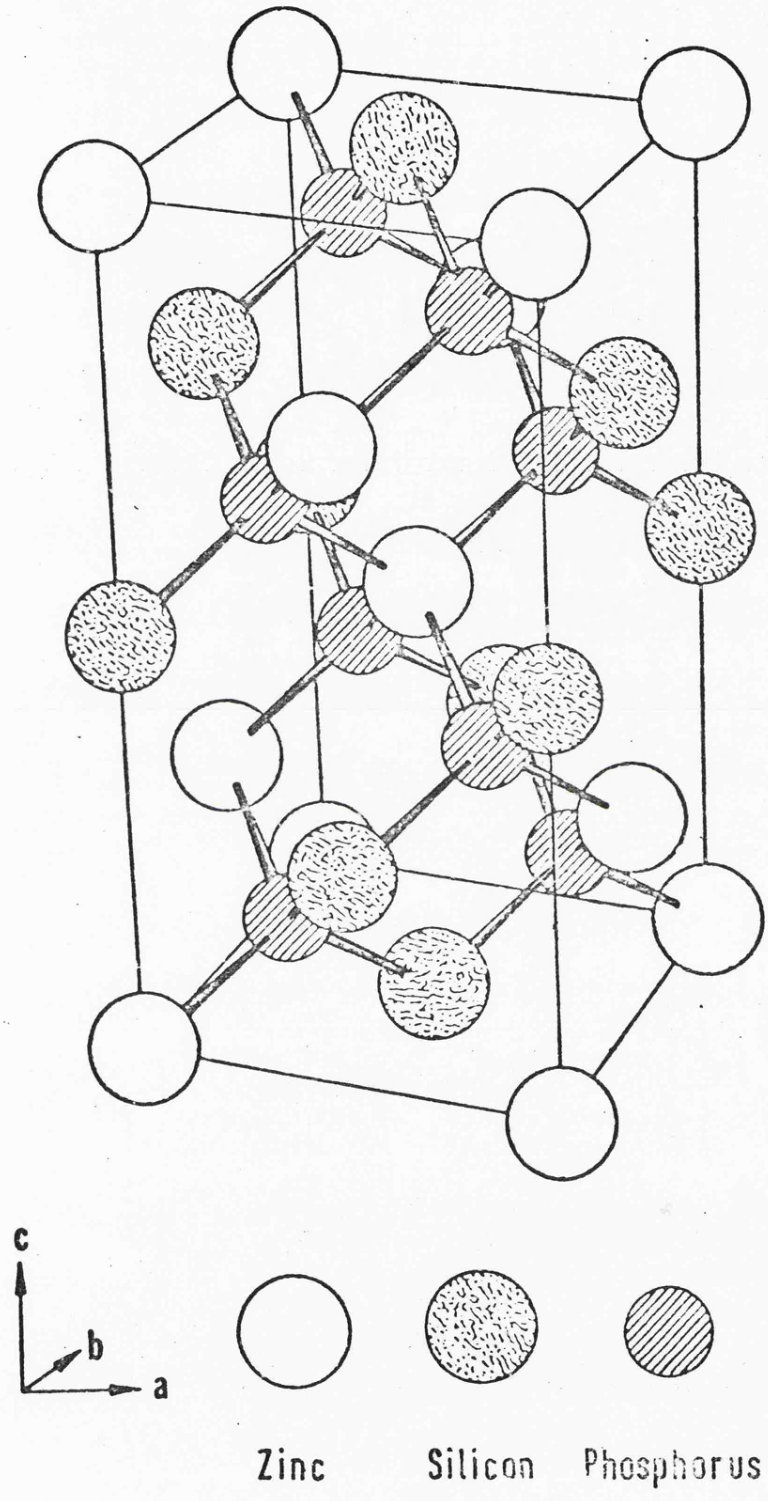

Fig. 1.1 The chalcopyrite structure

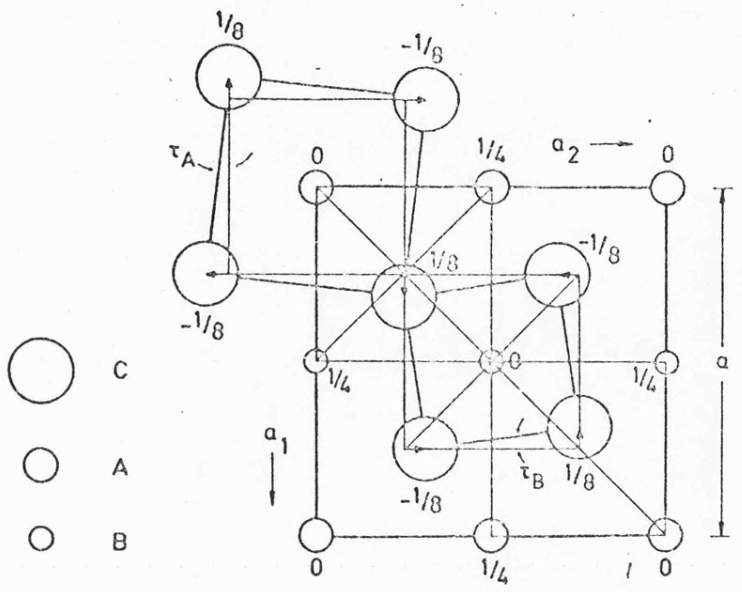

Figure 1.2 Atomic arrangement in the chalcopyrite structure for $x > 1/4$

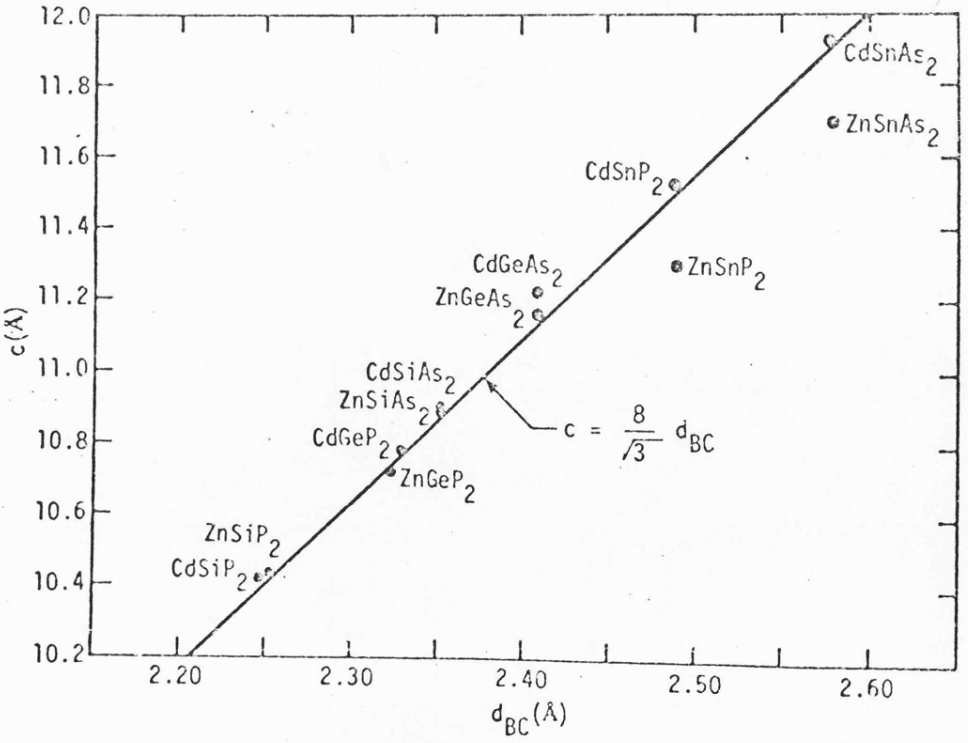

Figure 1.3 Lattice constants c vs. B-C bond lengths.

Because of this the ratio of the lattice parameters, $\frac{c}{a}$, varies slightly from its ideal value of 2. This is characterised by $2 - \frac{c}{a}$, called the tetragonal compression, which is positive or zero for all II IV V_2 compounds.

The unit cell dimensions a and c can easily be determined from x-ray powder photographs. The value of x, however, requires the interpretation of x-ray diffraction intensities which is much more difficult. It has been done using single crystals by Abrahams and Bernstein (1970, 1971, 1974) for $ZnSiP_2$, $CdSiP_2$ and $CdGeAs_2$ and by Lind and Grant (1973) for $ZnGeP_2$ and $ZnSiAs_2$. Other results obtained from powder diffraction, which are less accurate, are also available. A summary of II IV V_2 lattice parameters is given in table 1.1.

The chalcopyrite structure is completely determined once c a and x are known, and bond angles and lengths may be calculated. Abrahams and Bernstein (1971) observed that the BC_4 tetrahedra in $ZnSiP_2$ and $CdSiP_2$ were very nearly regular and only the AC_4 tetrahedra distort much as x varies from $\frac{1}{4}$. In the approximation of regular BC_4 tetrahedra they showed from geometry that:

$$x = \tfrac{1}{2} - \left[\frac{c^2}{32a^2} - \frac{1}{16} \right]^{\frac{1}{2}} \qquad 1.1$$

They compared bond lengths calculated on this approximation with those expected from the tetrahedral radii (Van Vechten and Phillips (1970)) and found good agreement, although the BC bond length was consistently shorter than predicted.

Lind and Grant (1972) plotted c against BC bond length for several II IV V_2 compounds (fig. 1.3) using data similar to that of table 1.1 and showed that:

$$c = \frac{8}{\sqrt{3}} (BC),$$

TABLE 1.1

Lattice Parameters of II IV V_2 compounds

	a	c	c/a	x	
$ZnSiP_2$	5.399	10.435	1.933	.2691	Abrahams and Bernstein (1970)
$ZnSiAs_2$	5.606	10.890	1.943	.2658	Lind and Grant (1973)
$ZnGeP_2$	5.464	10.708	1.960	.2582	Lind and Grant (1973)
$ZnGeAs_2$	5.672	11.153	1.966	.250*	Vaipolin (1972)
$ZnSnP_2$	5.651		2.000	.239*	Rubenstein and Ure (1968)
$ZnSnAs_2$	5.851		2.000	.231*	Vaipolin (1972)
$CdSiP_2$	5.680	10.431	1.836	.2968	Abrahams and Bernstein (1971)
$CdSiAs_2$	5.885	10.881	1.849	.298*	Valov et al (1973)
$CdGeP_2$	5.740	10.775	1.877	.283*	Valov et al (1973)
$CdGeAs_2$	5.943	11.216	1.887	.2785	Abrahams and Bernstein (1974)
$CdSnP_2$	5.902	11.513	1.951	.265*	Vaipolin (1972)
$CdSnAs_2$	6.094	11.918	1.956	.262*	Vaipolin (1972)

* Indicates that x was measured from powder diffraction data, and is probably less accurate than other values.

A more comprehensive set of references may be found in Shay and Wernick (1975). Those quoted here are 'best' values.

which is the result expected for perfect BC_4 tetrahedra, was obeyed by all the II IV V_2 compounds except for $ZnSnC_2$ compounds. These have $\frac{c}{a} = 2$ in spite of having $x \neq \frac{1}{4}$ (Vaipolin et al (1968), Pfister (1963)) where the approximation is clearly invalid if these compounds do in fact have the chalcopyrite structure, about which there is some doubt (Montfort et al (1975)).

Phillips (1974) has attempted to explain the observed tetragonal compressions in terms of the electronegativities of the atoms, and obtained a moderate fit for small compressions for:

$$2 - \frac{c}{a} = .60X_A + .25X_B + .15X_C + .01$$

Better agreement was obtained by Noolandi (1974) using:

$$2 - \frac{c}{a} = \alpha R_A^{\beta} R_C^{\gamma} (X_A - X_B)^2$$

where the empirical constants were found to be: $\alpha = .089$; $\beta = 5.383$ and $\gamma = -1.323$ if the tetrahedral radii R_A and R_C are in Å.

Weaire (1975) has obtained a similar expression to that of Noolandi (1974) by rather simpler arguments, but using only two empirical constants:

$$2 - \frac{c}{a} = K_A (X_A - X_B)^2$$

where $K_{Zn} = 0.2$ and $K_{Cd} = 0.45$

An attempt to explain a similar effect was made by Abrahams and Bernstein (1973) who found that the difference between the measured x-parameter and that calculated for perfect BC_4 tetrahedra could be estimated as:

$$\Delta y = .0049X_A + .0254X_B - .0236X_C$$

which depends to a large extent on $(X_B - X_C)$, showing the connection between the perfection of the BC_4 tetrahedra and the covalency of the B - C bond.

None of these semi-empirical approaches has been entirely successful, and a quantitative understanding of the tetragonal compressions in ternaries may have to await a more fundamental method.

1.3 Crystal growth of II IV V_2 compounds

II IV V_2 compounds were first prepared by direct reaction between their constituent elements by Goodman (1957). Since then a considerable amount of effort has been directed towards controlling the size and quality of crystals. Three basic crystal growth methods have been used.

(1) Melt growth by directional solidification

In this technique the constituent elements are mixed in stoichiometric or nearly stoichiometric proportions, sealed in an evacuated silica ampoule, heated to above the melting point of the compound and then cooled slowly in an imposed temperature gradient. Techniques based on this approach have been widely used for low melting point II IV V_2 compounds. The greatest problems seem to be multiple nucleation and the formation of cracks (Borshchevskii et al (1967)). The latter is thought to be due to anisotropic contraction on cooling and/or the transformation from a high temperature disordered form to the chalcopyrite structure.

(2) Vapour Transport

The group II and group V elements which make up II IV V_2 compounds are volatile, but it is usually necessary to introduce a carrier for the non-volatile group IV element in order to grow II IV V_2 compounds from the vapour. The most commonly used carrier has been I.

The II IV V_2 compound, either prereacted or formed in situ from the elements, is sealed with a small amount of carrier in a silica ampoule. When this is heated in a temperature gradient, crystals grow by vapour transport from the hot source material to the cool part of

the tube. Vapour grown crystals can be of high crystal quality, but unfortunately they are often rather small.

(3) Solution growth

In this technique a low melting point metal is included with the compound in a sealed ampoule so that crystals grow from solution in the metal as the melt is cooled. The solvent can either be one of the components of the crystal (growth from a non-stoichiometric melt) or a fourth element which is not incorporated into the crystals grown. This method has great advantages in some cases, and was used in the present work. It is discussed more fully in Chapter 2.

The amount of work which has been done on crystal growth of II IV V_2 compounds is such that is is not possible to summarise it here. It has been reviewed by Borshchevskii et al (1967) and Shay and Wernick (1975) and a table of the growth methods which have been applied to II IV V_2 compounds is given by Pamplin (1974).

The best developed faces for all II IV V_2 compounds as grown are (101) and (112) oriented and the crystal growth direction is $\langle 111 \rangle$ irrespective of the growth technique. Vapour growth yields both needles and platelets (Buehler and Wernick (1971)) while solution growth usually gives needles. The shapes of the needles are shown in Figure 1.4 in relation to the crystallographic unit cell.

1.4 Optical Properties

In view of the similarity between the II IV V_2 and III V compounds it is to be expected that their physical properties will be closely related. This has been found to be the case and much of the interpretation of optical measurements on the II IV V_2 compounds has relied on this approach.

Because they are more numerous than the III V compounds, a wider range of properties should be obtainable with the II IV V_2 compounds.

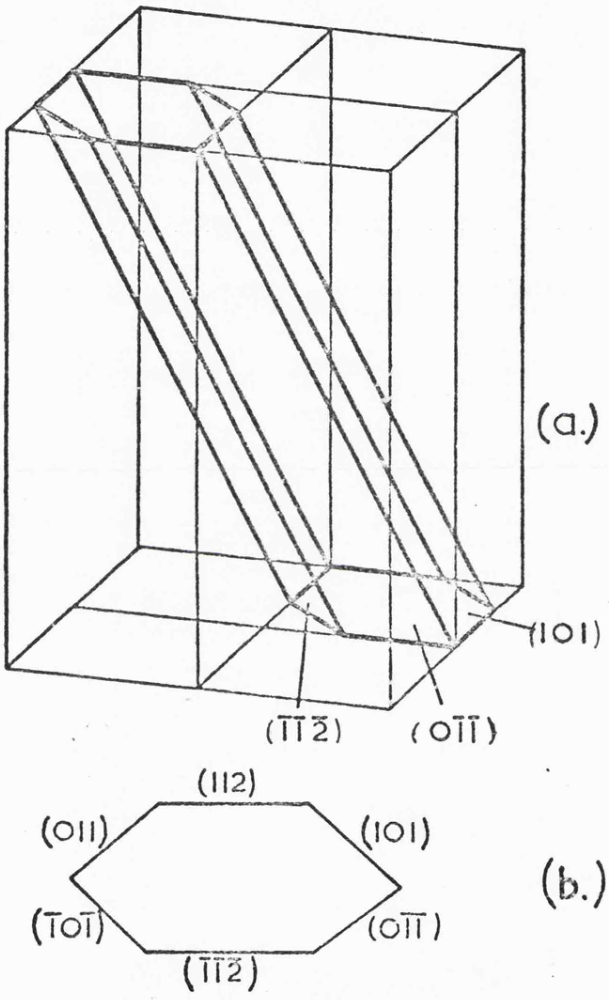

Fig. 1.4 Schematic diagrams of the crystal habit of $ZnSiP_2$, showing (a) the prismatic shape of the crystals, and (b) the cross-section of the crystal perpendicular to the growth direction.

There are also several interesting new properties which arise in the II IV V_2's because of the lower symmetry and larger unit cell. Since the structure is uniaxial the optical properties become anisotropic. This has given rise to possible applications of the II IV V_2 compounds as non-linear optic materials.

Other optical properties related to the band structure are discussed in detail in Chapter 3 in connection with the results of the present work.

The band gaps of the II IV V_2 compounds are listed in Table 1.2.

1.5 Electrical Properties

Data have now been published on the electrical properties of all the common II IV V_2 compounds, although in some cases it is not very detailed. Many of the compounds have a characteristic electrical type, and attempts to obtain the opposite type by doping yield high resistivity material. As shown in Table 1.2, all the Cd compounds except $CdSiAs_2$ can be obtained as low resistivity n-type material and all the Zn compounds except $ZnSiP_2$ as low resistivity p-type material but so far no more definite trends have emerged. It may be that the existing data are misleading. Miller and Clark (1975) have noted anomalies in the published data on ZnGeP and $CdGeP_2$ which they suggest might be due to surface conduction. This has been seen in $CdSnP_2$ (Knight et al (1972)).

Averkieva et al. (1970, 1971, 1972, 1973) have examined the effect of stoichiometry on the electrical properties of $ZnSiAs_2$ and $CdSiAs_2$ both by annealing and by growth from melts of different compositions, but were unable to draw any very firm conclusions about the processes taking place. No other detailed studies of this sort have been performed on II IV V_2 compounds.

The problems are similar in the I III VI_2 compounds. Tell et al. (1972) have performed annealing studies on several I III VI_2 compounds

from which it appears that by variations in composition the Cu compounds can be made p-type while the Ag compounds cannot, and that the In compounds can be made n-type, but Ga compounds cannot. The reasons for this are not understood at present, but at least there appears to be some systematic variation through the compounds.

So far the electrical properties of the ternary chalcopyrites are not well understood due to the relative complexity of the structure and the problems of non-stoichiometry.

TABLE 1.2

Some basic properties of II IV V_2 compounds at room temperature (after Shay and Wernick (1975) and other references cited in the text)

	Band Gap (eV)		μ_n (max) (cm^2/Vs)	μ_p (max) (cm^2/Vs)	n_{max} (cm^{-3})	p_{max} (cm^{-3})
$ZnSiP_2$	2.08	p*	200+	20	10^{18}	10^8
$CdSiP_2$	2.03	p*	150		10^{15}	
$ZnGeP_2$	1.99	p*		20		2.10^{14}
$ZnSiAs_2$	1.74	p*		180		10^{15}
$CdGeP_2$	1.72	d*	1000	50	10^{15}	10^{15}
$ZnSnP_2$	1.66	d*		55		5.10^{16}
$CdSiAs_2$	1.55	d*		500		4.10^{16}
$CdSnP_2$	1.17	d*	2000		10^{18}	
$ZnGeAs_2$	1.15	d*		23		4.10^{18}
$ZnSnAs_2$	.73	d*		200		10^{21}
$CdGeAs_2$	.57	d*	2500	1500	10^{18}	7.10^{15}
$CdSnAs_2$	.26	d*	11000	190	10^{18}	6.10^{17}

* p - pseudodirect gap, d - direct gap

\+ μ_n values greater than 1000 cm^2/Vs have been reported for occasional samples.

CHAPTER 2

Crystal Growth and Structure

2.1 Introduction

A considerable amount of effort has been devoted to the crystal growth of II IV V_2 compounds over the past fifteen years. All the compounds except $ZnSiP_2$ and $CdSiP_2$ have sufficiently low melting points for the crystals to be grown from the melt. For $ZnSiP_2$ however the melting point is so high (~1300 C according to Vaipolin et al. (1967)) with a large vapour pressure (~30 atmospheres) that only vapour growth or solution growth are possible without extensive high pressure facilities.

Vapour growth yields typically rather small crystals (Buehler and Wernick (1971)) and solution growth appeared to be more promising.

2.2 Previous work on the growth of $ZnSiP_2$

The existence of $ZnSiP_2$ was first reported by Folberth and Pfister (1958) although the method of preparation was not given. The first growth technique reported was halogen vapour transport (Akopyan and Zlatkin (1966) and Belle et al. (1965)). In a review article, Borshchevskii et al. (1967) described the growth of crystals as needles up to 10 mm long or, in some cases, as platelets with dimensions 6 x 1.5 x .1 mm^3 by iodine vapour transport. These crystals were frequently twinned and contained capillaries. They also reported the growth of crystals up to 25 mm long and 3.5 mm thick from a 20 mol% solution in Sn. They cite Vaipolin et al. (1965) as the original reference for solution growth.

Vapour transport growth was later described by Valov and Ushakova (1968), Mughal et al. (1969) and Buehler and Wernick (1971). Alekperova (1969b) measured the electrical properties of material grown from the vapour using fluorine as the transporting agent and gave a brief descri-

ption of the growth technique. The biggest crystals obtained by vapour transport were probably those of Mughal et al. (1969) the largest of which had dimensions 5 x 5 x 2.5 mm^3. Most were much smaller than this.

Solubility curves for $ZnSiP_2$ in Sn have been published by Springthorpe and Pamplin (1968), Vaipolin et al. (1967) and Mughal and Ray (1973), and for $ZnSiP_2$ in Zn by Alekperova et al. (1969a). These are reproduced in Figure 2.1 and show reasonable agreement in the slope of the curves, but rather serious discrepancies in the magnitude of the solubility at a given temperature.

Crystals grown by these workers by slow cooling from Sn solution were 1 - 2 cm long and 5 - 3 mm wide and thick. Stroud (1970) reported the presence of a considerable amount of Sn ($\sim \frac{1}{2}\%$) in $ZnSiP_2$ grown from Sn solution. Mughal (1971) found wide variations in the amount of Sn, up to about 5% in some crystals. Alekperova et al. (1969a) observed that crystals grown from Zn solution were more equiaxed than the needle-like Sn grown crystals, but were extremely fragile, due to very high solvent inclusion densities. All the Sn grown crystals were also reported to contain solvent inclusions running along the long axis of the crystals.

The solution growth of $ZnSiP_2$ has been discussed in some detail elsewhere (Humphreys (1973)). The major results of this work will be included here for the sake of completeness.

2.3 Solution Growth

In view of the difficulty found by previous workers in obtaining large single crystals by vapour transport, the method chosen was solution growth. The main reason for growing crystals from solution rather than from the melt is to reduce the growth temperature. In the case of $ZnSiP_2$ the need for this is mainly practical in that the melting point of the compound is too high for any material capable of withstand-

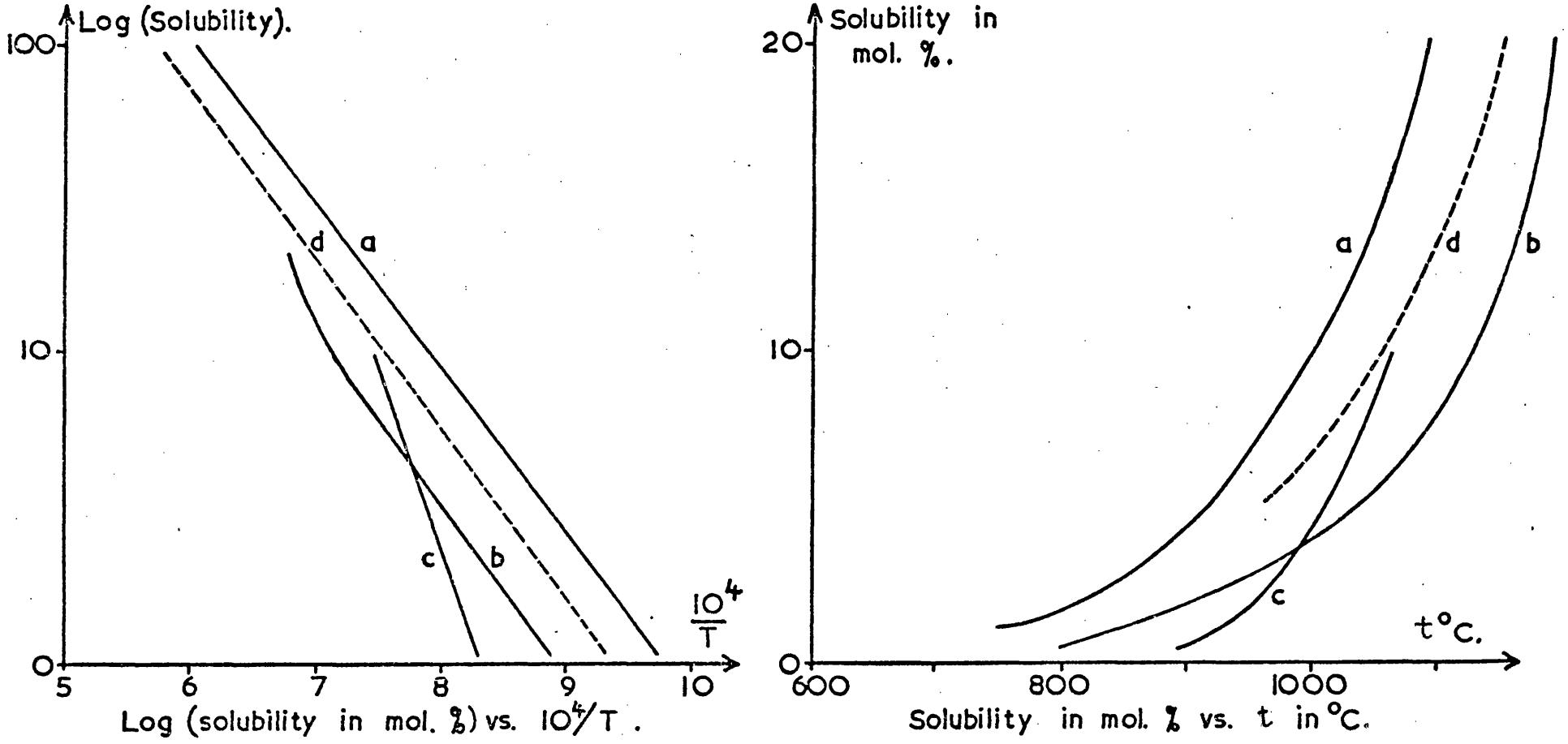

Fig. 2.1 Solubility curves for $ZnSiP_2$ in tin (solid lines) and zinc (dotted)
a Vaipolin et al. (1967), b Mughal and Ray (1973), c Springthorpe and Pamplin (1968),
d Alekperova et al. (1969)

ing the vapour pressure. In other cases it can be necessary if there is a phase change below the melting point, such as a transition from the disordered zinc blende structure to the ordered chalcopyrite one. No such transition has been observed in $ZnSiP_2$ but this is not surprising since all the growth techniques which have been used for $ZnSiP_2$ normally take place at least 200 C below the melting point.

There are, however, disadvantages to solution growth. The rate of growth which can be achieved under even moderately stable conditions is reduced, often by orders of magnitude compared to melt growth techniques, by the necessity of allowing time for diffusion of solute to the growing surface.

Since solution growth takes place over a wide range of temperature (several hundred degrees in the case of $ZnSiP_2$) the impurity distribution between the solid and the liquid, and also any deviations from stoichiometry in the crystals, may vary as growth proceeds, so that doping and composition may change along the length of the crystal. The bulk of the melt is also much larger than in the melt growth case, so that larger quantities of impurity may be present for a given impurity concentration.

There is a further disadvantage in that there may be some solid solubility of the solvent in the crystal. It is obviously highly desirable that this be as low as possible. The most commonly used solvent for $ZnSiP_2$ is Sn, but in view of the high concentration of Sn found by Stroud (1970) in material grown in this way the possibility of using another solvent in the present work was examined. A likely choice is Pb, which has been used by Miller (1974) in this laboratory for the growth of $CdGeP_2$ and $ZnGeP_2$ and by Bertoti and Somogyi (1971) as an eutectic with Bi for $ZnGeP_2$. In common with Miller's (1974) result for $CdSiP_2$ it was found in the present work that growth using Pb as solvent

failed for $ZnSiP_2$ due to broken ampoules, with some signs of reaction between the melt and silica.

Zn was selected as a solvent for $ZnSiP_2$ so as to reduce the problems of solvent contaminating the crystals, and also because Alekperova (1969b) reported that Zn solution grown material could be doped p-type. Alekperova's (1969a) observation that zinc solution grown crystals are fragile was confirmed in this work, the reason being a very high concentration of solvent inclusions. Solvent inclusions have always been reported in work on solution growth of II IV V_2 compounds and have normally been attributed to constitutional supercooling. This arises when the solution ahead of a growing crystal becomes supersaturated. Since there must be a concentration gradient near the crystal to induce solute diffusion towards the growth face of the crystal, crystals normally grow in a region more dilute than the rest of the solution, so that the bulk of the solution may be expected to be supersaturated if the solution is of a uniform temperature.

To reduce constitutional supercooling there are three measures which can be taken.

1. To grow the crystals as slowly as possible, reducing the concentration gradient near the crystals.
2. To make the bulk solution hotter than the crystals by imposing a temperature gradient.
3. To increase the transport of solute to the growing crystal by mixing the solution.

(1) is an obvious precaution but a limit is set on this by the thermal stability of the furnace and by the requirement of reasonable times for experiments. Cooling rates of the order of 1C/hr were used in the present work, when it was felt that thermal stability of the furnace was comparable with the cooling rate. There may well be considerable problems in maintaining any significant thermal gradient in

a solution of molten metal, although it was found by Fiegelson (1975) and in the present work that crystals could be induced to grow from the bottom of the ampoule by a temperature gradient. However it is doubtful whether a gradient large enough to have any significant effect on constitutional supercooling could be established. It was therefore decided to adopt method (3) as an aid to growth stability. This can conveniently be achieved for the sealed systems with which we are concerned by the use of an accelerated crucible rotation technique.

2.4 The accelerated crucible rotation technique (ACRT)

The object of using an ampoule which is not stationary is to mix the solution more thoroughly than is the case for the normal convective and diffusive mechanisms. In a sealed system the introduction of a paddle to rotate in the solution is not possible, and the simplest alternative is to rotate a vertical cylindrical ampoule about a vertical axis. Rotation at a constant angular velocity will only lead to a centrifugal force to alter convection, but if the angular velocity changes continuously so that the ampoule accelerates and then decelerates, a continuous shearing of the liquid layers will result due to the lag between the angular velocity of the ampoule walls and that of the middle of the solution. In this way, fairly thorough mixing can result.

This technique has been used for the flux growth of oxides by Scheel and Schulz-Dubois (1971). They also considered (Scheel and Elwell (1972a)) the optimum cooling program for solution growth, and suggested the use of local cooling to promote nucleation (Scheel (1972b)), an approach which has been used by Fiegelson et al (1975) in the solution growth of $CdGeAs_2$.

In the present work local cooling was not used, although by mounting the ampoule low in the furnace it was ensured that the bottom was cooler than the top. In order to achieve some control of nucleation,

a 'saw tooth' temperature program was used in the nucleation region. In other words, the ampoule was cooled to near the nucleation temperature, heated again through a few degrees, and then cooled to below the nucleation temperature, reheated again and so on. The intention of this approach was to induce nucleation and then dissolve off all but the largest crystals, so that the number of nuclei was reduced. This is similar to the procedure suggested by Scheel and Elwell (1972a).

After nucleation a non-linear cooling program was used so that the rate of cooling was smallest when the slope of the solubility curve was large and a more or less constant rate of mass deposition resulted. Cooling was continued until 5OC above the freezing point of the solvent, when the ampoule was inverted and replaced in the furnace so that the solvent was decanted. This not only made it easier to separate the crystals grown but also reduced the risk of the crystals being damaged as the solid solvent contracted on cooling.

2.5 Experimental

Silica ampoules were made using a stainless steel jet on the glassblowing torch (instead of the usual brass, since Cu is known to be a troublesome impurity) out of 3 - 4 cm diameter 'heralux' high purity tube. A 1 cm diameter tube for evacuation and sealing was attached at one end and the other sealed in a smooth curve. Ampoules were degreased with detergent and distilled water, filled with HCl/HNO_3 mixture, rinsed with distilled water and etched lightly with hydrofluoric acid. They were then rinsed thoroughly with distilled water and flame polished. Sometimes the ampoule was baked at 1000 C under vacuum before filling. No relationship between the cleaning methods used and results were noted provided the routine used was carefully carried out.

The elements were weighed out using a balance capable of reading to .1 mg. The effect of outgassing is uncertain, however and stoichio-

metry was probably no better than one part per thousand. The materials used were 5N pure or better and were obtained from Koch-Light Laboratories Ltd or Mining and Chemical Products Ltd. The metals (Zn and Sn) were etched in concentrated HCl to remove oxide film, washed repeatedly, and air dried. The phosphorus was ground under nitrogen to a suitable size and the silicon was ground rather smaller, to aid in reaction with the melt.

The materials were placed in the ampoule which was evacuated to about 10^{-4} torr. A small furnace around the ampoule was used to heat it to 200 C for several hours to assist with outgassing. After sealing under vacuum, the ampoule was positioned in a region of nearly uniform temperature in the furnace and was heated to 500 C at 30 C/hr, then at 6 C/hr to 650 C after which no free phosphorus remained and the temperature could safely be increased at 30 C/hr to 1150 C. The heating was carried out with the stirrer turned on to aid reaction of the phosphorus and silicon with the zinc. After some hours at 1150 C to ensure equilibrium, the furnace was cooled at 6 C/hr to where the nucleation temperature was thought to be from the solubility curves and the temperature program described above followed. Concentrations between 10 and 20 mol % were used

2.6 Apparatus

Cylindrical furnaces of 6 cm bore made by Severn Science Ltd were used. The temperature was controlled by a Eurotherm proportional temperature controller using a Pt/Pt 13% Rh thermocouple to sense the temperature.

The cooling rate was fixed by using a simple backing-off circuit, shown in Figure 2.2. The wiper of the helipot was driven through a variable ratio gearbox corresponding to variable heating and cooling rates. If a non-linear cooling program is required, this can be achieved by loading the output of the helipot.

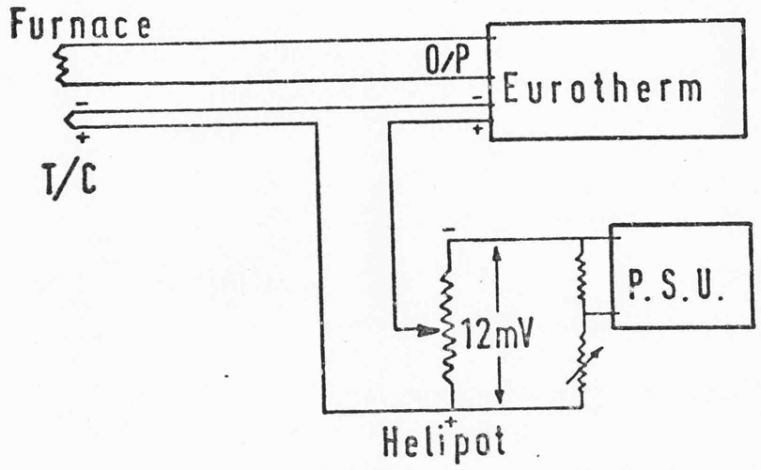

Figure 2.2 Thermocouple back-off circuit used to control the cooling rate of the furnace

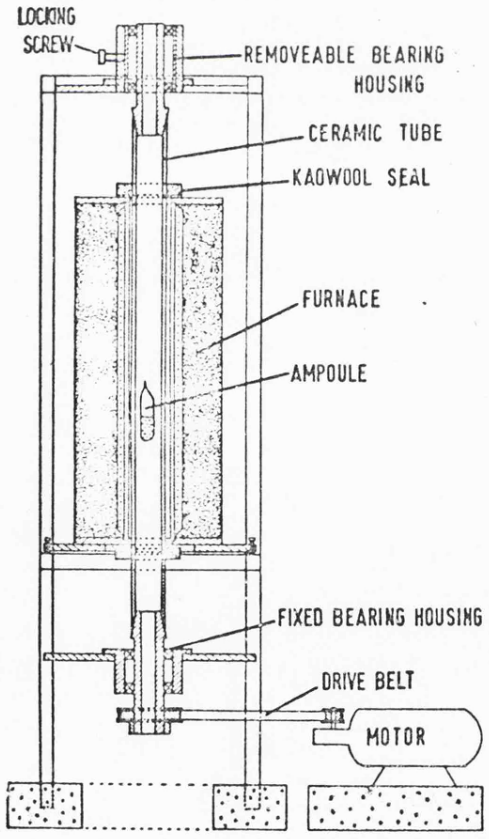

Figure 2.3 Accelerated crucible rotation furnace

A schematic diagram of the apparatus for ACRT is shown in Fig 2.3. The ampoule was contained in an alumina tube coaxial with and just narrower than the furnace tube. This alumina tube was mounted between steel cones which could rotate freely, and the bottom cone was driven by a motor via a toothed rubber belt. The top cone could be removed so that the furnace could be tilted and the alumina tube removed.

With this arrangement the rotation of the ampoule had to be stopped for the ampoule temperature to be monitored using chromel-alumel thermocouples mounted near it. Temperature control was by the thermocouple near the furnace windings. It is possible that the remoteness of the control thermocouple from the ampoule could make the temperature of the ampoule less stable but there was no way of checking this while the ampoule was rotating.

2.7 Results

The crystals grew in the form of an interpenetrant mass of clearly distinguishable single crystals. All (except a few thin platelets) contained solvent inclusions. Crystals grown from tin solution were needle-like as found by other workers (Springthorpe and Pamplin (1968)), and contained solvent inclusions parallel to the long axis. There was a tendency, however, for the (101) faces to be better developed when ACRT was used and for the width and thickness to be increased. Crystals grown from zinc solution were more equiaxed whether or not ACRT was used, and generally showed less well developed faces. A considerable reduction in the density of inclusions was found when ACRT was used, although they still posed considerable problems for obtaining thick, inclusion free optical specimens. The crystals were, however, greatly improved over those grown in stationary solutions.

There was an obvious difference in colour to be seen between the large crystals near the bottom of the ampoule and some rather smaller crystals near the top of the solution. It seems probable that the latter

grew at a relatively low temperature towards the end of a run when it is possible that some impurity had been exhausted from the solution or that the stoichiometry was changed due to the lower growth temperature. These crystals, designated as last grown, were bright red in colour, by contrast to the darker colour of the first grown crystals of the same thickness. Unfortunately very few such crystals of a size sufficient for optical and electrical measurements were grown. The 'last grown' crystals, however, showed much sharper optical absorption spectra and much lower absorption in the extrinsic region, which appears to the eye as a difference in colour.

Figure 2.4 shows some crystals grown from solution and demonstrates the difference between 'first' and 'last' grown crystals. Whereas first grown crystals were high resistivity p-type, the last grown were low resistivity n-type. This will be discussed in Chapter 4.

Some attempts at doping were made by including an impurity at the level of parts per thousand in the solution. A last grown Se doped crystal was found to be n-type with a different activation energy to undoped crystals, indicating that Se was in fact incorporated into the crystals, although a high resistivity p-type Se doped crystal was also found.

The introduction of Ga into the melt had no perceptible effect on any properties measured. Cu acted as a sensitising impurity for photoconductivity (Chapter 5) suggesting that it behaves as a safe trap in $ZnSiP_2$.

The impurity content of some crystals was assessed using arc emission spectroscopy. Concentrations more than a few parts per million should be detectable in this way, although it is difficult to make any quantitative estimate of concentrations of impurities in particular cases. In materials grown from Sn solution, large amounts of Sn were present and

Fig. 2.4 Crystals of $ZnSiP_2$ grown from solution by the Accelerated Crucible Rotation Technique.

Left: The largest crystal grown in this way, from Zn solution.

Centre: Two similar crystals grown from Zn solution, except that the top one is last grown and the bottom first grown.

Right: Two crystals grown from Sn solution, comparable in size to the largest obtainable without accelerated rotation.

The scale is in cm.

Mg, Al, Cu, Ag and Ca were also detected. This material is highly impure, therefore. Crystals grown from zinc solution on the other hand showed only trace impurities at levels where positive identification became difficult. Ca, Ag and Al were thought to be present in these quantities in some samples, while in others no impurities were detected at all. Similar impurity levels were detected in the elements used to make the $ZnSiP_2$. The Zn which was nominally 6N pure, contained Cu and Cd at the limit of detection. The Si contained Ca in similar concentration and the phosphorus used contained Mg and Ca.

While this method only detects some elements, it appears that the impurity content of crystals grown from Zn is satisfactorily low. The poor purity of the crystals grown from Sn is probably due to the impurities in the Sn, since Cu, Mg and Pb were all detected in unused Sn but not in that which had been used as a solvent. Al was also found, both in used and unused samples.

In particular, no difference was found between first grown and last grown crystals from Zn solution, although in one case it was thought that a trace of Sn was detected in a first grown sample. The difference in properties between them cannot definitely be attributed to any particular cause at present.

2.8 Crystal structure

All the measurements of lattice parameters of $ZnSiP_2$ reported in the literature show that it has the chalcopyrite structure. The best measurements are probably those of Abrahams and Bernstein (1970) who determined the lattice parameters and the x-parameter by single crystal x-ray diffraction using a sophisticated structural refinement technique. Their results and those of other workers are shown in Table 2.1.

In this work the lattice parameters were measured by x-ray powder diffraction in a Phillips camera with a Straumanis film mounting, using

cobalt K α radiation. The diffraction angles of the lines observed were determined by measurement with a vernier ruler. The Straumanis film mounting had the advantage that the camera radius need not be known since the positions corresponding to $\theta = 0^\circ$ and $\theta = 90^\circ$ can be determined directly from the measured positions of the lines and film shrinkage is automatically taken into account. It is assumed that the camera is cylindrical and that the film shrinks uniformly.

The interplanar spacing d between $\{hkl\}$ planes is given by:

$$\frac{1}{d^2} = \frac{h^2 + k^2}{a^2} + \frac{l^2}{c^2} = \frac{4 \sin^2\theta}{\lambda}$$

where λ is the x-ray wavelength and θ the diffraction angle.

The conditions limiting possible reflections for the space group $I\bar{4}2d$ are (Henry and Lonsdale (1965)):

$h + k + l = 2n$ for a general reflection; and

$2h + l = 4n$ for $\{hhl\}$ reflections

A simple computer programme written by Miller (1974) was used to calculate values of θ from the published lattice parameters of $ZnSiP_2$ and the measured lines were indexed by comparison with these using a knowledge of the systematic absences.

Errors arising from the absorption of x-rays by the sample and from displacement of the sample from the centre of the camera along the line of the x-ray beam both vanish for backscattering ($\theta = 90^\circ$). The measured values of the lattice parameters were extrapolated to $\theta = 90^\circ$ using a variety of correction functions to account for the angular dependence of the errors. This extrapolation was performed by a least squares fitting programme written by Lee (1970) and the correction function which gave the best fit to the data was used to obtain the lattice parameters. The error in these was estimated as $\pm .001$ Å for a and $\pm .002$ Å for c from the scatter resulting from the use of different correction functions,

TABLE 2.1

Lattice Parameters of $ZnSiP_2$ –

a(Å)	c(Å)	c/a	x	
5.399	10.438	1.9334		This work
+ 5.399	10.435	1.933	.2691	Abrahams and Bernstein (1970)
* 5.407	10.451	1.933		Mughal et al. (1969)
5.400	10.440	1.933		Springthorpe and Pamplin (1968) Stroud (1970)
5.400	10.441	1.933		Vaipolin et al. (1964a, 1964b)
5.399	10.435	1.933	.270	Vaipolin et al. (1967)
5.399	10.435	1.933	.271	Vaipolin et al. (1972)

* Not corrected for absorption and acentricity

\+ Single crystal measurement. Error in x $\pm$ .0004

Errors were quoted as $\pm$ .001 Å for a and $\pm$ .002 Å for c by all the above workers

as the errors obtained from the statistical standard deviations were unrealistically low.

The result obtained is shown in Table 2.1, together with those of other workers. No significant variation was found between 'first-grown' and 'last grown' crystals, or for any other samples measured. The lattice parameters are in agreement within the limits of experimental error with those of all other workers except for Mughal et al (1969) who used a Bjurstrom chart, and so did not correct for absorption and acentricity. Apart from this measurement, the results of different workers are in fairly good agreement, although there is a just significant variation in c. There is complete unanimity in c/a to $\pm$ .0005, or one part in 4000, and the value of c/a in the present work is quoted to an extra figure since many of the errors in a and c may be expected to be in the same sense, so that c/a may be considerably more accurate than either.

2.9 Thermal expansion of II IV V_2 compounds

Relatively little is known about the thermal expansion of II IV V_2 compounds. Measurements of this effect could be useful for interpreting the results of crystal growth experiments, both in the case of epitaxy, where differences in the contraction of substrate and layer could lead to deformation, and in melt growth, where anisotropic contraction is thought to be the cause of the cracking of boules. The possibility of the existence of a high temperature sphalerite phase on the evidence of differential thermal analysis for several II IV V_2 compounds suggests that this could also cause problems in crystal growth. It is also possible that measurements of thermal expansion could throw light on the nature of bonding in these materials.

The coefficients of thermal expansion of II IV V_2 compounds have been little investigated until recently. Kildal (1972) has measured this

property of $CdGeAs_2$ using an accurate optical technique over a rather limited temperature range, and Cervinka and Kaspar (1970) used x-ray diffraction on the same compound. Pfister (1963) quoted the lattice parameter of disordered $ZnSnAs_2$ at room temperature and 640 C and showed that $ZnSnAs_2$ disorders at about this temperature. Miller (1974) has measured the lattice parameters of $ZnGeP_2$ and $CdGeP_2$ above room temperature by the same technique as that described here. Kozhina and Borschchevskii (1971) have measured high temperature lattice parameters of several II IV V_2 compounds. Their results for $ZnGeP_2$ are significantly different from those of Miller (1974) even at room temperature, and may reflect a difference in preparation technique. Their results for $CdGeAs_2$ are in reasonable agreement with those of Cervinka and Kaspar (1970). They also found that the $ZnSnC_2$ compounds, which show no tetragonal compression at room temperature, expand isotropically with temperature.

2.10 Measurement of high temperature lattice parameters

The lattice parameters of $ZnSiP_2$ were measured using a 19 cm Unicam S150 high temperature powder camera, with a Van Arkel film mounting. With this arrangement the film is in two sections, one on each side of the x-ray beam, and their positions were marked by a series of pins which cast shadows on the film. The positions of the pins were calibrated using the room temperature powder pattern of α - Al_2O_3 and it was verified that the lattice parameters of $ZnSiP_2$ at room temperature measured with this camera agreed with those obtained using a conventional camera.

The sample was contained in a sealed silica tube 0.3 mm in diameter which was mounted in the centre of the camera. Except for a narrow gap to allow the x-rays to pass, the sample was surrounded by heater elements. The temperature was measured with a Pt/Pt 13% Rh thermocouple near the sample and the inside of the camera was evacuated for thermal insulation.

At high temperatures extra lines sometimes appeared due to the devitrification of the quartz, although this could be eliminated up to 1100 C by careful cleaning of the outside of the tube to remove finger marks. At 1100 C it was necessary to inhibit decomposition of the sample by nearly filling the empty space above it in the quartz tube with a quartz rod drawn out to be a good fit to the tube. After the measurement the sample was cooled to room temperature and its lattice parameters again measured. They were found to be the same as those taken on unheated samples, showing that no permanent change in the lattice parameters of the sample had occurred. Nevertheless a fresh sample was used for each measurement.

Copper K α radiation (filtered with Ni) was used for the high temperature work because the high power available makes for short exposure times (8 hours at 40 kV and 20 mA) and any effects of decomposition should be minimised. At room temperature, copper radiation gives no lines higher than 73^{o} but at higher temperatures an extra line indexed as (448) appears on the film at a high value of θ due to the increased lattice parameters. Since lines at as high θ values as possible are needed for optimum accuracy in extrapolating to $\theta = 90^{o}$ the appearance of the extra line was beneficial in maintaining accuracy to high temperatures where it would normally decrease due to the greater diffuseness of the lines.

Indexed photographs taken at room temperature and at 1100 C are shown in Figure 2.5.

2.11 Results and Discussion

The lattice parameters were calculated as described in section 2.8. and are shown as a function of temperature in Figure 2.6. The points are fitted within the limits of experimental error by straight lines and the coefficients of expansion calculated from their slopes are mean values for the temperature range considered. $ZnSiP_2$ expands faster along the a axis than the c axis so that the tetragonal

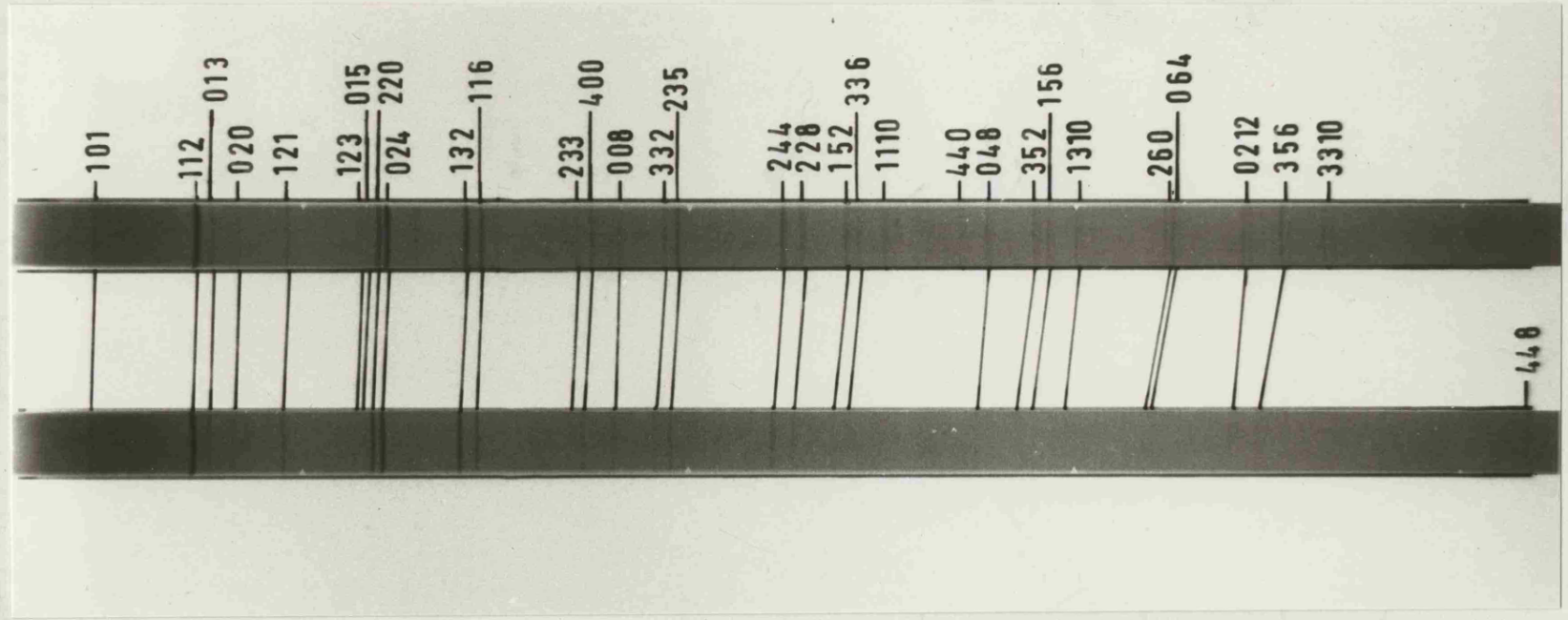

Fig.2.5 Indexed X-ray powder photographs of $ZnSiP_2$ using Cu Kα radiation; (a) room temperature, (b) 1100 C.

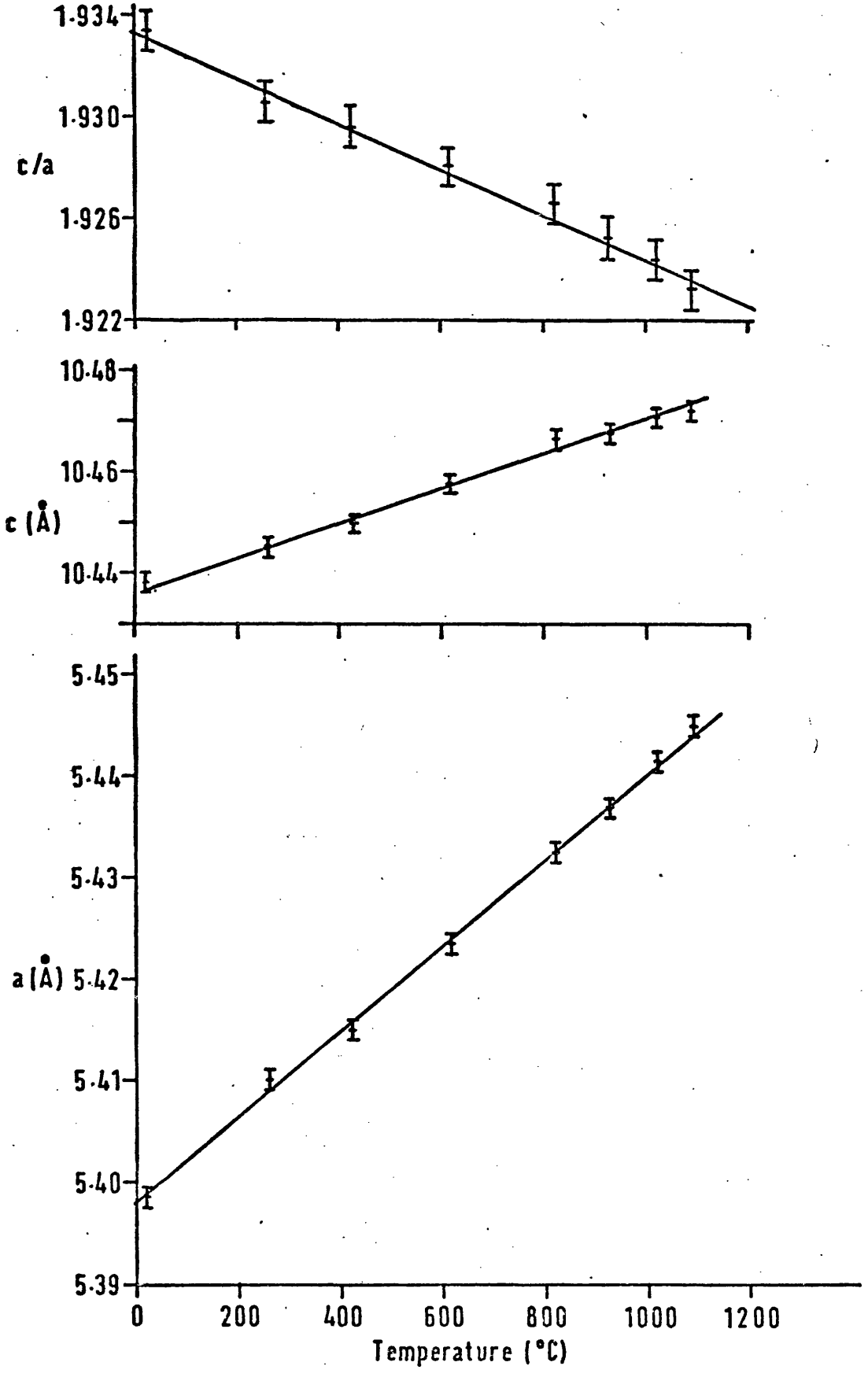

Fig.2.6 Temperature dependence of the lattice parameters of $ZnSiP_2$

compression increases with temperature. This can be understood in terms of the thermal expansion of the individual bonds in the crystal.

The bond lengths from geometry are (Abrahams and Berstein (1970)):

$$Zn - P = \left[a^2x^2 + \frac{4a^2 + c^2}{64} \right]^{\frac{1}{2}}$$

$$Si - P = \left[a^2(1 - x)^2 + \frac{4a^2 + c^2}{64} \right]^{\frac{1}{2}}$$

If regular SiP_4 tetrahedra are assumed, then:

$$Zn - P = \left[\frac{16a^2 + 3c^2}{64} - \frac{a}{4} \left(\frac{c^2}{2} - a^2 \right)^{\frac{1}{2}} \right]^{\frac{1}{2}}$$

$$Si - P = \frac{\sqrt{3}}{8} c$$

This approximation is known to be good at room temperature. However the thermal expansion of the crystal between room temperature and 1100 C is so small as to be comparable with the error in this approximation so that any change in the deviation from the approximation could have a significant effect. The thermal expansion coefficients of the bonds are only estimates, therefore, and could be subject to considerable errors.

The bond lengths given by this approximation are shown in Figure 2.7 plotted as functions of temperature. The coefficient of thermal expansion of the Zn - P bond was calculated to be $9.7\ 10^{-6}\ C^{-1}$ and that of the SiP bond $3.2\ 10^{-6}\ C^{-1}$. The coefficient of expansion of the Zn - P bond may be compared with Miller's (1974) value for the same bond in $ZnGeP_2$ of $8.9\ 10^{-6}\ C^{-1}$. No measurements of the thermal expansion of a Si - P bond were found for comparison except the results for $CdSiP_2$ by Kozhina and Borshchevskii (1971) which give an expansion coefficient of $.4\ 10^{-6}\ C^{-1}$, but the scatter of the experimental points is too large for this to have any meaning. Miller's (1974) value for the Ge - P bond in $ZnGeP_2$ of $4.8\ 10^{-6}\ C^{-1}$ is significantly larger than the present value for Si - P.

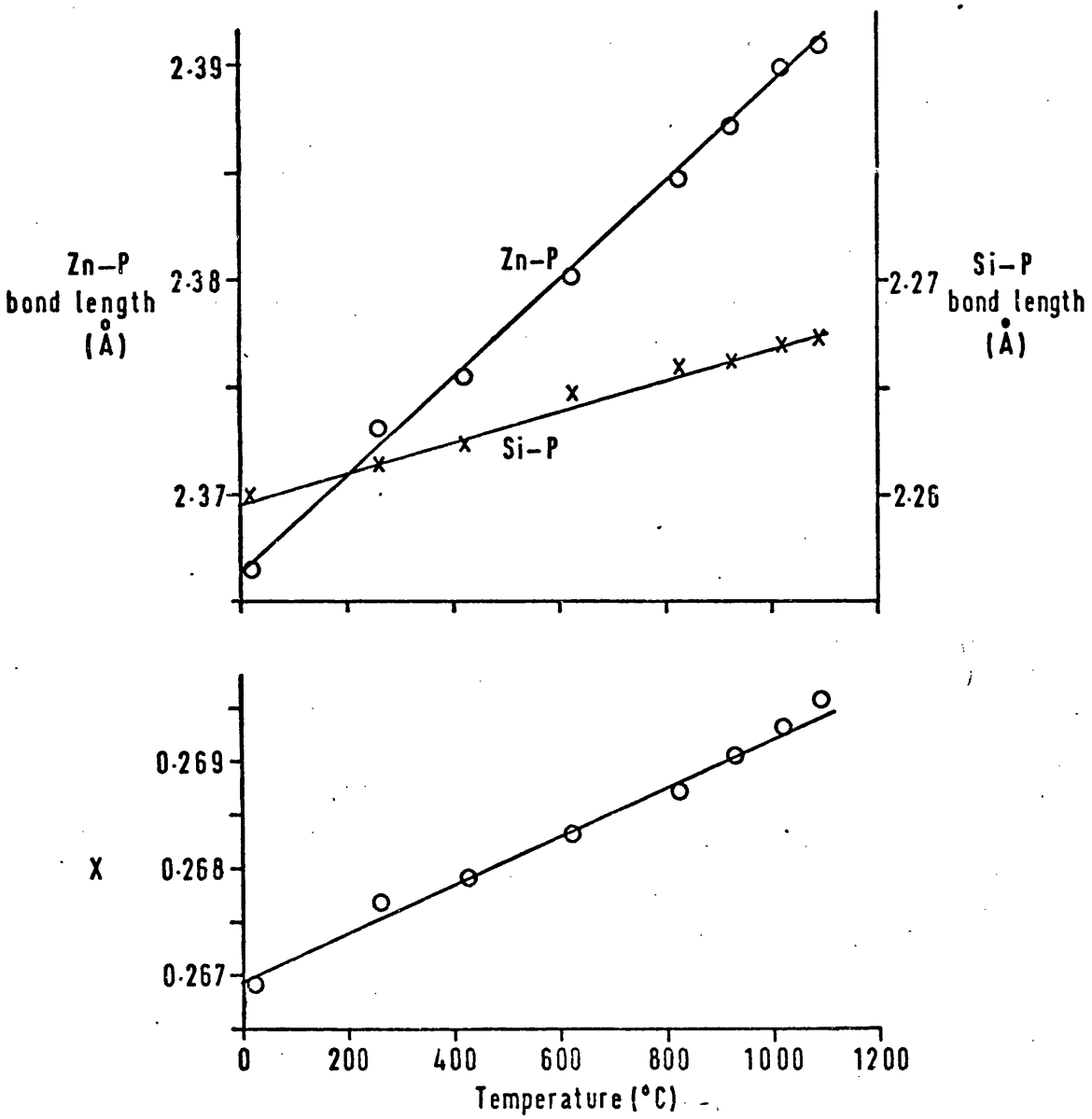

Fig. 2.7 Temperature dependence of x and bond lengths in $ZnSiP_2$, calculated assuming regular SiP_4 tetrahedra.

Covalent bonds are strong short range forces which characteristically have low coefficients of thermal expansion, whereas ionic bonds have much longer range. For example, the mean coefficient of thermal expansion of Si between 0 and 600 C is 2.0 10^{-6} C^{-1} (Pearson (1967)) while that of NaCl is about 50 - 60 10^{-6} C^{-1} (Enck and Dommel (1965)).

The large coefficient of thermal expansion of the Zn - P bonds is therefore attributed to its ionicity, while the Si - P bond is almost entirely covalent. The expansion of the Zn-P bond is comparable to that of ZnSe which is about 8.0 10^{-6} C^{-1} (Novikova (1966)). The expansion of the Si-P bond is between the values of 2.0 10^{-6} C^{-1} for Si and 5.3 10^{-6} C^{-1} for GaP (Novikova (1966)). No values could be found in the literature for the more appropriate analogues AlP and ZnS. The sizes of the bond thermal expansion coefficients are, therefore, similar to the values to be expected on the grounds of ionicity.

The coefficients of volume thermal expansion of the different II IV V_2 compounds for which data are available are similar despite the considerable variations in anisotropy, with values near 20 10^{-6} C^{-1}. A similar observation may be made in the case of the III V compounds values for which cluster around 17.5 10^{-6} C^{-1} in the same temperature range (Novikova (1966)). The similarity between these values reflects the close relationship between the II IV V_2 compounds and their III V analogues.

Weaire (1975) has suggested that the rate of change of the tetragonal compression with temperature should be proportional to the tetragonal compression. This conclusion was based on a consideration of the dependence of the internal energy of the crystal on the x-parameter and the close relationship between x-parameter and tetragonal compression. This is borne out surprisingly well by the available measurements as shown in Figure 2.8. The values for $CdSiP_2$ and $CdGeAs_2$ (Kozhina and Borshchevskii (1971)) are less accurate than the others, which

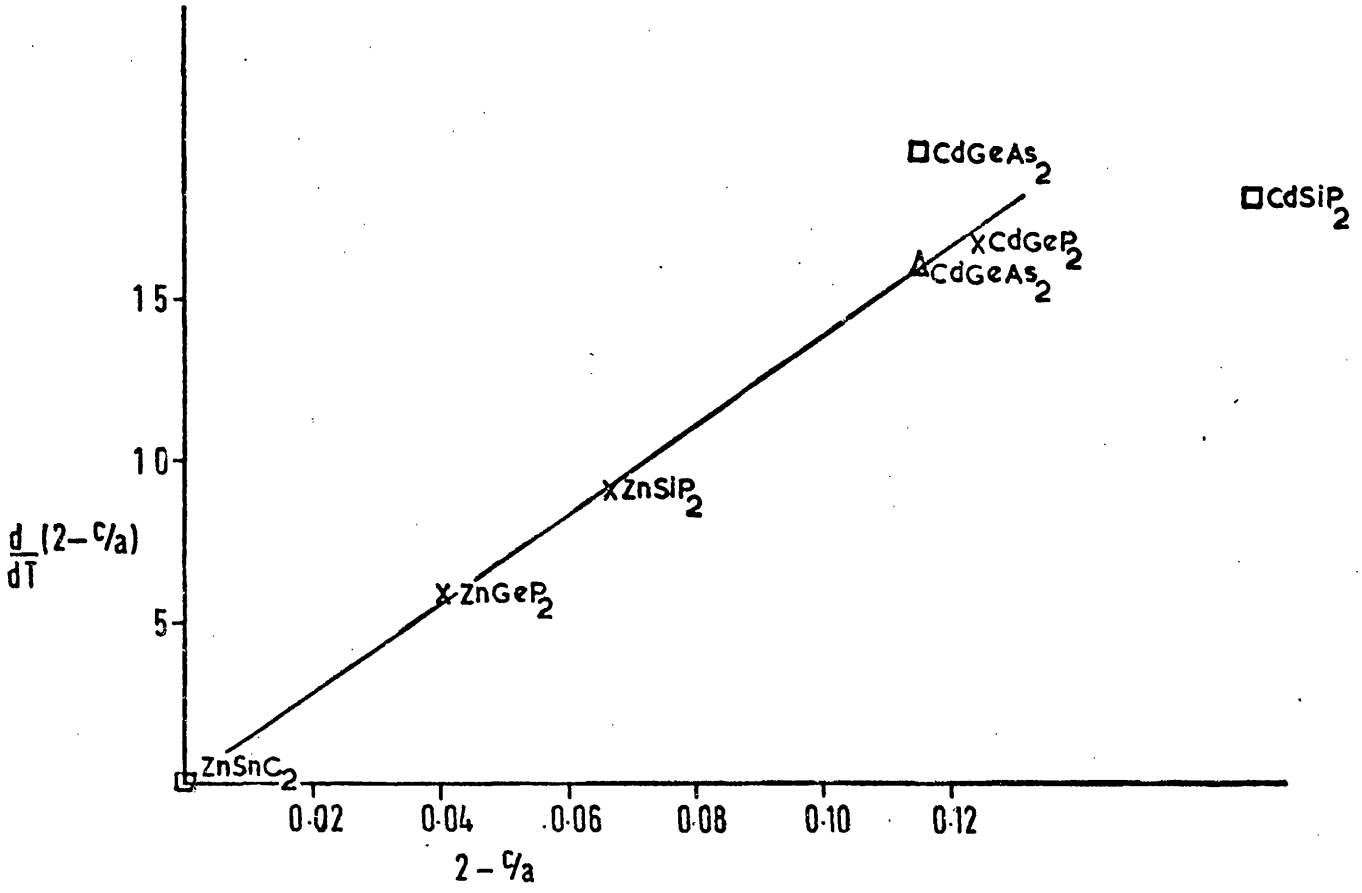

Fig. 2.8 Rate of change of tetragonal compression with temperature vs. tetragonal compression for several $II\,IV\,V_2$ compounds.

X $ZnSiP_2$ Present work ; $ZnGeP_2$, $CdGeP_2$ Miller (1974) ;

Δ $CdGeAs_2$ Cervinka and Kaspar (1970);

□ $ZnSnC_2$, $CdSiP_2$, $CdGeAs_2$ Kozhina and Borshchevskii (1971)

may account for them not lying on the straight line. Strictly the deviation of x from $\frac{1}{4}$ rather than the tetragonal compression should be plotted and the excellent agreement is perhaps some indication that the close connection between the x parameter and the tetragonal compression is maintained to high temperatures.

It is initially somewhat surprising that the tetragonal compression increases with temperature, since the tendency might be expected to be towards a more symmetric cubic structure at high temperatures. The explanation in terms of bond thermal expansions given here suggests why this should not be so. The point that II IV V_2 compounds cannot necessarily be expected to behave as slightly deformed cubic materials under all conditions is also illustrated.

CHAPTER 3

Optical properties and band structure

3.1 Introduction

It was pointed out in section 1.4 that the band structure of a II IV V_2 compound is expected to be very similar to that of its III V analogue. The perturbations which must be considered to change the III V band structure into that of a II IV V_2 compound are:

1. The presence of two different cation species, which result in a larger unit cell
2. The compression of the lattice in the c-direction
3. The shift of the anions away from $(\frac{1}{4}, \frac{1}{4}, \frac{1}{4})$ and related positions

Increasing the size of the real unit cell reduces the size of the Brillouin zone, which in chalcopyrite has a quarter of the volume of that in zinc blende. The effect of (1), therefore, is to embed the band structure of a III V compound into the chalcopyrite Brillouin zone. It will also perturb the energies of some of the bands by small amounts.

The two Brillouin zones are shown in Figure 3.1 with some important symmetry points marked. The way in which the points outside the smaller chalcopyrite zone map back into it was described by Chaldyshev and Pokrovskiĭ (1963)). The most important points transform as follows:

$\Gamma(0,0,0)$; $X(0,0,\frac{2\pi}{a})$; $W(0,\frac{2\pi}{a},\frac{\pi}{a})$; $W(\frac{2\pi}{a},0,\frac{\pi}{a})$; $\rightarrow$ $\Gamma(0,0,0)$

$L(\frac{\pi}{a},-\frac{\pi}{a},-\frac{\pi}{a})$ Σ $(\frac{\pi}{a},\frac{\pi}{a},0)$ $\rightarrow$ $N(\frac{\pi}{a},\frac{\pi}{a},0)$

$X(0,\frac{2\pi}{a},0)$; $X(\frac{2\pi}{a},0,0)$; Δ $(0,0,\frac{\pi}{a})$ $\rightarrow$ $T(0,0,\frac{\pi}{a})$

where a is the lattice parameter of the zinc blende structure and the tetragonal compression has been neglected. It should be mentioned that

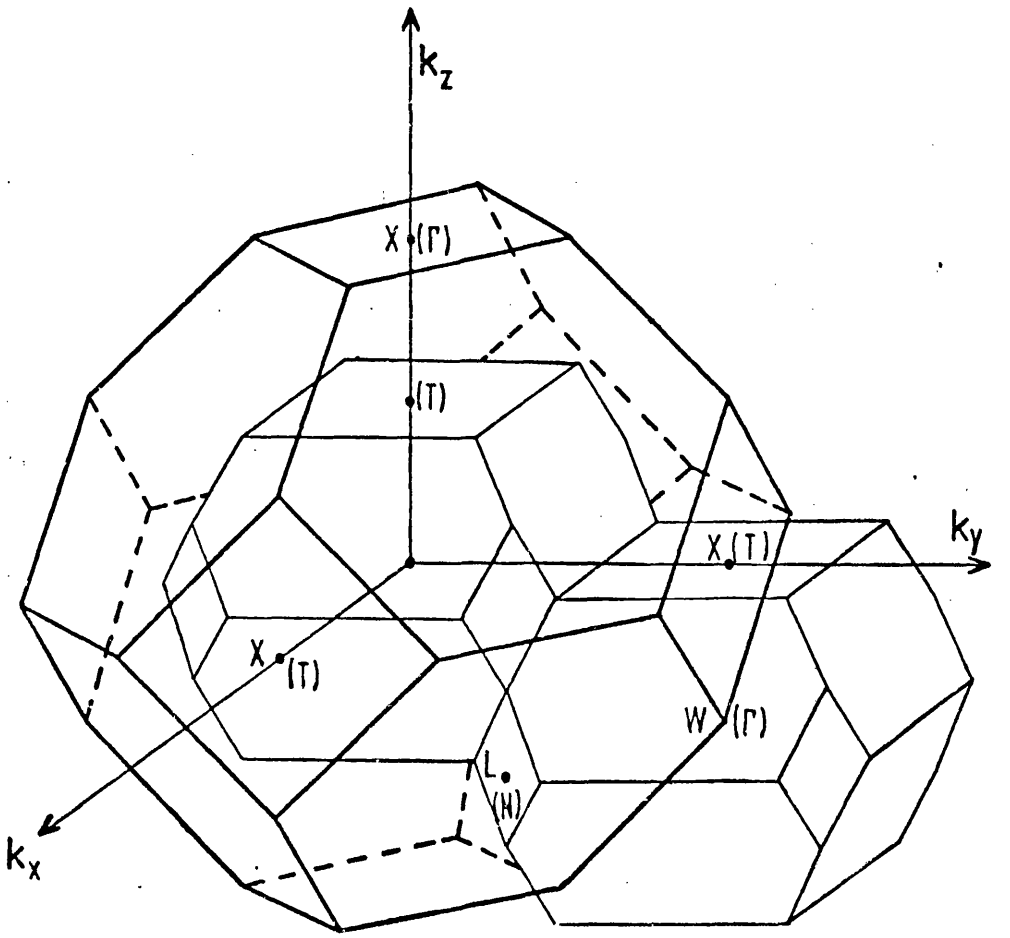

Fig. 3.1 Zinc Blende and Chalcopyrite Brillouin zones

the notation for labelling symmetry points, while the most widely used is not quite universal. The choice of notation for labelling irreducible representations also varies slightly. We shall use that most common outside the USSR which is the notation adopted by Shay and Wernick (1975).

The mappings shown illustrate two important points. The first is that all the points of a given symmetry in zinc blende do not all map to the same point in chalcopyrite (eg $X \rightarrow T, \Gamma$). The second is that one X-point maps back to the zone centre.

The band structures obtained in this way are of two types, shown in Figure 3.2 (neglecting spin-orbit interaction). If the III V compound has a direct gap, then the corresponding ternary will also be direct. If the III V is indirect with the lowest conduction band minima at X (eg GaP, AlP) then one of the X-points maps to Γ and the other two to T. One of the three indirect transitions (to the three equivalent X-points) of GaP becomes direct in the chalcopyrite Brillouin zone. Until other perturbations are considered the minima at Γ and T have nearly the same energy.

Since the mapping back process is due to the difference between the cations the strength of direct transitions between the valence band maximum at Γ and the conduction band minimum which maps back from X will depend on the difference between the cations. Shay et al. (1970a) called such transitions pseudodirect because their strength is proportional to the difference between the pseudopotentials of the cations.

When the tetragonal compression is included as a second perturbation the degeneracy between the mapped back conduction band at Γ and the minima at T is lifted. Balslev (1966) has shown that applying a uniaxial compression along the c-axis of GaP moves the (001) minimum to a lower energy than the (100) and (010) minima. Thus it is to be expected that the pseudodirect transition will be lower in energy

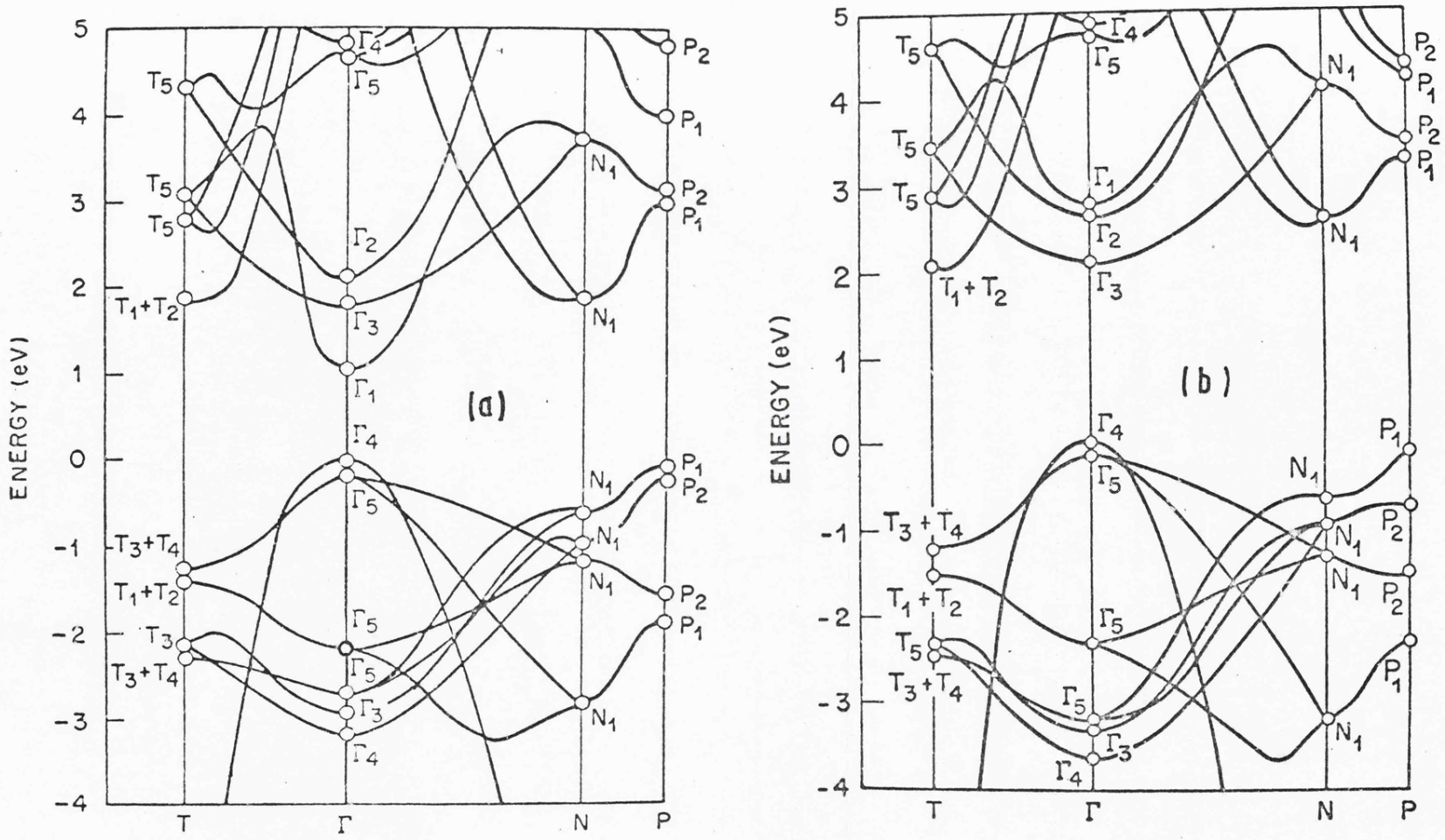

Fig. 3.2 Theoretical band structure of (a) direct and (b) pseudo-direct chalcopyrite compounds.

than the indirect one.

The presence of two cations and the tetragonal compression split the threefold degenerate (neglecting spin) Γ_{15} level into a non-degenerate Γ_4 and a doubly degenerate Γ_5 level. When spin is included, the Γ_5 level is again split, so that the valence band maximum of the II IV V_2 compounds is made up of three levels which are only spin-degenerate.

These changes are summarised in Figure 3.3. In this work the valence bands will be called V_1, V_2, V_3 (V_1 being highest in energy) and the lowest conduction band C, which greatly simplifies the nomenclature. This is the notation of Kildal (1972).

3.2 Selection rules

The presence of a unique axis in the chalcopyrite structure means that a II IV V_2 compound behaves differently under perturbations of different orientation so that, for example, the optical absorption coefficient is different for light polarised parallel and perpendicular to the c-axis. Whereas in the zinc blende structure transitions are only allowed or forbidden, in uniaxial crystals transitions may be allowed in one polarisation and not in the other. It is possible to predict with the aid of group theory the selection rules that determine which transitions are allowed under a particular set of conditions. The necessary character tables are given by Sandrock and Treusch (1964) and Chaldyshev and Pokrovski (1960), and the resulting selection rules for transitions between all the irreducible representations of the chalcopyrite structure by Poplavnoi et al. (1969)

The selection rules of particular interest are those corresponding to transitions near the lowest band gap of $ZnSiP_2$ which are included in Figure 3.3. The cases with and without spin orbit splitting are considered because it is a rather weak perturbation and transitions

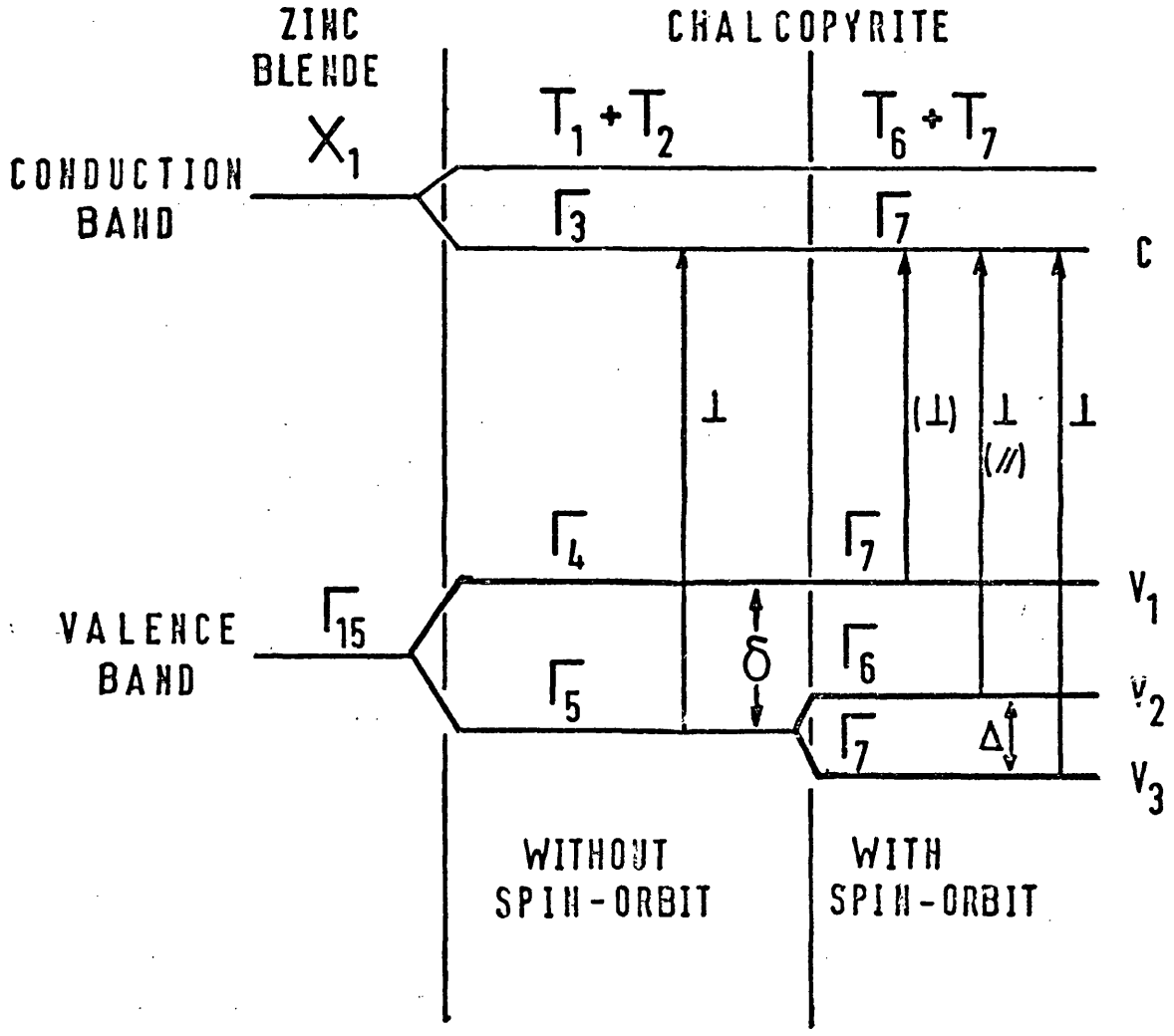

Fig. 3.3 Splittings of the bands and selection rules for $ZnSiP_2$

which are only allowed because of it are expected to have low oscillator strengths. None of the transitions shown in Figure 3.3 is allowed in zinc blende where they are all indirect.

Confusion can arise in discussing selection rules in chalcopyrites due to the presence of optical activity. This is not expected to disturb the selection rules appreciably because the effect is normally so small compared to birefringence. In optically active crystals without a unique axis light is propagated as left- and right-circular polarised forms with slightly different refractive indices. In the presence of both birefringence and optical activity light is propagated as elliptically polarised rays, and the birefringence is so much larger than the optical activity that these correspond to very nearly linear polarisations parallel and perpendicular to the unique axis (Nye (1957)). Optical activity has been observed in $AgGaS_2$ (Hobden (1968)) at a wavelength where the birefringence accidentally vanishes and it was confirmed to be small.

3.3 The Quasicubic Model

The magnitudes of the splittings of the valence bands due to spin-orbit coupling and the crystal field can be treated (Rowe and Shay (1971)) using the theory developed by Hopfield (1960) to interpret valence band splittings in II VI compounds with the wurtzite structure. This model considers these effects as perturbations mixing the p-like valence bands of the cubic case and is called a quasicubic model. Within this approximation the energies of the Γ_7 valence bands at $k = 0$ relative to the Γ_6 band are given by:

$$E_{1,\,2} = -\tfrac{1}{2}(\delta + \Delta) \pm \tfrac{1}{2}\left[(\Delta + \delta)^2 - \tfrac{8}{3}\Delta\delta \right]^{\frac{1}{2}} \qquad (3.1)$$

where δ is the crystal field splitting and Δ the spin-orbit splitting. Δ and δ may thus be obtained from experimental measurements of $E_{1,\,2}$. This model only incorporates the three valence bands, although

Kildal (1972) has shown that the splittings are the same at k = 0 when the Γ_1 conduction band is included by k.p theory. The quasicubic model also yields eigenfunctions which allow the ratios of oscillator strengths to be calculated.

3.3.1 Spin-Orbit Splittings

Spin-orbit splittings have been estimated for the III V compounds (Hübner (1970) with some success by using atomic spin-orbit splitting parameters (Herman (1963)) weighted by the ionicity to take account of the different amounts of time spent by the electrons on the cations and anions. The reason why this can be done is that the spin-orbit coupling Hamiltonian is $\frac{\hbar}{4 m_o^2 c^2} (\Delta V \times p).\sigma$, which is only significant inside the atoms where ΔV is large, so that spin-orbit splitting is mainly a property of the individual atoms involved, and only the ionicity is needed to account for the individual crystal concerned.

Hübner and Unger (1972) have applied this approach to estimating the spin-orbit splittings of the II IV V_2 compounds by using the average ionicity of the two bonds.

$$\Delta_{ABC_2} = \tfrac{1}{4}\left[(1 - f_i)(\Delta_A + \Delta_B) + (1 + f_i)\, 2\Delta_C\right] \qquad (3.2a)$$

where f_i is the mean ionicity of the bonds and $\Delta_A, \Delta_B, \Delta_C$ are the atomic spin-orbit splitting parameters of the atoms A,B,C. This equation yields good agreement with the values measured experimentally, although they are consistently overestimated slightly. Very similar results are obtained if the bonds are treated separately using Levine's (1973) ionicities, although the agreement with experiment is perhaps slightly better. Equation (3.2a) then becomes:

$$\Delta_{ABC_2} = \tfrac{1}{4}\left[(1 - f_{AC})\Delta_A + (1 - f_{BC})\Delta_B + (2 + f_{AC} + f_{BC})\Delta_C\right] \qquad (3.2b)$$

where f_{AC} and f_{BC} are the ionicities of the AC and BC bonds. Equation (3.2a) estimates the spin-orbit splitting of $ZnSiP_2$ as .070 eV, while

(3.2b) gives .069 eV, so that they agree closely in this case. The differences become more pronounced in compounds with larger spin-orbit splittings.

3.3.2 The Crystal Field splitting

The crystal field splittings of the II IV V_2 compounds have been calculated by a pseudopotential method (Poplavnoi et al. (1969), (1970a), (1970b), summarised by Goryunova et al. (1970)) with rather poor agreement with experiment. Since the accuracy of such calculations is limited (Poplavnoi (1969) claim an accuracy of .3 eV) it is not surprising that splittings in the range 0 - .25 eV are not predicted.

A more successful approach to explaining the observed crystal field splittings, if not to calculating them, is that of Shay (1971) who assumed that the tetragonal compression is the major perturbation responsible for the crystal field and therefore that the splitting should be given by:

$$\delta = \frac{3}{2} b \left(2 - \frac{c}{a}\right)$$

where b is the deformation potential of the III V analogue, $(2 - \frac{c}{a})$ is the tetragonal compression and the factor of $\frac{3}{2}$ accounts for the observed shift of the top valence band being only $\frac{2}{3}$ of the crystal field splitting according to the quasicubic theory in the limit of small crystal field.

The experimental values of the deformation potentials of the III V compounds show considerably scatter, depending on the measurement technique. The prediction of this equation that the crystal field splitting of a II IV V_2 compound should be approximately proportional to its tetragonal compression is borne out both for the II IV V_2 (Shay and Wernick (1975)) and the I III VI_2 (Shay et al. (1974)) compounds with slopes suggesting mean deformation potentials of - 1.2 and - 1.0 respectively. The close relationship between the tetragonal compression and

the rotation of the anion tetrahedra (equation 1.1) makes it difficult to rule out this as a possibly important perturbation. However the absence of a crystal field splitting in $ZnSnP_2$ (Krivaite et al (1973)) and $ZnSnAs_2$ (Kwan and Wooley (1971)), where the tetragonal compression is zero, is good evidence that the tetragonal compression alone contributes significantly to the crystal field which splits the valence bands.

3.4 Previous work on the band structure of $ZnSiP_2$

Since $ZnSiP_2$ is the isoelectronic analogue of $GaAlP_2$ and both GaP and AlP have indirect gaps with the lowest conduction band minima at or near X, it is to be expected that $ZnSiP_2$ will have a pseudodirect gap. Band calculations (Poplavnoi (1968), (1969)) are in agreement with this prediction, although the calculated band gap was 1.23 eV, whereas most experimental values are greater than 2 eV.

Most of the early experimental work on the band structure of $ZnSiP_2$ was rather inconclusive. The band edge determined from photoconductivity measurements can vary over a considerable range (Zlatkin and Novikov (1967)) due to differences in crystal quality. The measured absorption curves (see Figure 3.4) are approximately exponential and are therefore rather difficult to interpret in terms of a band gap. For some years the 'best'value was that of Goryunova et al. (1966) for a crystal of low carrier concentration. Examination of these results show that this steep absorption edge, although very different to all the other results on $ZnSiP_2$ is very similar to that of iodine doped ZnP_2 (the crystals were grown by vapour transport). The luminescence spectrum of crystals from the same source showed (Akopyan (1966)) a luminescence spectrum with many sharp lines similar to the results of Wardzynski et al. (1967) for ZnP_2. It seems plausible, therefore, that the often quoted result of 2.00 eV for the band gap of $ZnSiP_2$ is a result for ZnP_2.

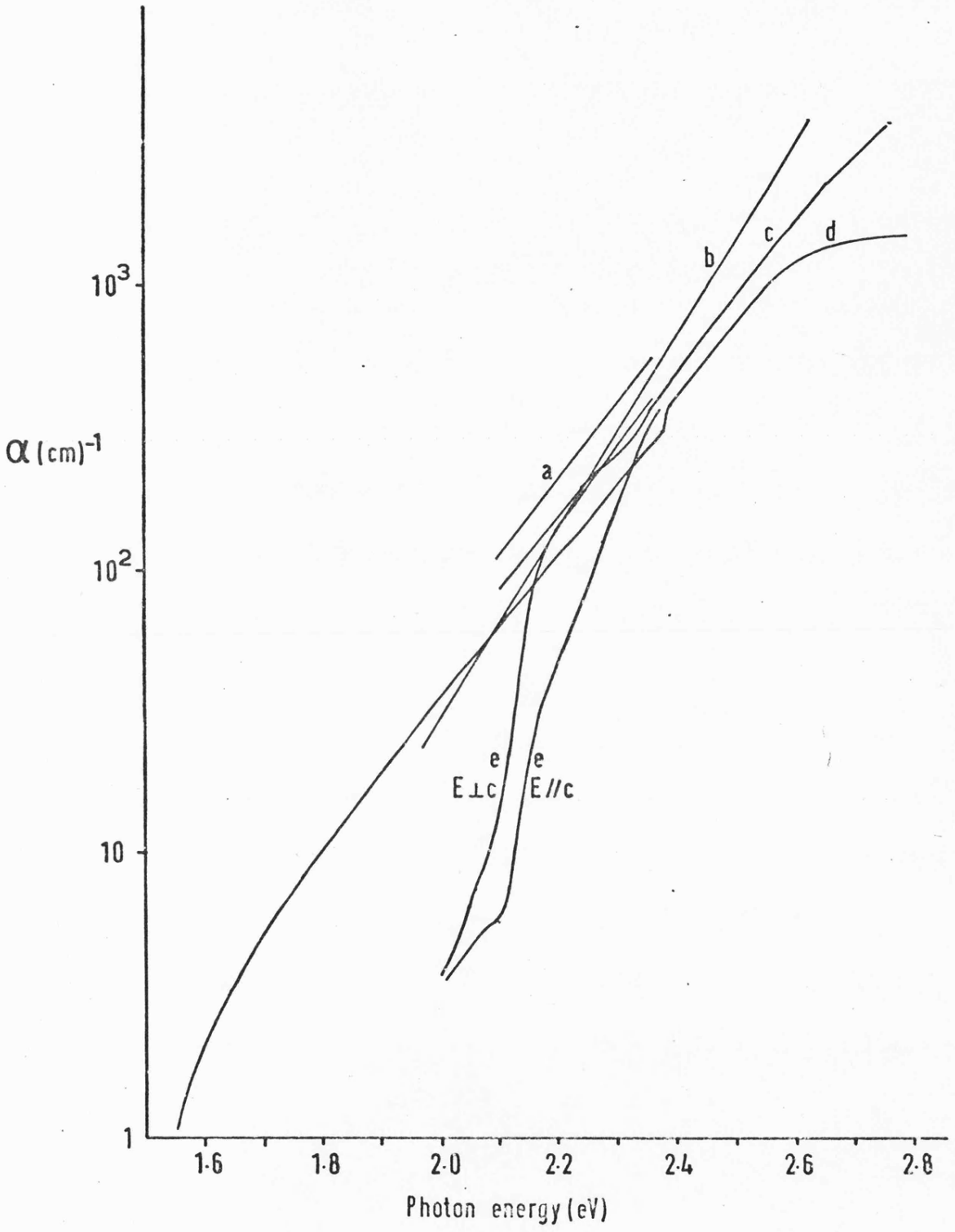

Fig. 3.4 Absorption of $ZnSiP_2$ (after Kruse and Schulze (1974)
a Bendorius et al. (1972), b Stroud (1970), c Kruse and Schulze (1974)
d Goryunova et al. (1966) e Sample 2; this work

Belle et al. (1965) observed structure on the absorption edge of $ZnSiP_2$ in the form of two peaks, but their magnitudes were not determined. Recently more detailed measurements have been made. Bendorius et al. (1972) showed that the absorption edge in $ZnSiP_2$ probably derives from the Γ - X transition in GaP by examining the pressure dependence of the absorption edge. Babonas et al. (1974a) have observed structure on the absorption edge of $ZnSiP_2$ by wavelength modulation and attributed the three peaks which they found to transitions from the three valence bands to the conduction band. Babonas et al. (1974b) measured the pressure dependence of the wavelength modulation peaks to confirm their origin at the X point in zinc blende. Gorban et al. (1974) have seen these singularities without wavelength modulation but attributed them to different levels of a single exciton which would require an exciton binding energy of more than 150 meV, an unusually large value for a semiconductor.

Electroreflectance, which has proved so valuable in determining the band structures of II IV V_2 compounds, yields anomalous results for $ZnSiP_2$. Figure 3.5 shows the electroreflectance spectra determined by Shay et al. (1973) and by Miller in this laboratory, both workers using crystals grown from tin solution in the present work. The spectra are qualitatively similar although the magnitude of the peak for E//c near 3.06 or 3.03 eV is greater in Shay's measurements. The region below 2.8 eV shows no structure, and there is not thought to be any particular significance in terms of band structure in the opposite sign of the signal in the two measurements in this region. The positions of the peaks given are marginally different, although this sort of error is to be expected and could be accounted for by the different conditions of the experiments.

The graphs show that the first structure appears at 2.96 or 2.93 eV, far above the observed absorption edges near 2 eV. More difficult

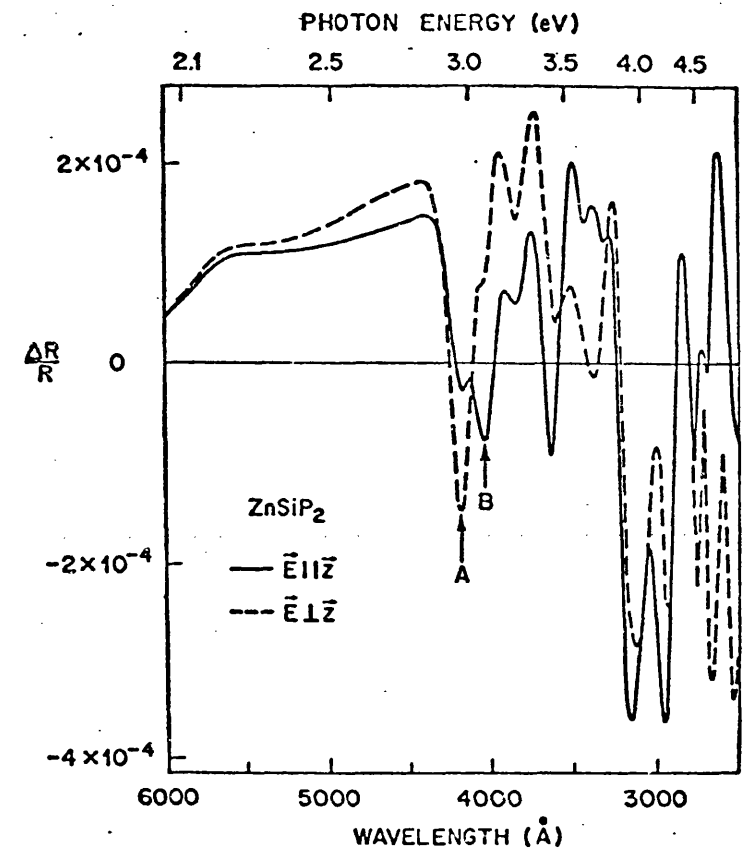

(a)

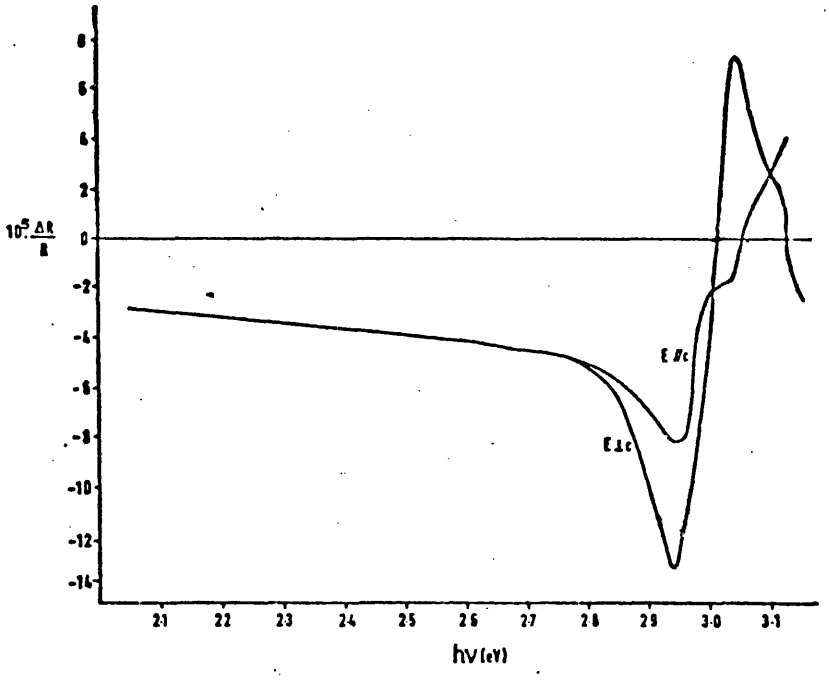

(b)

Fig.3.5 Electroreflectance spectra of $ZnSiP_2$

(a) Shay et al. (1973)

(b) Miller (unpublished)

to explain is the polarisation dependence of the spectra. A transition from V_1 to the Γ_1 conduction band, which is the lowest direct transition (excluding pseudodirect ones) in all other II IV V_2 compounds studied, should be polarised E//c whereas in this case it is clearly polarised $E \perp c$. This leads Shay et al. (1973) tentatively to suggest that the valence band ordering in $ZnSiP_2$ might be different from that in all the other II IV V_2 compounds. All the evidence in the present work indicates that this is not so, and another explanation must be sought.

The direct gap in GaP is at 2.79 eV at room temperature (Nelson et al. (1964)) and that of AlP has been variously estimated (Stirn (1972), Onton and Chicotka (1970)) at 3.3, 3.6 and 3.7 eV. The direct gap of $ZnSiP_2$ is therefore expected to be of the order of or greater than 3eV so that it is not surprising that no structure is seen below 2.9 eV. The band structures of Figure 3.2 show that the direct gaps at N, P and T are all thought to be of about the same magnitude. The most plausible explanation for the observed electroreflectance results seems to be in terms of transitions at some point in the Brillouin zone away from the zone centre.

Gallay et al. (1975) have performed electroreflectance measurements on $ZnSiAs_{2-x}P_x$ alloys and, by following the valence band to Γ_1 transition through a range of alloys of different compositions, estimated the position of the $V_1 - \Gamma_1$ transition at 3.42 eV in agreement with the ideas expressed above.

The low temperature ($\sim$2 K) luminescence measurements of Shay et al. (1970b), Nahory et al. (1970), Shah and Buehler (1971) and Shah (1972) show a series of lines at low temperatures caused by bound exciton decay with phonon replicas. The absence of a no-phonon line suggested to these authors that $ZnSiP_2$ has an indirect gap.

3.5 Experimental

3.5.1 Sample Preparation

Relatively thick crystals were required for the absorption measurements, since pseudodirect transitions were expected to be weak. Crystals had to be cut in such a way that solvent inclusions could be 'polished out' and still leave a reasonable thickness. This requirement dictated the orientation of the platelets produced and it was not possible to choose a particular orientation. Crystals up to about .8 mm thick were used.

Crystals were mounted with wax on a stainless steel polishing jig, shown diagrammatically in Figure 3.6, which permitted samples to be polished plane-parallel. They were lapped on 600 grade emery paper, carefully washed, and polished with 6μ diamond paste on a paper pad. This was followed by polishing on 1μ diamond and finished with .05μ Al_2O_3 on a microcloth. When a good scratch-free surface was obtained the crystal was removed from the jig by boiling in methanol, and the process repeated on the other side. Crystals were examined under a polarising transmission microscope to ensure that they were single and contained no inclusions.

The thickness of a crystal was measured by placing it between optical flats so that a wedge film was formed and illuminating it with sodium light. The fringe spacing over 100 fringes was measured using a travelling microscope and this information, coupled with the length of the wedge, gives the thickness of the crystal, since the wavelength of the light was known. This method was chosen because it elimated errors due to rounding of the edges of the crystal (the angle of the wedge was very small) and non-uniformity of the crystal thickness could be detected. The risk of damaging even a very fragile crystal is slight.

3.5.2 The Optical System

The apparatus used is shown diagrammatically in Figure 3.7. The

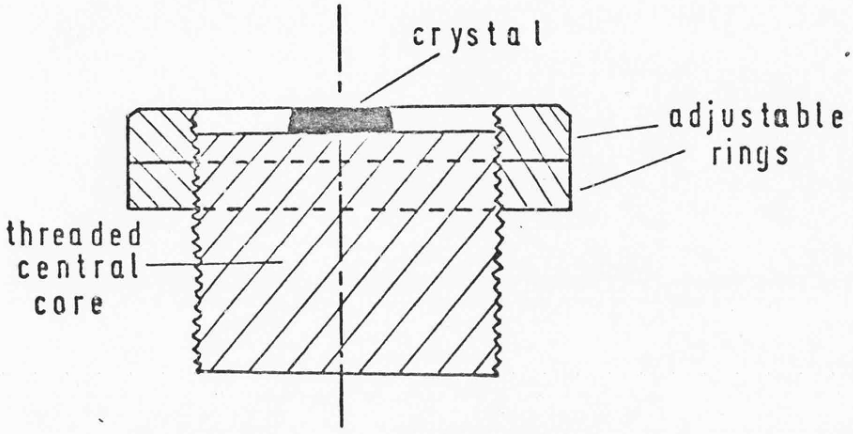

Fig. 3.6 Cross section of polishing jig

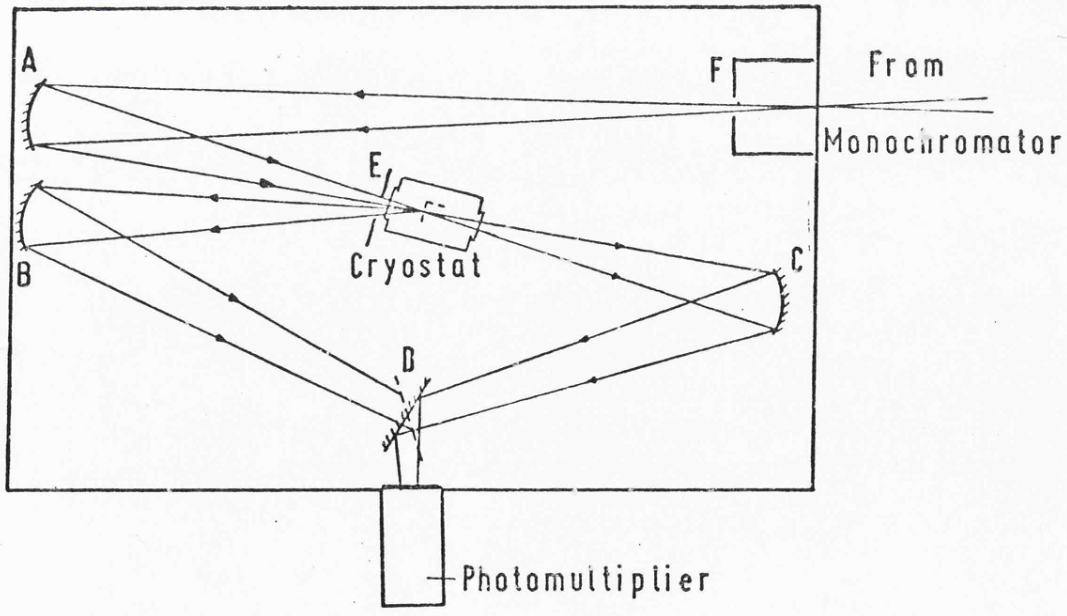

Fig. 3.7 Absorption apparatus

light from a water cooled 150 watt quartz-iodine bulb, which was run slightly below its maximum rated voltage for improved stability and lifetime, was focussed on the entrance slit of a Leiss double-prism monochromator. Before entering the monochromator, the light was mechanically chopped at 800 Hz. A reference signal was supplied by a photocell and light positioned on either side of the chopper.

After passing through the monochromator the light was plane-polarised using a sheet of polaroid, and was then focussed on to the sample by the mirror A of Figure 3.7. The baffle F was introduced to ensure that the mirror A was not overfilled. For absorption measurements a second baffle E just in front of the sample ensured that no light was transmitted round the sides of the plate on which the sample was mounted and the reflectance mirror was blanked off as a further precaution. These measures together reduced stray light to less than one part in 10^5.

The crystal was mounted over a spark eroded hole in a thin brass plate attached to a cold finger within the cryostat. The cold finger was connected to a thin steel rod which extended through a vacuum seal at the top of the cryostat, so that the rod and cold finger could be rotated about a vertical axis. A second plate with an identical hole in it was also attached to the cold finger, at right angles to the plate with the sample on it, so that the transmission through the crystal and the open hole could be compared by rotating the cold finger. For reflectance measurements, a freshly silvered mirror was mounted over the reference hole. Transmitted or reflected light was collected by the mirrors C or B, and it was deflected by a rotating plane mirror D into the photomultiplier. Rotating the mirror D determined whether transmitted or reflected light was detected. The photomultiplier used had an S20 photocathode response.

The signal from the photomultiplier was amplified by a variable

gain type 450 Brookdeal low noise amplifier and connected to the signal channel of a 9412A Brookdeal phase sensitive detector. The reference was taken from the photocell near the mechanical chopper and connected via a type 421 Brookdeal phase shifter to the reference channel of the phase sensitive detector. The magnitude of the signal was displayed on a Phillips 2422A digital voltmeter. The reasons for using a phase sensitive detection system were to eliminate signals due to external sources, which would not be chopped at the required frequency and would therefore not be detected, and also to permit the detection of small signals in the presence of photomultiplier noise and dark current.

The photomultiplier was supplied with 1.1 kV from an Oltronix A25k - 10R power supply which had a stability of .02% per hour. The measured signal, after allowing an hour for the system to stabilise, varied by less than .2% per hour under normal conditions.

3.5.3 Determination of the Absorption Coefficient

The optical absorption coefficient α is defined by:

$$I = I_o \exp(-\alpha d) \tag{3.4}$$

where I and I_o are the transmitted and incident light intensities and d the crystal thickness. When account is taken of multiple reflections within the sample it can be shown that (Kahan (1963)):

$$\frac{I}{I_o} = T = \frac{(1 - R)^2 \exp(-\alpha d)}{1 - R^2 \exp(-2\alpha d)} \tag{3.5}$$

where T is the transmission coefficient and R the bulk reflection coefficient. The measured reflectivity, r, is given by:

$$r = R(1 + T \exp(-\alpha d)) \tag{3.6}$$

Taking these equations together,

$$\alpha = \frac{1}{d} \ln \left[\frac{(A^2 + 4T^2)^{\frac{1}{2}} - A}{2T} \right] \tag{3.7}$$

where $A = T^2 - (1 - r)^2$

To measure α, it is necessary to measure both T and r at a particular wavelength and solve the above equation. The assumption has been made in this calculation that interference effects are negligible. In the present work a simple computer program written by Stroud (1970) was used to perform this calculation.

The absorption and reflection coefficients were measured at intervals of one minute of arc of rotation of the prisms, corresponding to a spacing of about .01 eV between points. More closely spaced measurements were made near sharp structure. The resolution used was normally about .001μ at .6μ, corresponding to a slit width of .1 mm. Measurements were made with .02 mm wide slits on sample 2 at liquid nitrogen temperature to ensure that the observed shape of the absorption edge was not limited by resolution. At this resolution, the problems of noise and stability became more significant and the lower resolution was preferred. The monochromator was calibrated regularly during this work using the known wavelengths of the lines from discharge lamps.

Attempts to measure the amount of stray light present in the absorption measurements (that is, light which was either non-monochromatic or reached the photomultiplier without passing through the sample) showed that it was at or below the noise level. If the sample and baffles were carefully set up, with the monochromator set at a wavelength above the absorption edge of the crystal no reliable measurements of light intensity could be made. This sets an upper limit on the stray light at less than one part in 10^5 which is the level of stray light expected from the monochromator used. No attempt has been made to correct for this rather small error.

A similar problem arises in the polarisation where the absorption coefficient is the greater. If the polaroid is not perfectly aligned with the crystal the small component of light not in the intended polarisation could become significant when the difference between the absorption

coefficients is large. If care was taken in aligning the polaroid with the crystal, this was not thought likely to give rise to large errors, and the close agreement found between the results of different runs supports this.

With the samples available in the present work it was not possible to cut crystals so that the absorption coefficient for E//c could be determined exactly. In $\{112\}$ platelets, the c-axis makes an angle of 36.3° with the crystal, and in $\{101\}$ platelets 27.4°. To eliminate differences due to crystal orientation all the results presented have been corrected for this assuming that (Shubnikov (1960)) the absorption coefficient for light polarised parallel to the projection of c in the plane of the crystal is given by:

$$\alpha_{//}\text{ (measured)} = \sin^2\theta\ \alpha_{//} + \cos^2\theta\ \alpha_{\perp}$$

where θ is the angle between the c-axis and the normal to the platelet, and $\alpha_{//}$, $\alpha_{\perp}$ are the absorption coefficients for light polarised parallel and perpendicular to c. Since $\alpha_{\perp}$ can always be measured for crystals of any orientation, the value of $\alpha_{//}$ can be found from the measured values provided the orientation is known.

The crystals were oriented by a combination of Laue back reflection photographs and the use of a polarising microscope. The Laue photographs gave the crystal orientation to within $\pm 3^{\circ}$ and also the positions of the crystallographic axes. The polarising microscope was then used to distinguish the c-axis since when an extinction is seen when the crystal is rotated between crossed polars, the light is either parallel or perpendicular to the c-axis. The polarising microscope was also used to align the crystal on the sample holder.

3.6 Results

The variation of absorption coefficient in both polarisations as a function of incident photon energy is shown in Figures 3.8 - 3.11 for several samples, in some cases at both room temperature and at

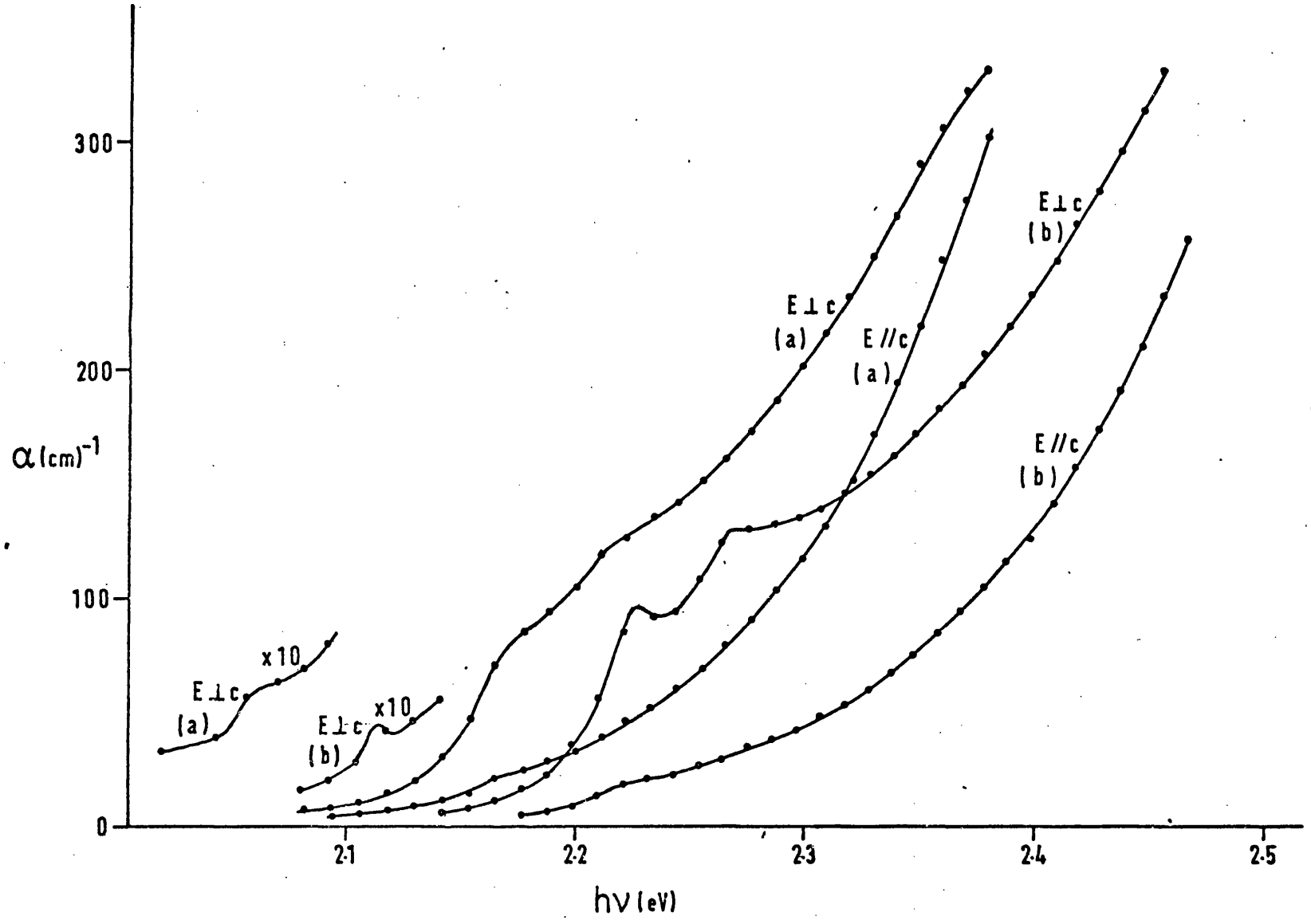

Fig. 3. 8 Absorption edge, sample 2 at (a) 290K, (b) 124K

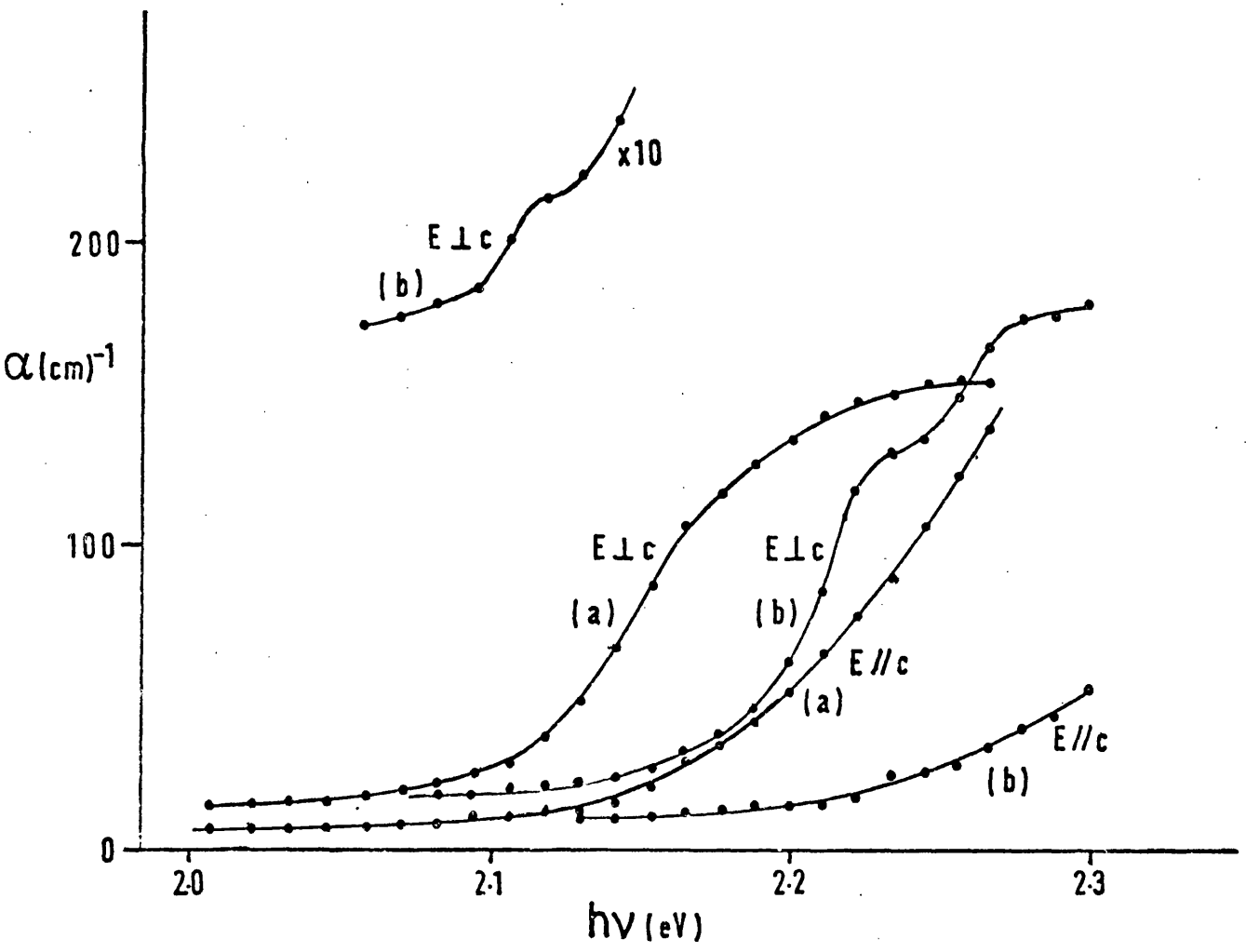

Fig. 3.9 Absorption edge, sample 11 at (a) 290 K (b) 110 K

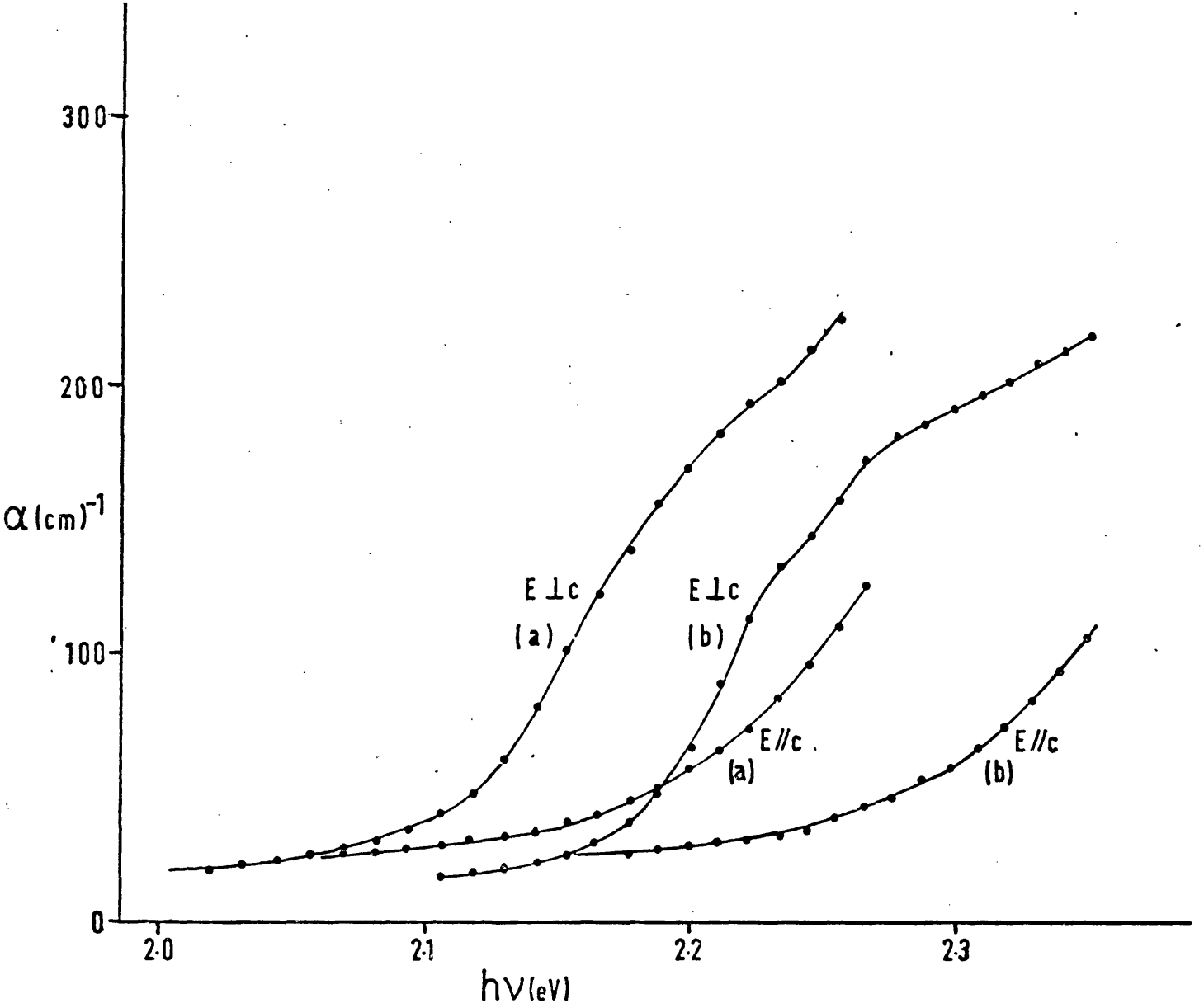

Fig. 3.10 Absorption edge, sample 1 at (a) 290 K, (b) 120 K

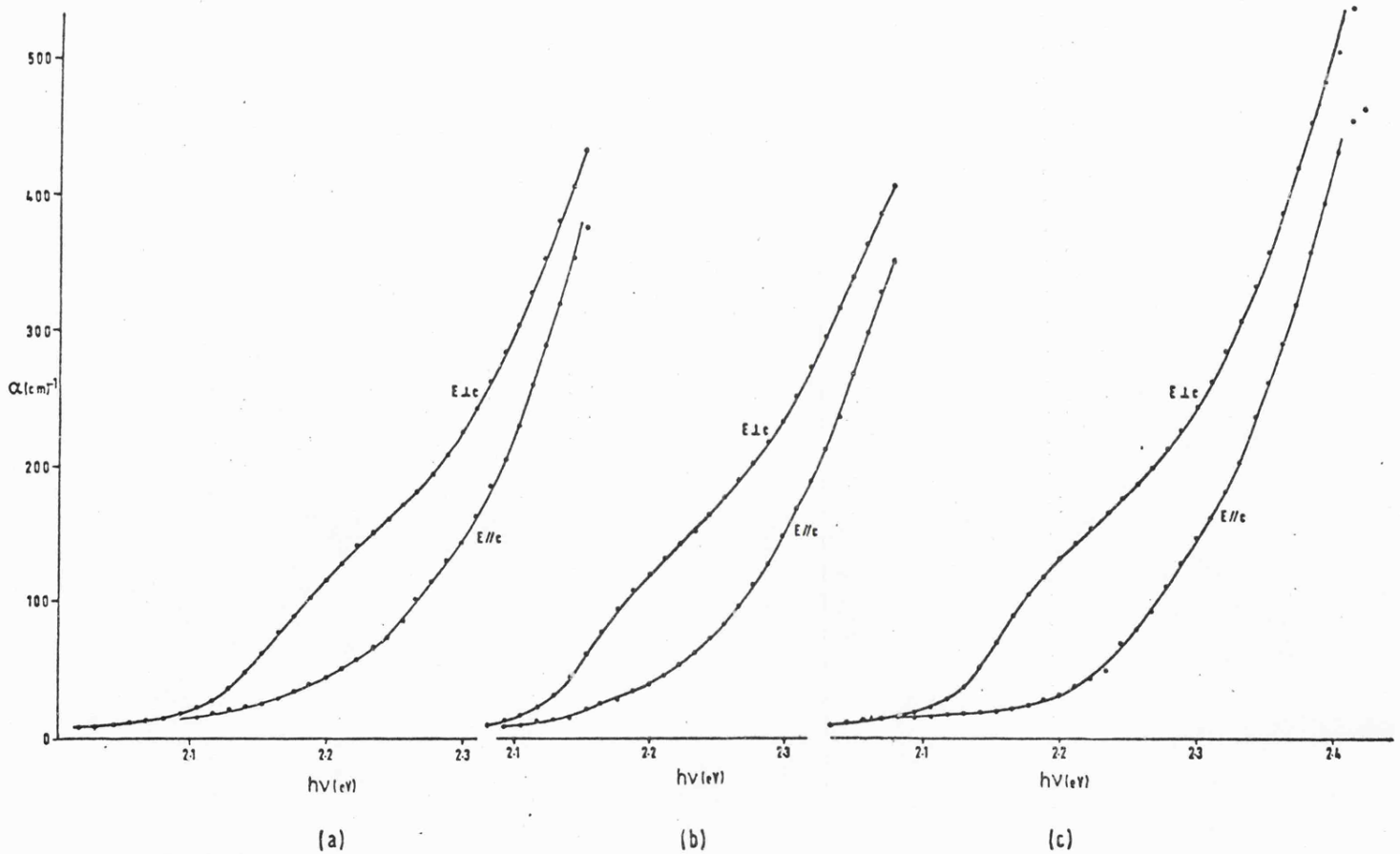

Fig. 3.11 Room temperature absorption results of (a) sample 4, Se doped, first grown; (b) sample 12, Se doped, last grown; (c) sample 17, Ga doped.

liquid nitrogen temperature. The points marked by filled circles on the graphs are representative experimental points to indicate the scatter, although in many cases the lines have been drawn to include other points not shown, especially near singularities in the curves.

The absorption curves are relatively gradual, and show considerable difference in both shape and magnitude depending on polarisation. There is also some structure shown in the E⊥c polarisation which varies considerably in clarity from sample to sample and with temperature. The curve which shows the structure most clearly is Figure 3.8 which refers to sample 2, a 'last grown' crystal, not intentionally doped, from solution in zinc. Curves on an expanded scale are also shown here for the lowest structure. At room temperature this was near 2.06 eV but is so weak (about 2 cm^{-1}) as to make it difficult to determine its strength. This will be discussed in more detail later. Further up the curve for E⊥c two changes of slope can be seen, after which it rises smoothly. In the E//c polarisation there is a suggestion of a change of slope near the middle peak, but it must be remembered that there may well be some component from E⊥c in the E//c measurements, and it is difficult to be certain about this. All this structure becomes considerably sharper at low temperatures.

The selection rules of Figure 3.3 show that the three pseudodirect transitions are allowed for E⊥c and the middle one is allowed for E//c. This is precisely the situation seen here, although whether the transition for E//c has in fact been observed is uncertain. The shape of the curves is characteristic of direct exciton absorption with some broadening. The major difference is that the scale is greatly reduced: in this case the absorption coefficient is near 100 cm^{-1} whereas for an ordinary direct transition, the absorption coefficient above the edge is of the order of 10^4 cm^{-1}.

For $E//c$, and $E \perp c$ at higher photon energies, the continuing smooth rise is not attributable to direct gap absorption, which should be nearly flat as a function of energy for parabolic bands. The smooth rise is also seen to be temperature sensitive, with a shallower slope at low temperatures than at room temperature. This behaviour is characteristic of indirect transitions. Indirect transitions are expected to take place to the $T_1 + T_2$ band which derived from X in GaP and is expected to be at higher energies than the minimum which mapped back to Γ. Indirect transitions are also expected to take place to this minimum. The only reason that indirect transitions are not normally seen associated with a direct gap is that they are normally much weaker.

There are therefore expected to be six indirect transitions from the three valence bands to the two lowest conduction bands which will be relatively closely spaced in energy and each will presumably have several different thresholds corresponding to emission and absorption of different phonons. A plot of $\alpha^{\frac{1}{2}}$ for $E//c$ against energy which should be linear for an indirect transition shows a steadily increasing slope (Figure 3.12). This is qualitatively the behaviour expected, but it is not possible to separate the effects of the individual transitions.

The behaviour of the difference between the absorption coefficients in the two polarisations is interesting. It shows relatively little temperature dependence except for the clarity of the structure and the band edge shift, and may therefore be attributed mainly to pseudodirect transitions. This corresponds to the assumption that the indirect absorption is independent of polarisation. This approach will be used to compare the results with theory. It is somewhat uncertain how good this approximation will be, but in view of the agreement which can be obtained with the theory, it is hoped that the errors are not too serious. Certainly it is a better approximation to the pseudodirect absorption than the absorption in the perpendicular polarisation alone.

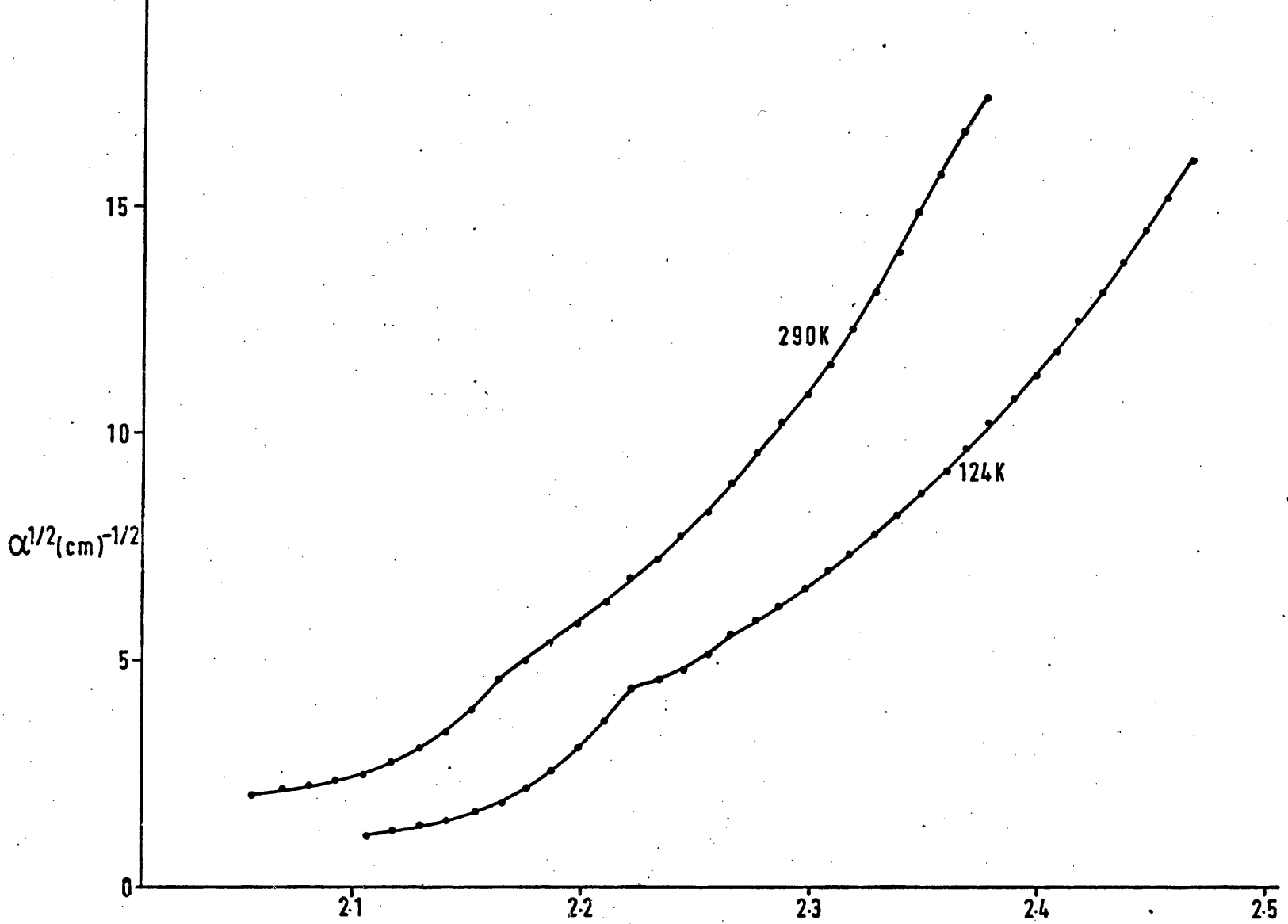

Fig. 3.12 Square root plot of absorption coefficient for E//c.

3.7 Discussion

The eigenfunctions calculated by Hopfield (1960) allow the relative intensities of the pseudodirect transitions from the three valence bands to the conduction band to be calculated. These eigenfunctions are, using Kildal's (1972) notation and sign convention:

$$V_2 \qquad \left|\frac{X + iY}{\sqrt{2}} \uparrow\right\rangle$$

and $$\left|\frac{X - iY}{\sqrt{2}} \downarrow\right\rangle$$

$$V_{1,3} \qquad \left[1 + 2\left(1 + \frac{3E_{1,2}}{2\Delta}\right)^2\right]^{-\frac{1}{2}} \left|\frac{X - iY}{\sqrt{2}} \uparrow\right\rangle + \left[1 + \frac{1}{2\left(1 + \frac{3E_{1,2}}{2\Delta}\right)^2}\right]^{-\frac{1}{2}} |Z \downarrow\rangle$$

and $$\left[1 + 2\left(1 + \frac{3E_{1,2}}{2\Delta}\right)^2\right]^{-\frac{1}{2}} \left|-\frac{X + iY}{\sqrt{2}} \downarrow\right\rangle + \left[1 + \frac{1}{2\left(1 + \frac{3E_{1,2}}{2\Delta}\right)^2}\right]^{-\frac{1}{2}} |Z \uparrow\rangle$$

where Δ is the spin orbit splitting, X, Y, Z are the valence band basis functions and have the symmetry of atomic p-functions, $\uparrow$ and $\downarrow$ refer to spin orientation and $E_{1,2}$ are the energies of the V_1 and V_3 bands relative to V_2.

Light polarised parallel to c interacts only with $|Z\rangle$ and that polarised perpendicular to c with $|X\rangle$ and $|Y\rangle$ (eg. Kittel (1963)) so that:

$$\langle C | p_x | Z\rangle = \langle C | p_z | X\rangle = \langle C | p_z | Y\rangle = 0$$

where C is the conduction band wave function.

The intensity of the V_2 - C transition for E//c is zero in this approximation therefore. Group theory requires that the other two transitions are not allowed for E//c so:

$$\langle C | p_z | Z\rangle = 0 \quad \text{by symmetry.}$$

Setting $$P' = -\frac{i\hbar}{m_o} \langle C | p_x | X\rangle \quad , \tag{3.8}$$

the matrix elements for the three transitions are given by:

$$V_{1,3} - C \qquad -\frac{\hbar^2}{m_o^2} \langle C | p_x | V_{1,3}\rangle^2 = \left[1 + 2\left(1 + \frac{3E_{1,2}}{2\Delta}\right)^2\right]^{-1} P'^2$$

$$V_2 - C \qquad -\frac{\hbar^2}{m_o^2} \langle C | p_x | V_2 \rangle^2 = P'^2$$

and the values of the matrix elements in $ZnSiP_2$ are:

$$V_1 - C \qquad \frac{P'^2}{36}$$

$$V_2 - C \qquad P'^2$$

$$V_3 - C \qquad \frac{P'^2}{1.03}$$

In obtaining these values the spin orbit splitting and E_1, E_2 have been used, which will themselves be obtained by curve fitting using the above intensities. However a good estimate of these values can be made by inspection of the absorption curves and used in curve fitting to give better values so that ultimately a self consistent 'best' set of splittings can be obtained. These are the values used above.

The relationship between the matrix element and the absorption coefficient for an unbroadened exciton is given by (eg. Moss et al. (1973)):

$$\alpha = \frac{2\pi A R^{\frac{1}{2}}}{1 + \exp(-2\pi\gamma)} = \frac{\alpha_o}{1 + \exp(-2\pi\gamma)} \qquad (3.9)$$

where $\gamma = \left(\frac{R}{h\nu - E_g}\right)^{\frac{1}{2}}$ and $A = \frac{1}{2} \frac{2^{5/2} \pi e^2 m_r^{3/2} P'^2}{m_o^2 n \varepsilon_o c h^3 \nu}$

and the factor $\frac{1}{2}$ instead of $\frac{1}{3}$ appears in A because only the degeneracy between $|X\rangle$ and $|Y\rangle$ need be taken into account since $|Z\rangle$ does not mix with the conduction band. R is the ground state exciton binding energy, given on a hydrogenic model by:

$$R = \frac{m_r e^4}{8\varepsilon_o^2 \varepsilon^2 h^2} \qquad (3.10)$$

where m_r is the reduced mass of the electron-hole pair. Provided m_r and hence R is a constant independent of the valence band involved in the transition, the ratios of the absorption coefficients α_o for the three transitions should be the same as the ratios of the matrix elements.

To justify this assumption it is necessary to determine the conduction and valence band effective masses. Poplavnoi (1969) gave values for the conduction band effective masses. The valence band effective masses can be estimated using Kildal's (1972) kp theory, taking the energy of the Γ_1 conduction band as 3.42 eV above the top valence band (Gallay et al. (1975)). In this way we obtain the values shown in Table 3.1. The values for the Γ_1 band are shown for completeness only. The theory is clearly inadequate, since three out of the six hole effective masses are unrealistic or not given. Assuming these are fairly large and assigning them an arbitrary value of the free electron mass, the reduced masses are estimated as .16, .18 and .18 for the three excitons using (Harper and Hilder (1968)):

$$\frac{1}{m_r} = \tfrac{1}{3}\left[\frac{2}{\mu_t} + \frac{1}{\mu_l}\right] \quad , \text{ where } \frac{1}{\mu_{t,l}} = \frac{1}{m_{e\,t,l}} + \frac{1}{m_{h\,t,l}} \tag{3.11}$$

The similarity between the values obtained is due to the dominance of the transverse electron effective mass. Provided the other values are fairly large in comparison, variation in exciton reduced mass will be small, even though the actual values used here are subject to considerable uncertainty.

The theory predicts, therefore, that the lowest energy peak will be weak, while the other two are of nearly equal strength. Equation 3.9 does not give good agreement with experiment because of the broadening of excitons in solids.

Sell and Lawaetz (1971) have published curves for the absorption due to a Wannier exciton broadened by Lorentzians of various widths. A fit using these curves was made to the difference between the absorption coefficients in the two polarisations, on the assumption that this quantity is mainly due to pseudodirect transitions and also that the V_2 - C absorption for E//c is negligible. The lowest energy V_1 - C exciton was neglected in this analysis as being weak.

TABLE 3.1

Effective masses in $ZnSiP_2$ in units of free electron mass

	Γ_1	C	V_1	V_2	V_3
m_t	.151	.18	(- 1.09)	.58	.62
m_l	.146	.9	.23	-	(- 1.2)

Values for C from Poplavnoi et al.(1969)

The remainder from Kildal's (1972) theory

m_t, m_l are transverse and longitudinal masses

The magnitude of the $V_2 - V_3$ splitting (E_2 in equation 3.1), the broadening parameters of the two excitons and the exciton binding energy were adjusted to give a good fit, and α_o was chosen so that theory and experiment agreed on the flat portion of the curve at 2.3 eV. Sell and Lawaetz (1971) only show curves for particular values of broadening parameters and intermediate ones were obtained by interpolation. The theoretical ratio of intensities between the transitions was assumed. The fitting was done by hand and the result is probably not the best possible fit. Nevertheless as can be seen in Figure 3.13 very reasonable agreement with experiment was obtained. The values used were: R = 22 meV, α_o = 49 cm^{-1}, E_2 = .042 eV and broadening parameters of 0.75 and 1.0. The value of R may be compared with that calculated on a hydrogenic model for $m_r = 0.18\ m_o$ and (Holah (1972)) $\varepsilon \doteq 11$ which gives R = 20 meV.

The fall off in the experimental curves at high energies is due to stray light effects and was found in all samples at low values of transmission.

The strength of the V_1 - C transition can be estimated from the theoretical intensity ratios as having α_o = 1.5 cm^{-1}, which is in agreement with experiment so far as it is possible to measure so low an absorption coefficient.

The value of α_o may also be used to estimate the matrix element for pseudodirect transitions by including specifically the value of A in equation 3.9.

$$\alpha_o = \tfrac{1}{2} \frac{2^{3/2}\, e^2\, m_r^{3/2}\, R^{\frac{1}{2}}\, P'^2}{n\, \varepsilon_o\, c\, \hbar^4\, E_g} \qquad (3.12)$$

Substituting R = 22 meV, Eg = 2.252 eV, n = 3.1 (Stroud (1970)), $m_r = .18 m_o$ and α_o = 49 cm^{-1} the matrix element is estimated as:

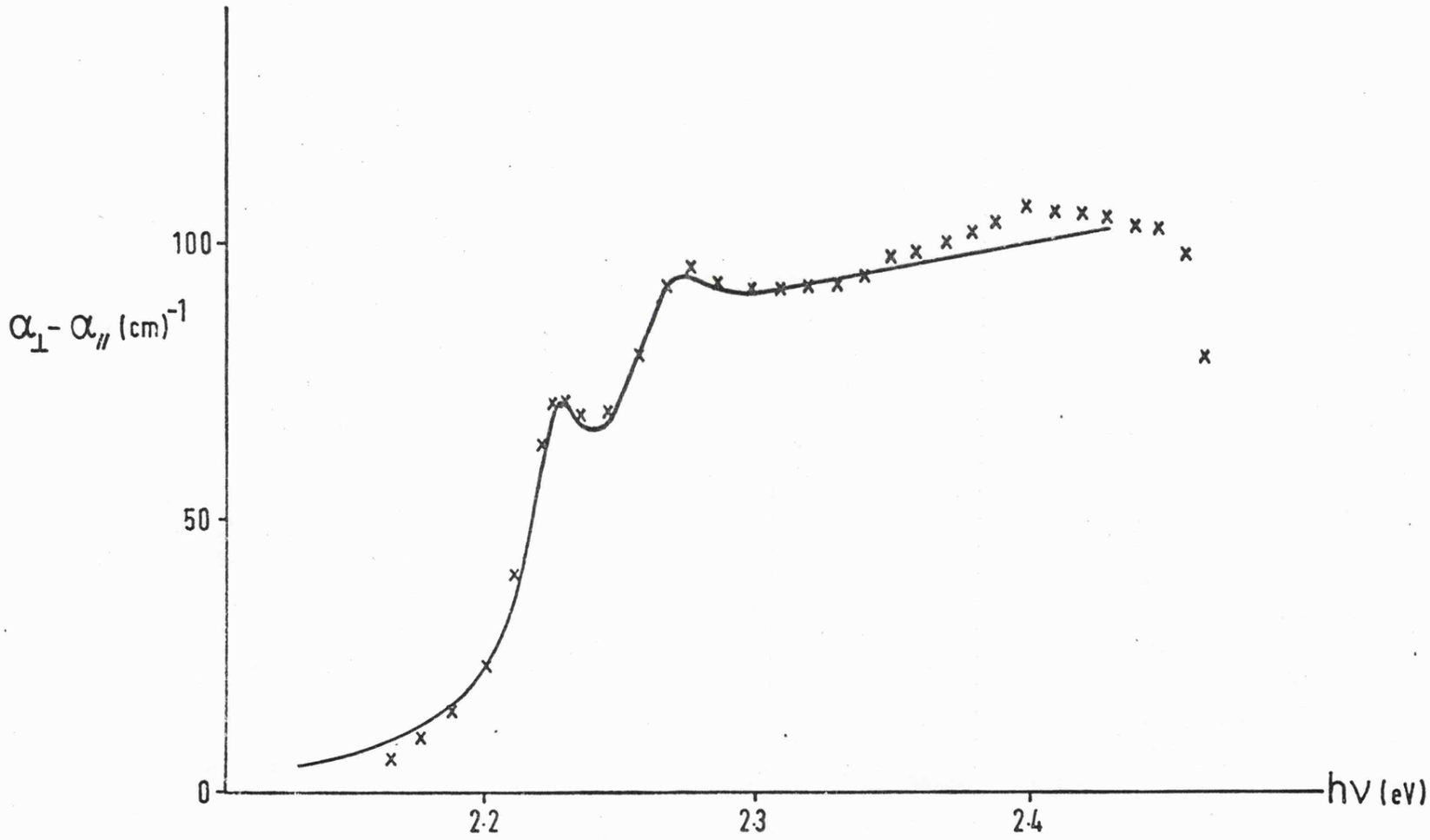

Fig. 3.13 Theoretical fit to the experimental results for sample 2 at 124 K using $\alpha_o = 49\ cm^{-1}$, R = 0·022 eV, broadening parameters 0·75 and 1·0 and theoretical curves from Sell and Lawaetz (1971)

$$P'^2 = \frac{\hbar^2}{m_o^2} \langle C | p_x | X \rangle^2 = \frac{\hbar^2}{m_o^2} \langle C | p_y | Y \rangle^2$$

$$= \frac{\hbar^2}{2m_o} \times 0.015 \text{ eV}$$

The matrix elements for direct transitions in the III V compounds do not vary much from compound to compound and have an average value of (Ehrenreich (1961))

$$P^2 = \frac{\hbar^2}{2m_o} \times 20 \text{ eV} .$$

so that pseudodirect transitions in $ZnSiP_2$ are more than a thousand times weaker than ordinary direct transitions.

Kildal's (1972) k.p theory applied to the II IV V_2 compounds neglects mixing between the lowest conduction band and the valence bands of $ZnSiP_2$. The effect of including this pseudodirect interaction will be to introduce terms into the transverse effective masses of the bottom two valence bands of the order of:

$$\frac{2E_g}{\hbar^2 P'^2} = 150 \, m_o$$

Such terms add as reciprocals, and this is so large as to be totally negligible. The conclusion may be drawn, therefore, that mixing between bands related by pseudodirect matrix elements is so weak as to have negligible effect on the effective masses.

A fit similar to the one performed on the low temperature data was attempted with the room temperature results, as shown in Figure 3.14. Since the structure is so much less well defined, the values of α_o, E_2 and R were not allowed to vary so that the only variable parameters were the band gap and the broadening parameter. A moderate fit was obtained which allowed the temperature dependence of the band gap to be calculated. This was found to be $3.1 \, 10^{-4}$ eV/K, compared to a value

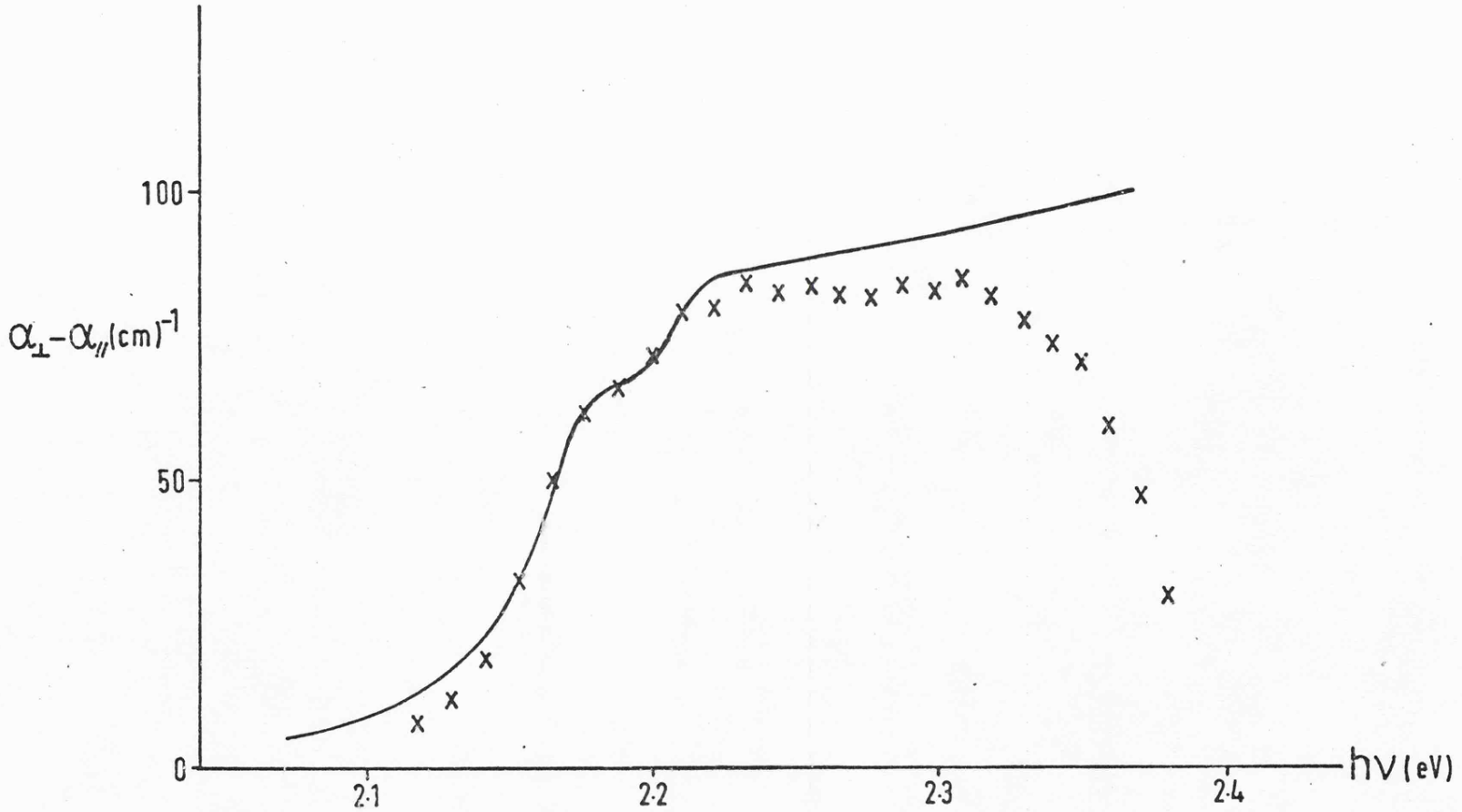

Fig. 3.14 Theoretical fit to the experimental results for sample 2 at room temperature using broadening parameters 1·0 and 1·5

of 3.2 10^{-4} eV/K for GaP over this temperature range (Panish and Casey (1969)).

The energies of the band to band transitions after taking into account the exciton binding energy are shown in Table 3.2. The values are slightly larger than those quoted by other workers because of the exciton binding energy and the way in which it is accounted for. The splittings between the valence bands, however, agree fairly well.

3.8 Valence band splittings in $ZnSiP_2$

From the band gap energies obtained in the previous section the values of E_1 and E_2 can be obtained and the spin-orbit and crystal field splittings calculated from equation 3.1. This gives a spin orbit splitting of .056 eV which is in reasonable agreement with the theoretical value of .07 eV calculated by Hübner and Unger (1972) or .069 eV using Hübner's theory but treating the cations separately with Levine's (1973) ionicities. The theoretical and experimental spin-orbit splittings of the II IV V_2 compounds are compared in Figure 3.15 showing the generally good agreement with theory.

The crystal field splitting is calculated to be - .130 eV. No exact theory exists to estimate this parameter but Shay's (1971) observation of the strong correlation between tetragonal compression and crystal field splitting is borne out for this result, as shown in Figure 3.16. The uncertainty in the deformation potentials of the III V compounds makes more accurate comparison with theory difficult.

The agreement between these experimental results and the trends observed in other II IV V_2 compounds, however, is very good, which is reassuring in view of the doubts cast by the electroreflectance results (Shay (1973)) on the applicability of the quasicubic model to $ZnSiP_2$. It has been shown here to compare well with the experimental results, not only in the valence band splittings but also in the predicted

TABLE 3.2

Band gap energies in $ZnSiP_2$

	Low temperature			Room temperature		
	(a)	(b)	(c)	(a)	(b)	(c)
	124K	77K	80K	290K	300K	300K
V_1 - C	2.136	2.12	2.114	2.082	2.07	2.058
V_2 - C	2.252	2.23	2.226	2.200	2.16	
V_3 - C	2.294	2.27	2.262	2.242	2.21	

a Present work

b Babonas et al. (1974a)

c Gorban et al. (1974)

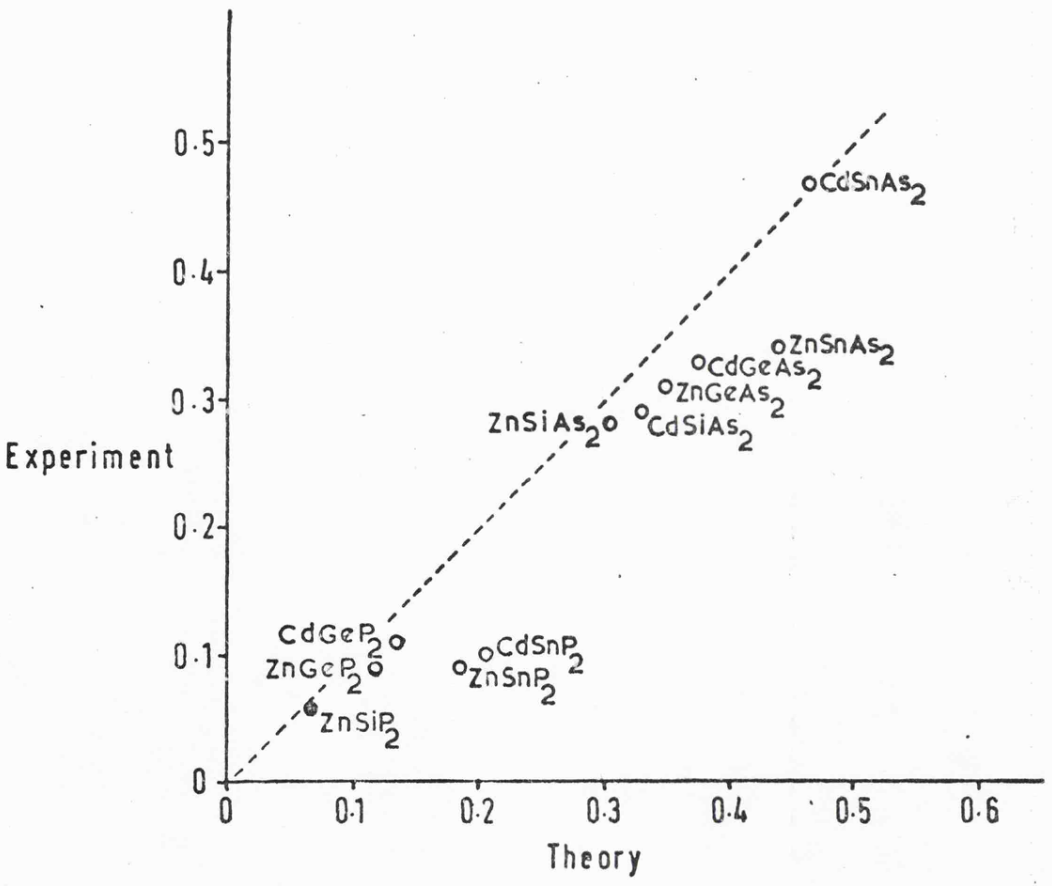

Fig. 3.15 Comparison of theoretical and experimental values of spin-orbit splitting.
Exprimental values (except $ZnSiP_2$) from Shay and Wernick (1975)
Theoretical values calculated using Levine's (1973) ionicities.

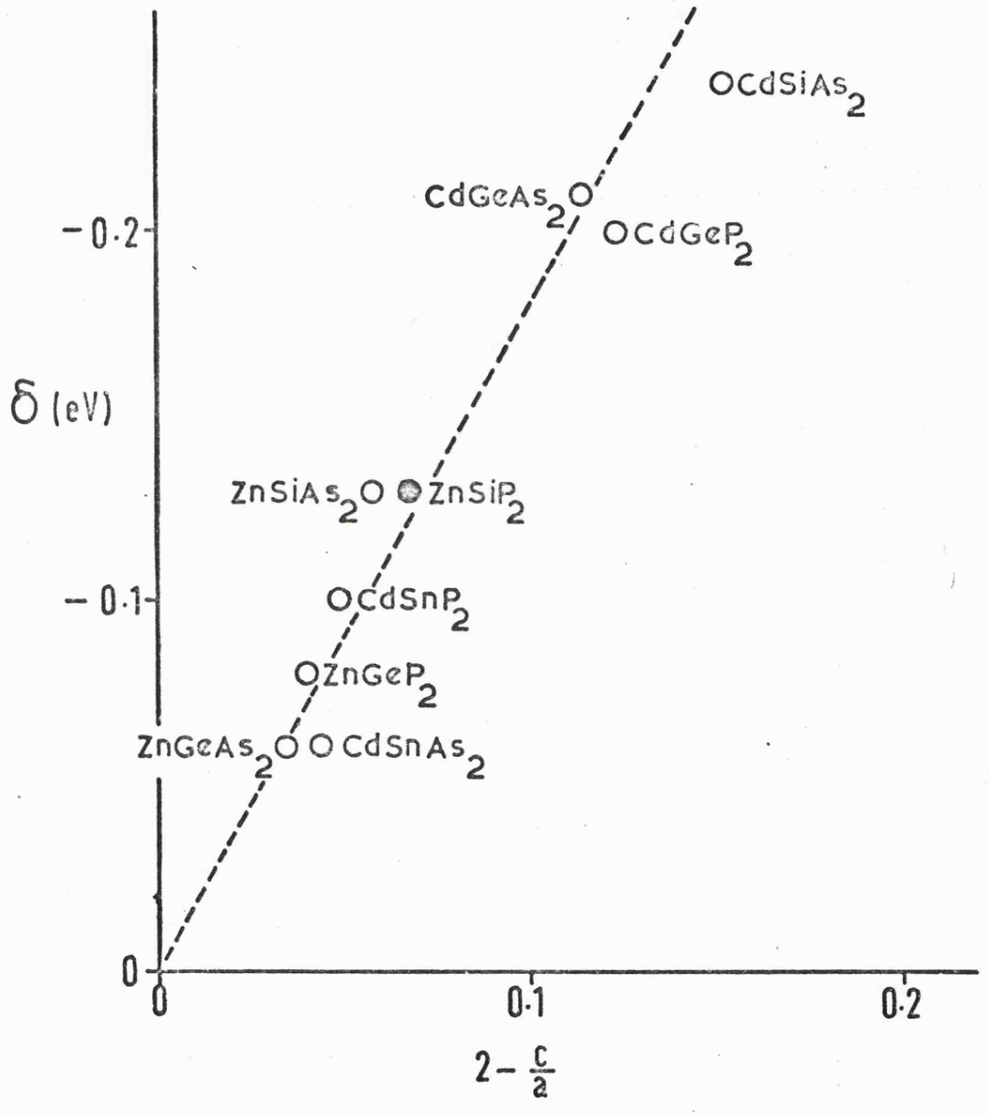

Fig. 3.16 Crystal field splitting vs. tetragonal compression for the $II\,IV\,V_2$ compounds
The broken line corresponds to a deformation potential b=−1·2

oscillator strengths.

3.9 Absorption below the fundamental edge

The transmission of a number of crystals of $ZnSiP_2$ in the infra-red was examined using a commercial spectrophotometer, a Unicam SP 700. A crystal was mounted over a hole in a thin aluminium plate after the 100% transmission level had been set without the crystal. A similar plate with a hole in it was placed in the reference beam throughout these measurements so that the sample and reference beams should be identical with the exception of the presence of the crystal. For polarised measurements a sheet of HR (infra-red transmitting) polaroid was introduced into both beams. Due to the construction of the instrument, it was not possible to perform measurements away from room temperature or to carry out reflectance measurements, so the absorption coefficient could only be estimated.

Some transmission curves are shown in Figure 3.17, plotted as transmission coefficient, so that crystal thickness must be considered in assessing these curves. The slight discontinuities at 15,000 cm^{-1} are artifacts of the system due to changing the detector from a photomultiplier to a lead sulphide detector. The 'cleanest' sample, as in the fundamental absorption measurements, was sample 2, which transmitted between 50 and 60% of the incident light over the entire range below the absorption edge.

Sample 1, a 'first-grown' crystal, shows a long shoulder on the absorption edge to below .1 eV. A band tail like this is characteristic of very impure semi-conductors, and could be due to transitions from the valence band to empty impurity levels in the forbidden gap, or from filled impurity states to the conduction band. The electrical measurements of Chapter 4 show an acceptor activation energy of .77 eV for this sample so that the Fermi level can be fixed somewhere near .7 eV above the valence band. Since, broadly speaking, states below the Fermi level are

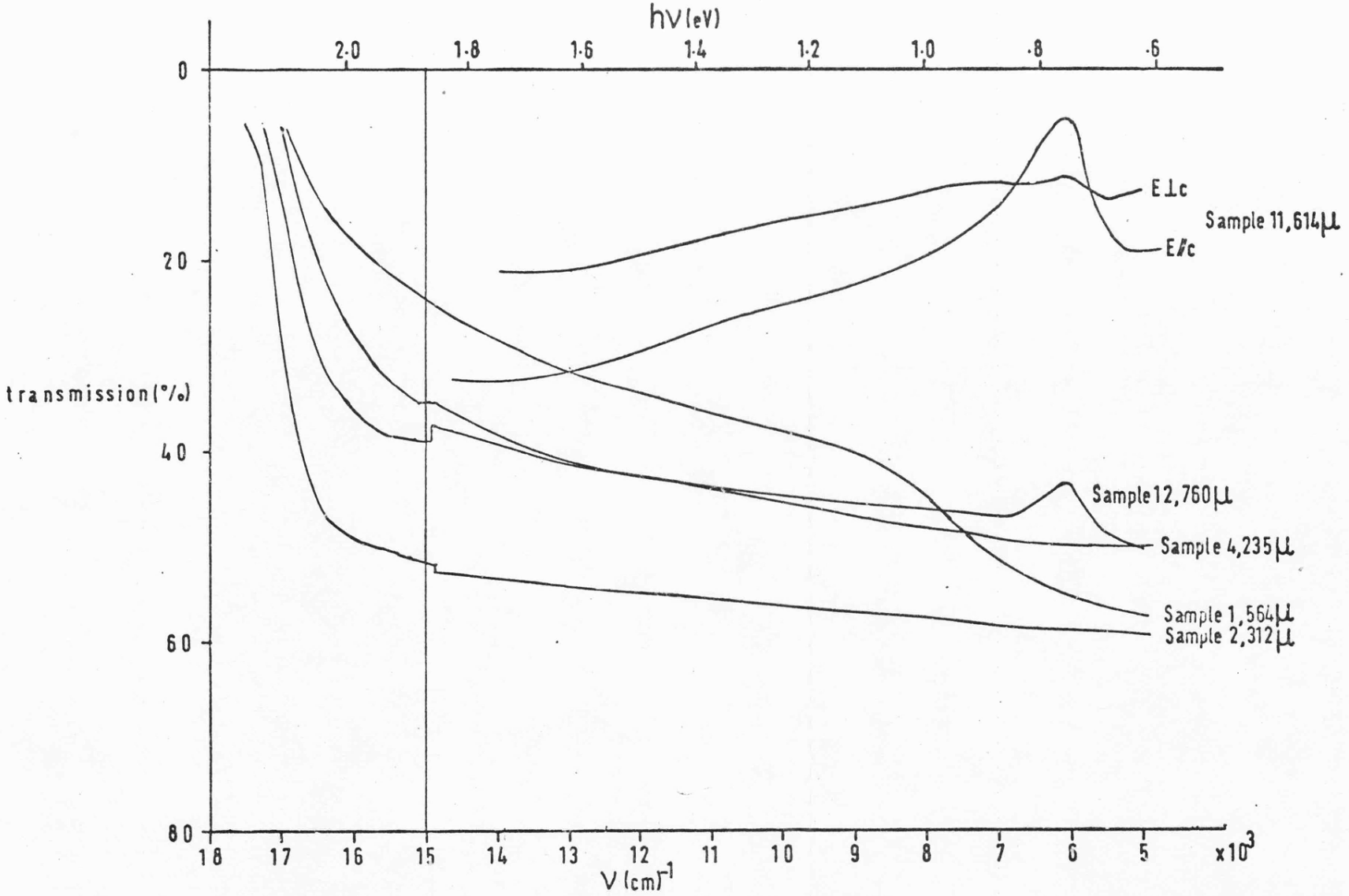

Fig. 3.17 Transmission of several samples of $ZnSiP_2$ in the infra-red.

full and those above it empty, transitions from impurity states to the conduction band are likely down to about 1.2 eV and transitions from the valence band to empty impurity states to about .7 eV. The transparency of this sample below .6 eV is as good as that of sample 2 so it is tempting to identify the major contribution to residual absorption in this sample as due to valence band-impurity transitions. However, sample 4 is also p-type with a similar activation energy and does not show this behaviour. This could be due in part to this sample being rather thin.

Samples 11 and 12 show more interesting behaviour, with a peak just below .8 eV. Such a peak was observed by Mughal (1971) in material grown from Sn solution, which he attributed to excitation from deep impurities to the conduction band, but he found that it was absent in copper doped material ($\sim 10^{6} \Omega$ cm). An approximate calculation reveals that it is improbable that impurity states $\sim$.8 eV below the conduction band are empty at this carrier concentration, which makes this explanation unlikely. In the present work it was found to be absent in sample 2 ($n = 3.10^{15} cm^{-3}$) whereas sample 12 ($n \div 3.10^{16} cm^{-3}$) shows it, as does sample 11, whose carrier concentration was not measured, but should be similar to other tin solution grown material ($\sim 10^{17} cm^{-3}$). It was not seen in any p-type material.

In GaP, Spitzer et al (1959) have reported a similar peak with a maximum at about 2.8 μ or .35 eV. This has been attributed by Allen and Hodby (1963) to transitions from the X_1 conduction band minimum, or shallow donors associated with it, to the X_3 conduction band minimum. More recent work (Abagyan (1971)) shows that at room temperature and above, the peak is due to $X_1 - X_3$ transitions, while at lower temperatures transitions from shallow donors to X_3 become more important.

In the chalcopyrite structure, X_1 and X_3 become Γ_3 and Γ_2. The selection rules show that direct transitions between these bands are allowed for E//c and forbidden for E$\perp$c. This is the polarisation

dependence for the .8 eV peak in $ZnSiP_2$ shown in Figure 3.17 for sample 11 and on a larger scale in Figure 3.18 plotted as absorption coefficient. This was calculated using reflection coefficient measured for this sample below the band edge and assuming that it remains constant in the infrared. This is a rather unsatisfactory procedure but it does permit the correction for crystal orientation to be performed for E//c. The peak is almost entirely absent for $E \perp c$ and the remaining trace shown could be accounted for by misalignment of the polaroid with the crystal.

The shape of the peak is similar to that seen in GaP, showing a fairly sharp edge on the low energy side and an approximately exponential fall on the high energy side. Attempts to detect photoconductivity associated with the peak were unsuccessful, as should be the case for $\Gamma_3 - \Gamma_2$ transitions, but the possibility that the rather crude arrangements made for this measurement were inadequate cannot be excluded.

The peak is considerably narrower than in GaP being about .1 eV wide at half the maximum, whereas that in GaP is about .3 eV wide. A recent theory by Lawaetz (1975) suggests that the greater the $X_1 - X_3$ splitting, the more similar are the effective masses of the two bands. Since the peak for direct $X_1 - X_3$ transitions wouldbe a δ-function if the two bands had identical effective masses, when they would be parallel in k-space, this narrowing of the peak is qualitatively to be expected, since the energy of the peak, and therefore the size of the $\Gamma_3 - \Gamma_2$ splitting is about double the equivalent splitting in GaP. The possibility that shallow donors rather than the Γ_3 band itself are involved cannot be ruled out, however. The observed polarisation dependence should be produced in both cases, since the wave functions of electrons bound to shallow donors could be expanded in terms of the conduction band wave functions, provided the donors are sufficiently shallow.

The magnitude of the $\Gamma_3 - \Gamma_2$ splitting in $ZnSiP_2$ is not easy to predict. According to Van Vechten (1969) the $X_1 - X_3$ splitting in III V

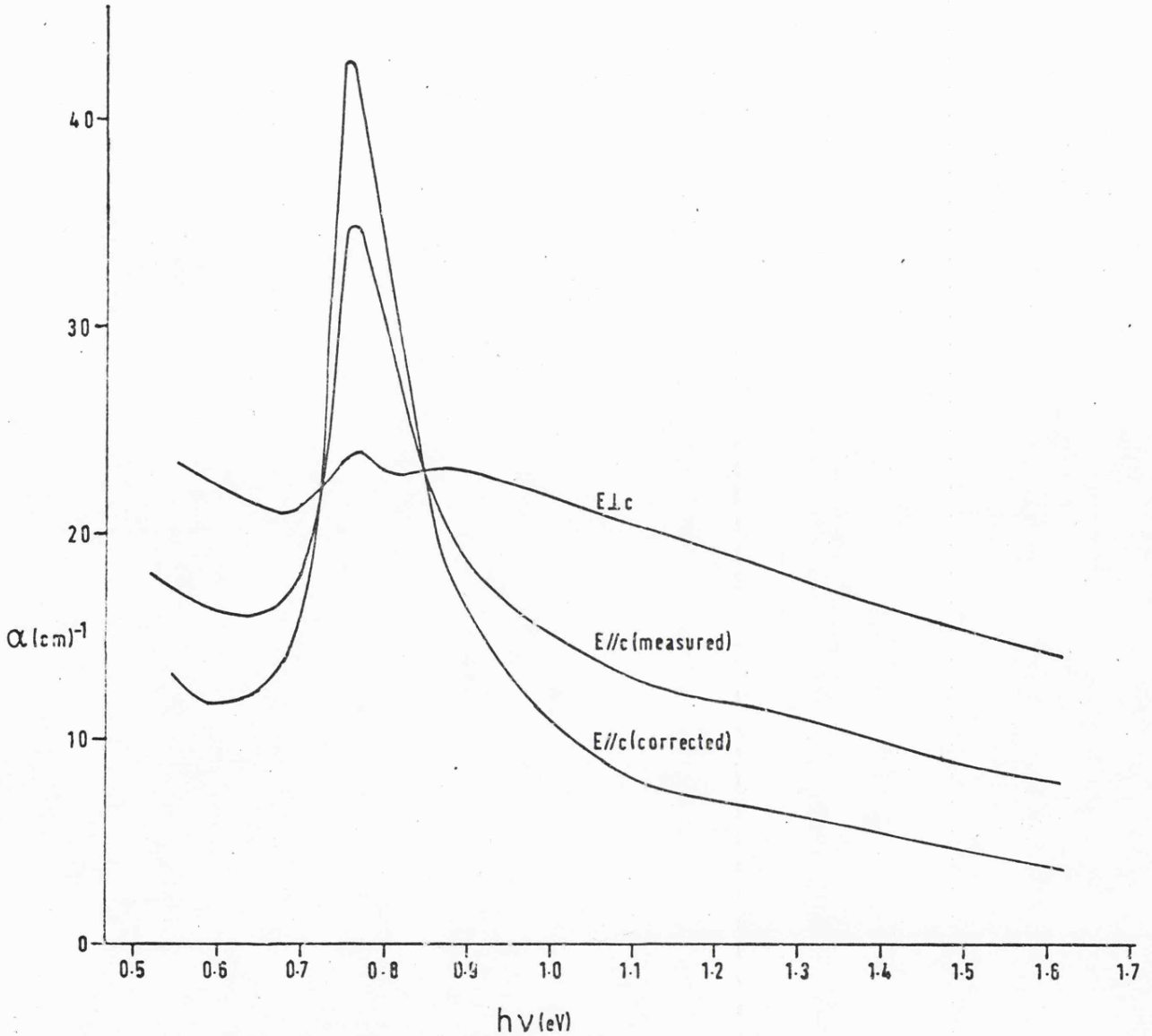

Fig. 3.18 Polarised absorption coefficient of sample 11 in the infra-red.

compounds is proportional to the mean heterapolar band gap. This quantity has two values in $ZnSiP_2$ (Levine (1973)) corresponding to the two types of bond in the chalcopyrite structure, and it is not clear how to treat the splitting in this case. There are, in addition, the various non-cubic potentials which could also change the splitting. Pseudopotential calculations of the $X_1 - X_3$ gap in III V compounds are highly unreliable (Pollack et al (1966)) and no useful comparison between the energy of the peak and theory can be made at present. A tentative identification of the peak with $\Gamma_3 - \Gamma_2$ transitions can be made for the following reasons:

1. The polarisation dependence of the peak obeys the predictions of group theory for this transition;
2. The peak is only seen in low resistivity n-type material;
3. The shape of the peak is similar to that in GaP;
4. No photoconductivity was detected corresponding to the peak in absorption.

If this is the correct assignment the energy of the $\Gamma_3 - \Gamma_2$ splitting can be put at $\sim .7$ eV, which corresponds to the sharp rise on the low energy side of the peak. No peak corresponding to $\Gamma_3 - \Gamma_1$ transitions, (a pseudodirect transition) was detected, but these transitions are forbidden at k = 0 so this is not at all surprising.

Also of interest is the polarisation dependence of the absorption coefficient of sample 11 away from the peak. This may be due to free carrier absorption since the conduction band minimum is highly anisotropic: according to Poplavnoi (1969) $\frac{m_{//}}{m_{\perp}} = 5$, so that the free carrier absorption should be greater for $E \perp c$ than for $E // c$. This interpretation must remain speculative since no low temperature measurements were possible in the infra-red. Measurements of the anisotropy of the infra-red absorption on the rig used for the fundamental absorption measurements showed similar anisotropy at room temperature and at low temperature, so free carrier absorption seems improbable as an explanation. The

residual absorption could be due to band tails caused by the low quality of the Sn solution grown crystals, since the residual absorption of sample 12 (grown from Zn solution) is relatively low. A third possible explanation lies in indirect transitions from the Γ_3 level to other conduction band states. Impurity absorption can also be polarisation dependent.

CHAPTER 4

Electrical Properties of $ZnSiP_2$

4.1 Previous work on the electrical properties of $ZnSiP_2$

The first report in the literature of the electrical properties of $ZnSiP_2$ is that of Vaipolin (1964a) who found mobilities of about 1000 cm^2/Vs and carrier concentrations near 10^{17} cm^{-3} at room temperature. The growth technique was not reported. The results of subsequent workers are summarised in Table 4.1 classified according to growth technique.

The materials grown from Sn solution is fairly consistent, with conductivities near 1 $(ohm\ cm)^{-1}$, electron concentrations between 10^{16} and 10^{17} cm^{-3}, mobilities of the order of 100 cm^2/Vs and donor activation energies rather less than .1 eV. The sole exception is the result of Ray (1971). By contrast zinc solution grown crystals are reported as both high resistivity p-type and low resistivity n-type. Vapour grown material also seems to vary from semi-insulating to fairly low resistivity. Crystals grown from the vapour using iodine as a carrier are usually low resistivity, although high resistivity material grown using I as carrier has also been reported (Shay et al. (1973)).

There is a larger scatter in the donor activation energies in Table 4.1 than can be attributed to experimental error. Most authors seem to have used the compensated approximation, but some may have determined activation energies from plots of R_H vs. $\frac{1}{T}$ rather than $R_H T^{3/2}$, which can make a significant difference to the result. It has been suggested (Siegel and Ziegler (1974)) that the same donor is responsible for the n-type conduction in most $ZnSiP_2$, but that its activation energy decreases as its concentration increases. This has been observed in other semiconductors and seems likely.

Table 4.1 Electrical properties of $ZnSiP_2$ determined by previous workers

(approximate values only)

Reference (first author only)	σ $(\text{ohm cm})^{-1}$	n (cm^{-3})	μ (cm^2/VS)	ε_d (ε_a) (eV)
Sn Solution				
Bychkov (1965)				
Goryunova (1965b)	1 - 3	10^{17}	70 - 100	.08
Springthorpe (1970)	2	$8\ 10^{16}$	150 - 200	.09
Stroud (1970)	1	$6\ 10^{16}$	100	.058
Ray (1971)	10^{-2} - 10^{-4}		100 - 1350	.17
Mughal (1971)	1 - 2	$3 - 5\ 10^{16}$	80 - 210	.047
Siegel (1974)	.4 - 1	$3 - 5\ 10^{16}$	70 - 115	.063 - .071
Zn Solution				
Alekperova (1969b)	$3\ 10^{-2}$	$4\ 10^{17}$	95	
	10^{-6}	p-type		
Ziegler (1973)	$8\ 10^{-10}$	p-type	2 - 6+	(.7)
Siegel (1974)	.1 - 1	$3 - 5\ 10^{16}$	150 - 230	.077 - .092
Vapour transport				
Goryunova (1966)		$5\ 10^{13}$ - $1\ 10^{19}$	80 - 210	
Alekperova (1969b)*	$2\ 10^{-3}$ - $3\ 10^{-2}$	$3\ 10^{15}$ - $5\ 10^{18}$	75 - 90	
Stroud (1970)	.1	$3\ 10^{16}$	21	

+ T = 530 K

* The values of n, σ and μ quoted in this reference appear to be mutually contradictory

All workers agree that $ZnSiP_2$ is naturally n-type, and that attempts to dope it p-type yield high resistivity material, possibly due to a self-compensation mechanism. Only two observations of p-type $ZnSiP_2$ have been reported of which only one (Ziegler et al (1973)) was a detailed investigation. This will be discussed later when the results of the present work are considered.

Data on the effective masses in $ZnSiP_2$ is sparse and probably not very accurate. Goryunova (1965b) concluded from the temperature dependence of photoconductivity that $m_e = .4\ m_o$, and also obtained a value between $.08\ m_o$ and $.13\ m_o$ from the Moss-Burstein shift of the absorption edge (Goryunova (1966)). Mughal (1971) estimated that $m_e = .475\ m_o$ from thermoelectric power data. More recently Siegel and Ziegler (1974) estimated $m_e = .11\ m_o$ from the variation of carrier concentration with temperature in the saturation region.

In some of the early work theoretical values around $.08\ m_o$ are quoted based on Gashimzade's (1963) attempt to apply k.p theory to the chalcopyrites. This is not appropriate to $ZnSiP_2$ as it does not take into account the pseudodirect nature of the band gap.

The best theoretical value is probably that of Poplavnoi et al (1969) who found a transverse mass of $.18\ m_o$ and a longitudinal one of $.9\ m_o$, giving a density of states effective mass of about $.3\ m_o$. This is the value which will be used in calculations in this work.

4.2 Summary of the theory of electrical properties

The theory of electrical properties is well known for many situations, and only the results required will be quoted here. The notation is that of Smith (1959). The equations given apply only to n-type material, but analogous expressions may be obtained in the p-type case.

In an extrinsic non-degenerate n-type semiconductor which contains both donors and acceptors in significant concentrations, the carrier con-

centration, n, is given by:

$$n^2 + (N_a + N_c')n - N_c'(N_d - N_a) = 0 \qquad (4.1)$$

where N_a, N_d are acceptor and donor concentrations, and

$$N_c' = \left(\frac{2\pi m_e kT}{h^2}\right)^{3/2} \exp\left(-\frac{\varepsilon_d}{kT}\right) = \tfrac{1}{2} N_c \exp\left(-\frac{\varepsilon_d}{kT}\right) \qquad (4.2)$$

where ε_d is the donor activation energy.

Equation 4.1 can be simplified if $N_c' \ll N_a < N_d$, when it becomes:

$$n = \frac{N_d - N_a}{2N_a} N_c \exp\left(-\frac{\varepsilon_d}{kT}\right) \qquad (4.3)$$

This is known as the compensated approximation, since it applies when donors and acceptors are present in comparable concentrations. The analogous expression for negligible acceptor concentration is probably not applicable here, but may have been used by Ray (1971), since the activation energy it yields from a given set of results is about double that from equation (4.3).

The position of the Fermi level, E_F, is given by:

$$n = N_c \exp \frac{E_F}{kT} \qquad (4.4)$$

provided the electrons in the conduction band are non-degenerate.

The quantities measured experimentally are Hall constant, R_H, and conductivity, σ . The Hall constant is related to the carrier concentration if only one type contributes by:

$$R_H = \frac{r}{ne} \quad , \qquad (4.5)$$

and r is a number near unity which depends on the scattering mechanism. We shall assume that r = 1.

Since N_c contains a factor $T^{3/2}$, equation 4.3 implies that a plot of $\ln (R_H T^{3/2})$ against 1/T should have a slope of ε_d/k, and an intercept of $\ln\left(\frac{2 N_a}{N_d - N_a} \frac{T^{3/2}}{e N_c}\right)$. The value of the donor activation energy

can be determined reasonably accurately, but the compensation ratio determined from the intercept is subject to considerable uncertainty, both because it is extrapolated and because the effective mass involved in N_c is not definitely known.

The theory described here applies to a simple two band model for an isotropic semiconductor with spherical constant energy surfaces and parabolic bands. In $ZnSiP_2$ the bands are expected to be anisotropic, with a density of states effective mass given by $(m_l\ m_t^2)^{\frac{1}{3}}$, where m_l and m_t are the longitudinal and transverse effective masses. No account could be taken of the probable anisotropy of the conductivity tensor in this work, because crystals large enough to be cut in any desired orientation were not available.

The use of a two band model is probably adequate in the temperature range used in this work. There are (as shown in the previous chapter) subsidiary valence band maxima .12 and .16 eV below the top of the band and a subsidiary conduction band minimum estimated to be about .23 eV above the bottom of the band. All of these might become significant at high temperatures. In particular the curve fitting process used by Siegel and Ziegler (1974) in the saturation region up to 1000 K to find effective masses might lead to erroneous results. Such effects are well known in GaSb and GaAs where the subsidiary minima are .08 eV and .38 eV respectively from the lowest conduction band minima (Madelung (1964)).

The Hall mobility is defined as

$$\mu_H = R_H \sigma$$

and is related to the conductivity mobility by the factor r which appeared in equation 4.5

$$\mu_c = \frac{\mu_H}{r} = \frac{e\tau}{m_e} \qquad 4.6$$

The mobility is limited by the conductivity relaxation time τ which is determined by the scattering process. It is sometimes possible to make statements about the nature of the scattering process by examining the temperature dependence of mobility, although this is only really successful on fairly high quality material. At low temperatures the mobility in impure material often varies as $T^{3/2}$ indicating scattering by ionised impurities (in this context 'impurity' includes all point defects). At higher temperatures scattering by optic phonons, acoustic phonons and space charge regions and intervalley scattering are thought to be the most significant mechanisms. Scattering from neutral impurities, dislocations and other carriers are usually considered negligible.

If the mobility is limited by only one of these mechanisms, it is expected to vary as $T^{-3/2}$ for scattering by acoustic phonons, $T^{-\frac{1}{2}}$ for space charge scattering (Weisberg (1962)) which is due to inhomogeneities in doping or to microscopic precipates, and in more complicated ways for intervalley and optical phonon scattering.

The analysis of Toyama (1968) of the temperature dependence of mobility in GaP suggests that if space-charge scattering were eliminated the room temperature mobility of GaP would be $\sim$180 cm^2/Vs, limited by intrinsic scattering processes. The situation is expected to be similar in $ZnSiP_2$ except that intervalley scattering should not be important, which suggests, all other things being equal, a maximum room temperature mobility of about 500 cm^2/Vs in $ZnSiP_2$. However, the increased number of optic modes at the zone centre which map back from other points in the Brillouin zone could reduce this.

4.3 High resistivity material

When high resistivity samples of a high band gap semiconductor such as $ZnSiP_2$ are encountered, the probability is that the material is compensated rather than extremely pure. Some of the II VI compounds can only be prepared with one electrical type, and are high resistivity if dopants

are added to try to change their type. On the other hand, high resistivity GaAs and GaP can be prepared even though they can be doped both n- and p-type. High resistivity material results if the Fermi level is well separated from both valence and conduction bands.

If a crystal contains N_d shallow donors, N_a shallow acceptors and N_t deep acceptors per unit volume, with $N_d > N_a$ and $N_t > N_d - N_a$, the shallow levels will be fully ionised, and the level which fixes the carrier concentration will be the deep acceptors, so the material will be high resistivity. Such material is high resistivity because of the relative concentrations of doping centres.

In the case of a material with a characteristic type like the II VI compounds the mechanism is though to be rather different. When a shallow acceptor is introduced into a naturally n-type material, a native donor (eg a vacancy) is created nearby. The electron from this donor falls into the acceptor level, liberating an energy $E_g - \varepsilon_a - \varepsilon_d$. If this energy is greater than that required to form the native defect, then this will happen spontaneously, so that all the acceptors whose energy is low enough will be compensated automatically. A self compensation mechanism like this is a possible cause for the characteristic types of some II IV V_2 compounds. The possibility cannot be ruled out at this stage, however, that, in some of the II IV V_2 compounds at least, the high resistivities observed are due to the presence of a deep level in high concentration (O and Cu are possible impurities which are found in many compounds to have deep levels and to appear in fairly high concentrations) which resists attempts to dope the material.

In connection with high resistivity material, it is worthwhile to estimate the intrinsic carrier concentration at various temperatures for comparison with observed values. Assuming that the band gap is 2.08 eV at room temperature and varies with temperature as $-3.1\ 10^{-4}$ eV/K, and that the density of states effective masses are .3 m_o and .6 m_o for

electrons and holes respectively, at 290K $n_i = 5.8\ cm^{-3}$, at 440K $n_i = 2.8\ 10^{7}\ cm^{-3}$ and at 1000 K $n_i = 8.7\ \ 10^{14}\ cm^{-3}$, so that intrinsic electrical properties will probably not be observed.

Averkieva (1973) has observed intrinsic conduction in $ZnSiAs_2$ (E_g (300K) = 1.74 eV, pseudodirect gap) at temperatures above about 1200 K in a system which ensured that the crystal composition did not change. At least this temperature would probably be necessary to observe intrinsic conduction in $ZnSiP_2$.

4.4 Van der Pauw's Technique

Conventional Hall effect measurements have the disadvantage that they require specially shaped crystals. In the present work it was desirable to keep the crystals as large as possible for optical measurements. Van der Pauw (1958) has shwon that electrical measurements can usefully be made on plane-parallel platelets of general shape, provided they are uniform, contain no isolated holes and are thin compared to their diameter. This theory applies for samples with four contacts which are well separated and on the edge of the sample. He showed that under these conditions:

$$\rho = \frac{\pi d}{\ln 2} \left(\frac{R_{AB,\,CD} + R_{BC,\,DA}}{2} \right) f\left(\frac{R_{AB,\,CD}}{R_{BC,\,DA}} \right) \qquad 4.7$$

where f is given by:

$$\frac{R_{AB,\,CD} - R_{BC,\,DA}}{R_{AB,\,CD} + R_{BC,\,DA}} = f \operatorname{arccosh}\left(\tfrac{1}{2} \exp \frac{\ln 2}{f} \right)$$

and $$R_H = \frac{d}{B}\ \Delta R_{BD,\,AC} \qquad 4.8$$

where ρ is the resistivity, d is the thickness of the sample, B the magnetic field and $R_{AB,\,CD}$ is the voltage between contacts C and D divided by the current flowing between contacts A and B, and the contacts are labelled in cyclic order. The function f was obtained from the graph

published by Van der Pauw (1958). There is an implicit assumption in using this method, that is that the conductivity is isotropic. In $ZnSiP_2$ this is not in fact expected to be the case because the electron effective mass is thought to be about five times greater parallel to the c-axis than perpendicular to it (Poplavnoi (1969)). In p-type $ZnSiP_2$ the hole effective masses should have the opposite anisotropy (see section 3.11). This was not investigated in the present work due to the lack of the large size of crystals required to cut specimens of desired orientation. Van der Pauw's technique under these conditions yields some sort of average value appropriate to the crystal orientation. Since the crystals used make nearly the same angle with the c-axis (within about 10^{o}) it is not expected to cause any great discrepancies between one sample and another.

4.5 Experimental Apparatus

Since it was observed in the early stages of this work that some of the crystals of $ZnSiP_2$ had high resistivities, a rig was designed and built which was capable of measuring conductivity and Hall effect for crystal resistances up to about 10^{10} ohms. The basic requirements are:

1. The insulation resistance between any pair of wires must be very much greater than the crystal resistance. Very good insulators are readily available; in this work glass, teflon and alumina were used.

2. For reasonable time constants, the capacitances between the leads must be low. This can be achieved by using thin wires and keeping them well separated and as short as possible.

3. The system must be electrostatically screened rather carefully, and earth loops avoided.

4. A high input impedance meter is needed. A Keithley model 610 C solid state electrometer was used, which had an imput impedance greater than 10^{14} ohms, and also incorporated internal shunt resistances so that

it could be used to measure current directly.

The electrical circuit is shown in Figure 4.1. This circuit supplies a voltage from two Ever-Ready B121 15V batteries (or equivalent) between any pair of contacts on the crystal, selected by the two switches I1 and I2. The voltage across any pair of contacts can then be measured using switches V1 and V2. The current flowing can be determined from the potential drop across a resistance in series with the crystal, although more often in practice the series resistance was switched to open circuit and the electrometer internal resistances used, which were calibrated by the manufacturers before starting measurements . The switches used were Elma type 03 wafer switches, with rated leakage resistance of better than 10^{12} ohms.

The wires labelled 1 and 2 in the diagram were not only used as leads to the crystal, but also in conjunction with the constantan wires $1'$ and $2'$ formed thermocouples directly connected to the crystal. To avoid problems with leakage to earth through the cold junction and increased lead capacitance, a switch was incorporated in the constantan sides of the thermocouples.

Only four copper leads to the crystal are shown in the diagram, although six were in fact built in to allow conventional measurements to be made if required.

The construction of the cryostat is shown somewhat simplified in Fig 4.2. The samples were mounted on a copper cold finger but electrically insulated from it by an alumina sheet. Wires were connected to ohmic contacts on the sample with air drying silver paste, which also held the sample in place. They then passed through a teflon spacer and into glass tubes which ran directly to the box containing the switches. The glass tubes were made vacuum tight by sealing them at the top with silicone rubber.

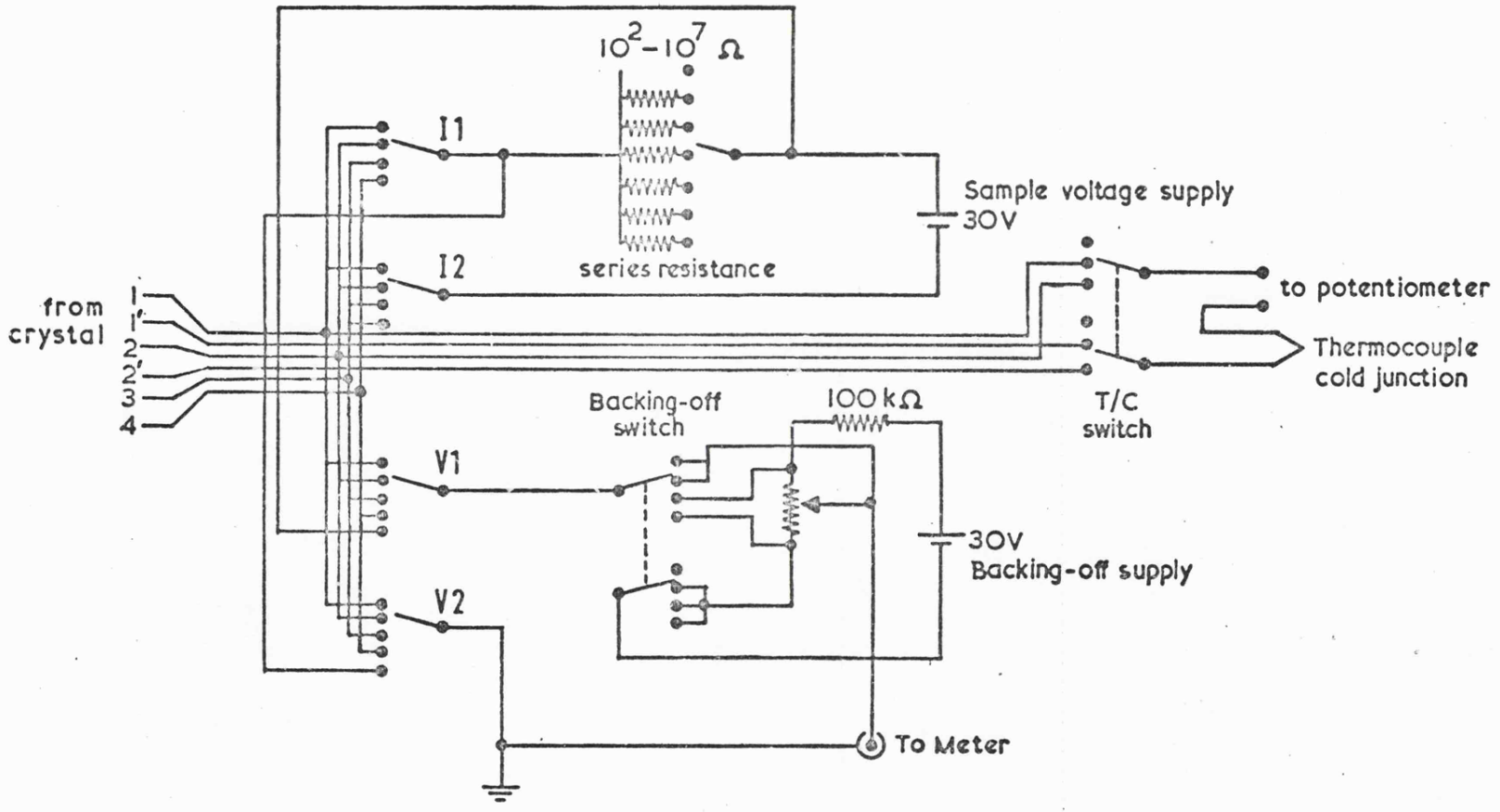

Fig. 4.1 Wiring diagram of Hall effect and conductivity rig

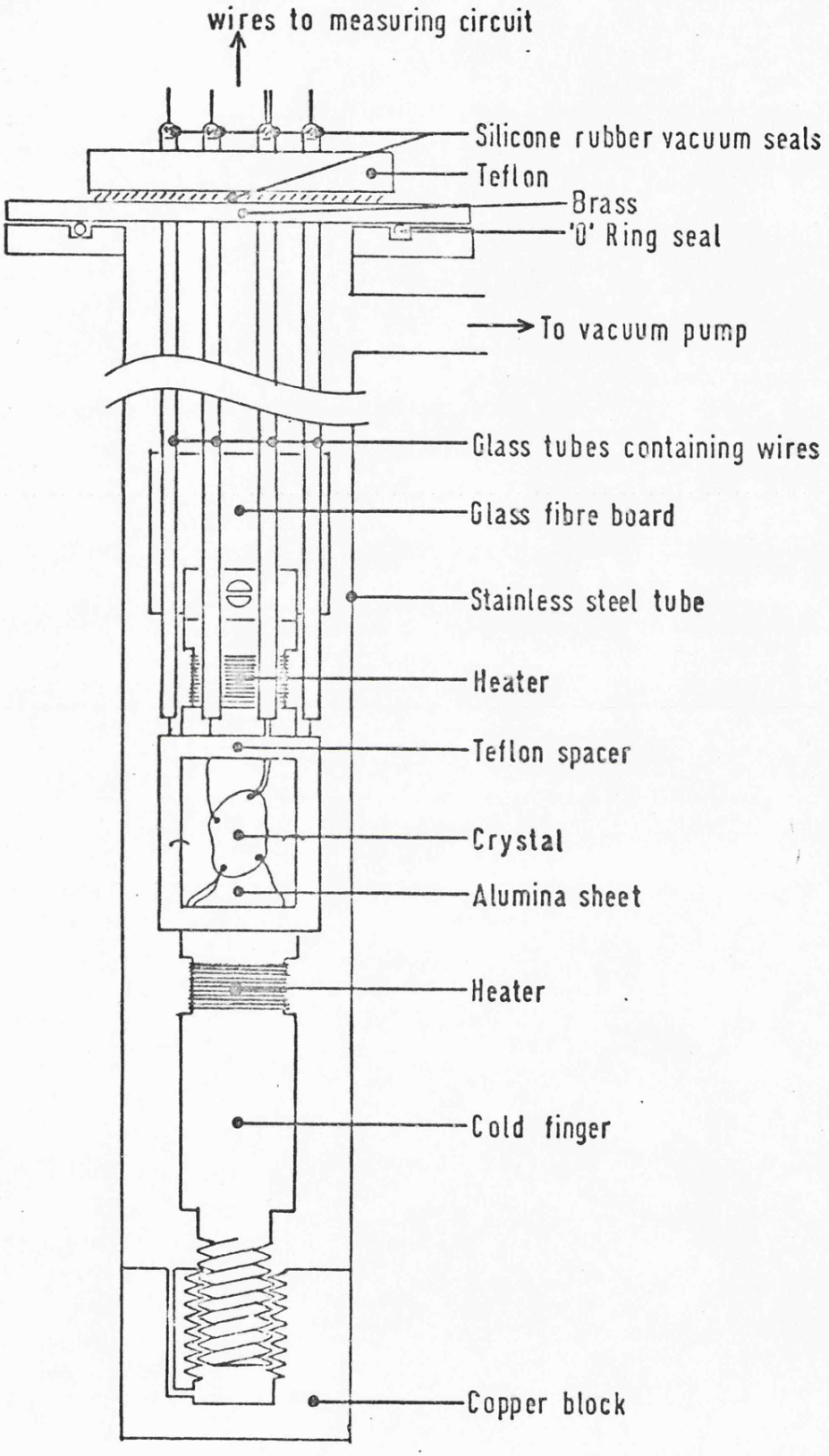

Fig. 4-2 Simplified diagram of Hall effect and conductivity rig
Not to scale

The whole assembly was held together by three lengths of brass studding (not shown in diagram) connecting the glass fibre board which supported the cold finger to the brass plate which formed the vacuum seal at the top. At intervals this studding supported teflon spacers holding the glass tubes in position.

The wires to the heaters and from a control thermocouple were contained in a stainless steel tube which ran down the centre between the glass tubes. This was earthed to screen out any ac which might be superimposed on the dc heater current, either due to poor smoothing or pick-up in the external leads. The heaters were non-inductively wound.

The temperature could be reduced to about 85K by immersing in liquid nitrogen the copper block into which the cold finger was screwed. Temperatures between this and room temperature could be achieved using the heaters on the cold finger. The current through these was controlled by simple feedback system designed by E. F. Lambson which compared the output of a thermocouple in contact with the cold finger with a voltage preset on a ten-turn potentiometer, and gave a current proportional to the difference. The crystal took about ten minutes to reach a steady temperature. Above room temperature the liquid nitrogen was removed.

With this system the leakage resistance was greater than 10^{12} ohms, although under damp conditions it was necessary to introduce some silica gel into the box containing the switches to remove moisture. The limiting factor on the highest resistance that could be measured was the time constant determined by the lead capacitances.

Hall effect measurements were performed by moving a Newport type A water cooled electromagnet, with a type C 154 power supply, so that the sample was between the pole pieces. These were not tapered (which gives improved field uniformity at the expense of some field strength) and the spacing was 3.2 cm. With a magnet current of 10A a field of 0.9 T was obtained, measured with a Scientifica Hall probe calibrated against a

standard permanent magnet. Measurements were performed by backing off the standing voltage between the appropriate pair of contacts using the supply built in to the system (see Fig 4.1) and rotating the magnet through 180^{o} between a maximum and minimum to measure the voltage change, which is twice the Hall voltage. Both noise and drift can cause trouble in these rather sensitive measurements, and in some cases it was necessary to smooth the output from the electrometer with an R - C circuit and record the change on a chart recorder, so that repeated measurements could be made and the effects of drift eliminated.

Measurements of both Hall effect and conductivity were made using all possible configurations of contacts in both polarities to eliminate the effects of temperature gradients and sample non-uniformity.

The samples were lapped and polished as for the optical measurements and then etched in hot 5 HNO_3: 1 HCl with a few drops of HF for about a minute. This produces a surface which is easily wetted by molten metal. Sn contacts were attached to the sample with a soldering iron using hydrazine hydrochloride flux as recommended by Alekperova (1970). These contacts were made ohmic with a 200 V pulse applied between the contact and the underside of the crystal just below the contact. The high resistivity material was heated to ~200 C to lower the crystal resistance so that breakdown took place. The voltage pulse had to be repeated several times in some cases until ohmic contacts were achieved.

4.6 Results

The electrical conductivity and Hall constant were measured for seven samples over a range of temperatures between 470 K, determined by the melting point of solder and the crystal contacts, and about 85 K. Measurements could be performed on high resistivity crystals only above room temperature. Four of the samples (two 'last grown' from Zn and two from Sn) were found to be fairly low resistivity n-type, and the other three ('first grown' crystals from Zn) were high resistivity p-type.

The results obtained are summarised in Table 4.2. The electron and hole effective masses were assumed to be .3 m_o and .6 m_o respectively in calculating the compensation ratios and Fermi energies.

4.6.1 N-type material

The two crystals grown from Sn solution have very similar properties (Fig 4.3) both to each other and to the published results of other workers summarised in Table 4.1. The measurements on sample 9 were performed with conventional six contact Hall effect geometry, rather than by Van der Pauw's technique. Sample 10 had a slightly higher activation energy than sample 9, and a second impurity level became significant at low temperatures. The activation energies of .066 and .068 eV are in good agreement with those published.

The two n-type crystals grown from Zn solution differ considerably (Fig 4.4). Sample 12 was nominally Se doped, and sample 2 was not intentionally doped. Sample 2 shows similar characteristics to the results reported by Siegel and Ziegler (1974) with a donor energy of .092 eV which is comparable to the highest they found, indicating low donor and acceptor concentrations according to their analysis. Sample 12, on the other hand, had an activation energy of only .042 eV, determined from equation 4.1 rather than 4.3 and using a curve fitting process similar to Siegel and Ziegler (1974) only performed by hand. The data could be fitted equally well in this temperature range using an effective mass of .3 m_o as with .1 m_o, with a donor energy of .042 eV. The curve drawn on the graph applies to both fits for the parameters shown. According to Siegel and Ziegler (1974), at a concentration of $5.7\ 10^{17}$ cm^{-3}, the donor which is normally responsible for electrical conduction in $ZnSiP_2$ is expected to have ε_d = .074 eV. The value of .042 eV found here suggests that this is a different donor, presumably Se. This value may be compared to the binding energy expected of a hydrogenic impurity in $ZnSiP_2$, which is .034 eV if m_e = .3 m_o and ε = 11.

TABLE 4.2 Electrical properties of $ZnSiP_2$ samples

n-type material at 290K

Sample No	Solvent	Dopant	σ $(\text{ohm cm})^{-1}$	n (cm^{-3})	μ_n cm^2/Vs	ε_d (eV)	E_F (eV)	$\frac{N_d}{N_a}$
2	Zn	-	$5\ 10^{-2}$	$3.1\ 10^{15}$	135	.092	- .18	1.06
12	Zn	Se	$2\ 10^{-1}$	$2.8\ 10^{16}$	48	.042	- .12	1.09
9	Sn	-	2.2	$8.0\ 10^{16}$	160	.066	- .10	1.64
10	Sn	-	1.6	$8.2\ 10^{16}$	126	.068	- .10	1.53

p-type material at 370K

Sample No	Solvent	Dopant	σ	p	μ_p	ε_a	$E_F + E_g$	$\frac{N_a}{N_d}$
1	Zn	-	$8.2\ 10^{-8}$	$4\ 10^{9}$	22	.77	.70	15
3	Zn	Ga	$6.4\ 10^{-7}$	$2\ 10^{10}$	15	.75	.65	34
4	Zn	Se	$6.0\ 10^{8}$	$6.3\ 10^{9}$	5	.70	.69	4.4

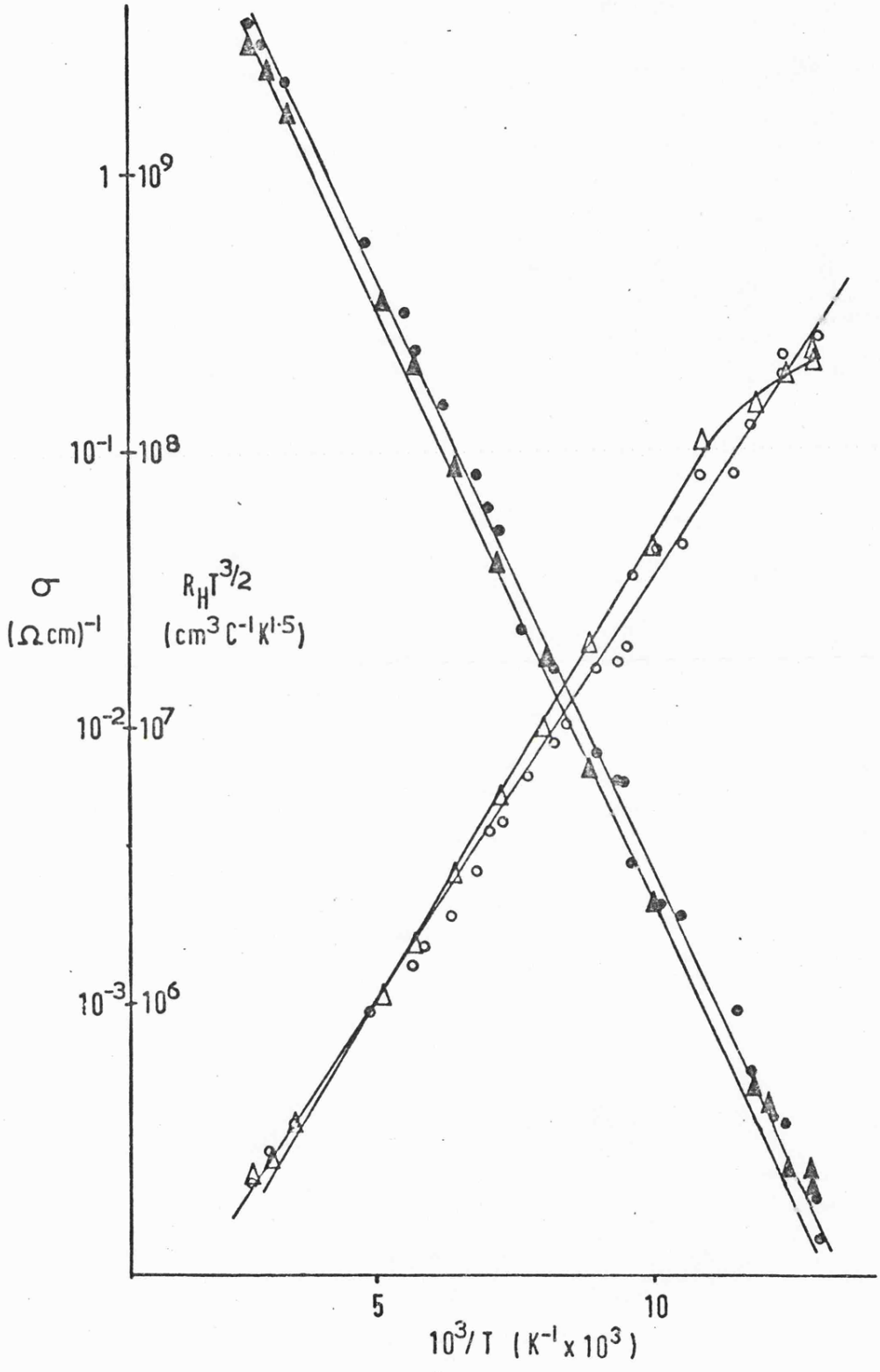

Fig. 4.3 Logarithmic plots of $R_H T^{3/2}$ and σ for n-type samples grown from Sn solution.
○, ● sample 9; Δ, ▲ sample 10: both undoped.

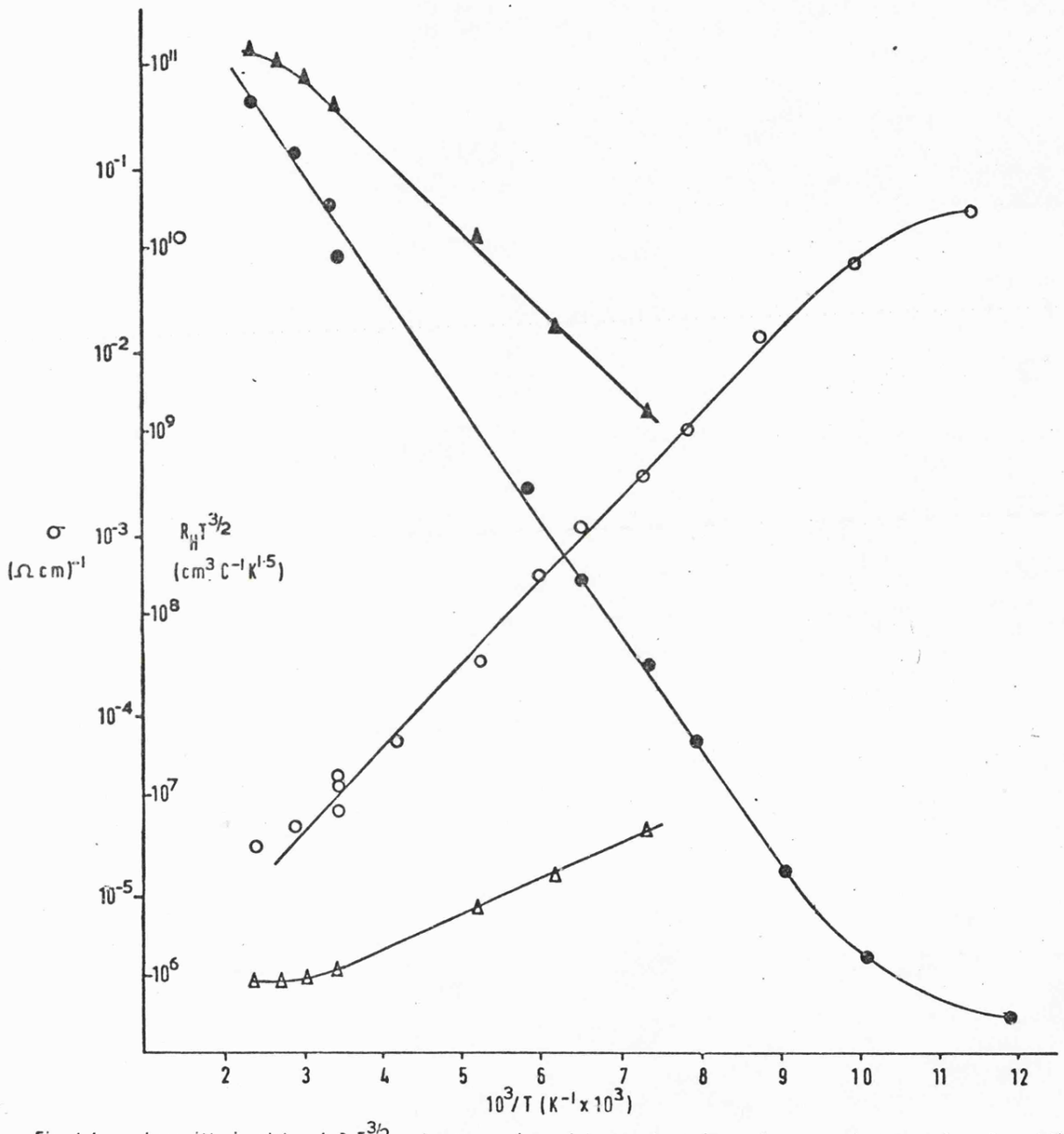

Fig. 4.4 Logarithmic plots of $R_H T^{3/2}$ and σ vs reciprocal temperature for n-type samples grow from Zn solution. ○,● sample 2, undoped; △,▲ sample 12, Se doped. The line drawn for sample 12 is a fit obtained for $N_a = 2.10^{18}\ cm^{-3}$, $N_d - N_a = 1.74.10^{17}\ cm^{-3}$ if $m^* = 0.3\,m_0$ and $N_a = 3.8.10^{17} cm^{-3}$, $N_d - N_a = 1.88.10^{17} cm^{-3}$ if $m^* = 0.1\,m_0$

The zinc grown material is rather more closely compensated than the Sn grown, although the actual magnitudes of the compensation ratios are uncertain due to the possibly large errors in the effective mass.

The mobilities of the n-type samples as functions of temperature are shown in Fig 4.5. All increase from low temperature approximately as $T^{3/2}$, although there is considerably latitude in this due to scatter of points. This is the result of plotting the slowly varying product of two quickly varying quantities so that any fluctuation in temperature has a large effect on the result. If the increase with temperature of these mobilities is due to the decreasing effect of ionised impurity scattering, then sample 2 has about double the ionised impurity content of samples 9 and 10 and sample 12 about seven times it. At high temperatures, the mobility of electrons in Sn solution grown material seems to decline slightly, while that of Zn grown material remains roughly constant. The results for Sn grown samples are in agreement with those of other workers quoted in Table 4.1, but the Zn grown results do not seem very similar to those of Siegel and Ziegler (1974), who found more or less constant mobilities at low temperature, which declined at high temperature. The mobility in the Se doped sample is considerably lower than in the others, as might be expected as a result of the increase in the number of scattering centres due to doping.

The room temperature Hall mobilities of electrons observed here and by other workers are comparable with the largest values observed for GaP, suggesting that the maximum mobility is considerably higher. The amount of ionised impurity scattering at low temperatures gives an indication of the room which still exists for improvement in crystal quality. Whether the values greater than 1000 cm^2/Vs measured by Vaipolin (1964a) and Ray (1971) were in error or whether they represent good crystals of quality which have not been grown elsewhere is uncertain. It is possible that their orientation was different from the (101) or (112) slices

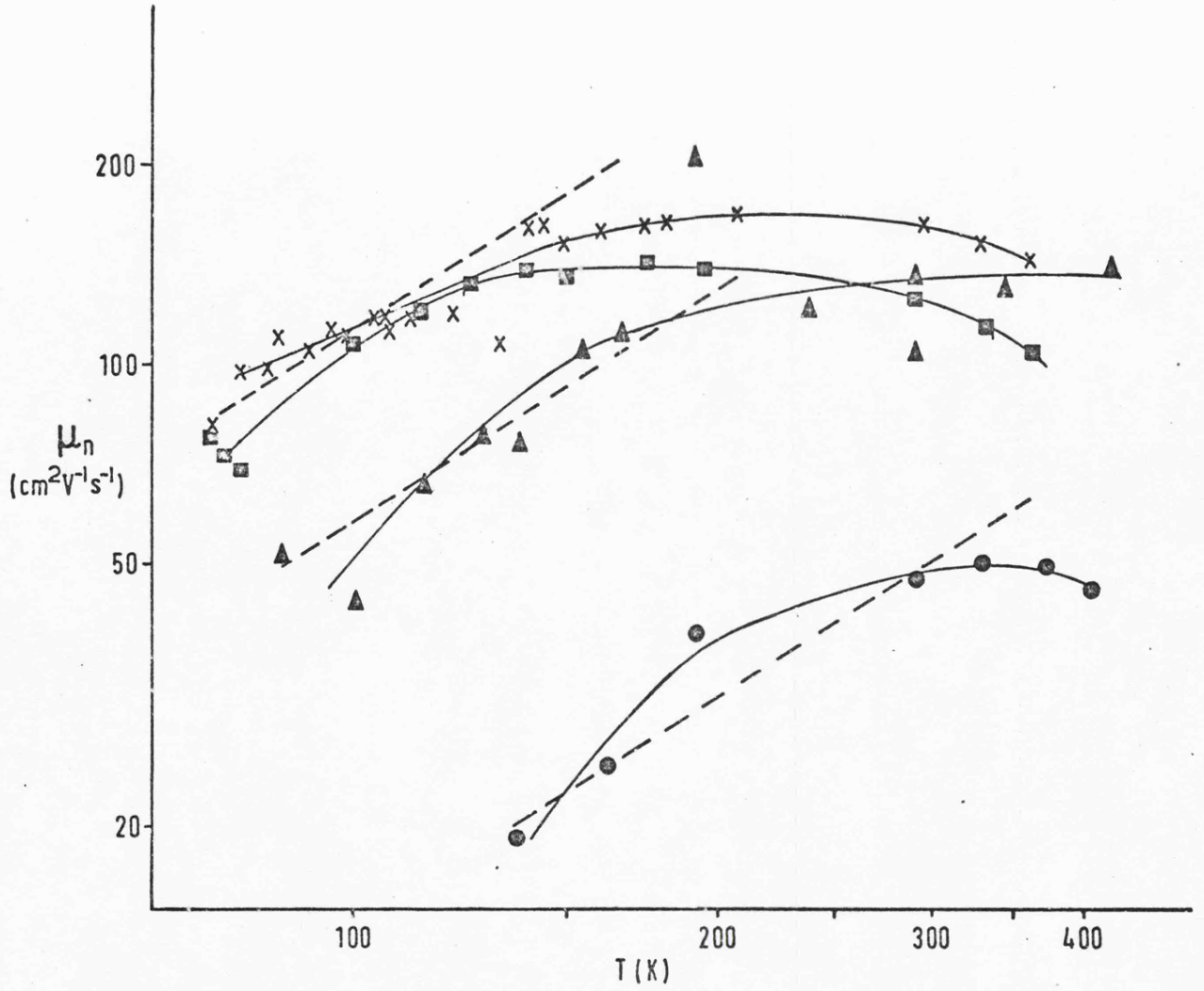

Fig. 4.5 Log-log plot of the Hall mobility of electrons as a function of temperature
● sample 12, Se doped; ▲ sample 2, undoped; x, ■ samples 9 and 10, both undoped and grown from Sn solution
The dotted lines correspond to a slope of $T^{3/2}$ for comparison.
The full lines are smooth curves drawn through the experimental points for clarity.

normally used and that the conductivity was measured in a direction of low effective mass.

4.6.2 P-type material

The temperature dependence of conductivity and Hall constant of the three p-type crystals examined are shown in Fig 4.6 over a relatively narrow range of temperature above room temperature. Measurements could not be performed outside this range because the crystal resistance became too large.

It is clear from the similarity in the slopes of the curves that the activation energies are very similar. Carrier concentrations vary from 7 10^{7} cm^{-3} (sample 1, 320 K) to 1.2 10^{12} cm^{-3} (sample 3, 440 K). These are much greater than the intrinsic concentrations calculated for these temperatures. The impurity activation energies were found to be near .75 eV. Presumably all shallow donors and acceptors are compensated. If, as is likely, there is a self compensation process involved, this implies that the energy required to create the compensating donors is greater than about 1.4 eV since the .75 eV acceptors are relatively uncompensated.

The effects of doping on these samples are not very clear, although the Se doped is more closely compensated than the undoped crystal, and the Ga doped the least compensated, which is as would be expected if Ga and Se are acting as acceptors and donors respectively and the other dopant concentrations are fixed, although if the mechanism is one of self compensation, the compensation ratio should be relatively unaffected by doping. However, it is impossible on the evidence available to be certain whether the differences in compensation are due to 'random' variations between samples, or whether they are really caused by doping, and it would require measurements on a large number of crystals to determine this. The difference between the compensation ratios of samples 1 and 4 is within the limits of experimental error.

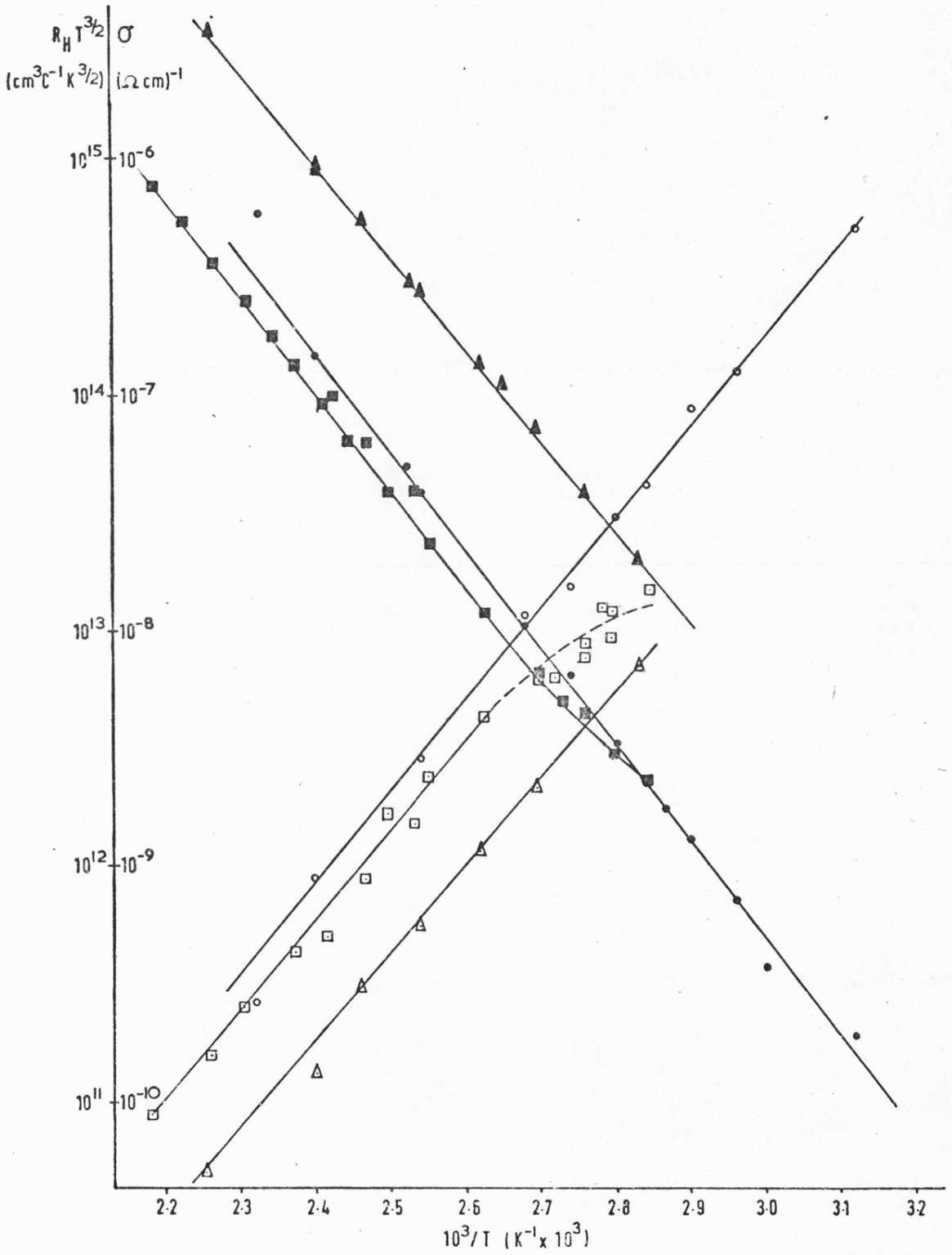

Fig. 4.6 Logarithmic plots of $R_H T^{3/2}$ and σ vs. reciprocal temperature for high resistivity p-type samples.
●, ○ sample 1, undoped; ▲, △ sample 3, Ba doped; ▣, □ sample 4, Se doped.
Filled in symbols refer to conductivity and open ones to Hall constant

The temperature range for these measurements is so narrow that it is difficult to determine the trend in mobility, as shown in Fig 4.7. It would appear, however, that the mobility of sample 3 declines with increasing temperature rather less fast than $T^{-3/2}$, and that of sample 4 increases with temperature, and that of sample 1 is roughly constant. Ziegler et al (1973) have reported the results of similar measurements at rather higher temperatures, which show mobilities varying as $T^{-3/2}$. Their highest value extrapolated to 400K was a mobility of 12 cm^2/Vs and most were considerably lower. The higher mobilities found here may indicate an improvement in crystal quality due to the use of accelerated crucible rotation in crystal growth.

The possibility that the conduction seen here is due to leakage through a thin surface layer should be considered. In the present work the Hall constants of the samples were observed to vary with a constant activation energy over three orders of magnitude. The good agreement with the results of Ziegler et al, (1973) indicates that with a sufficiently wide temperature range this wouldbe maintained over about eight orders of magnitude. For small surface layer thicknesses ($\sim 1\ \mu$) the carrier concentration in the surface layer would have to vary up to about $10^{19} - 10^{20}\ cm^{-3}$ to account for Ziegler's results. It seems unlikely that a consistent activation energy would be maintained over this range. This is at least an indication that true bulk conduction is being observed.

The transmission spectrum of sample 1 in the infra-red also agrees qualitatively with this being the case. As shown in Fig 3.17 it shows good transparency for photon energies less than about .7 eV, which is about the same magnitude as the separation between the Fermi level and the valence band. Above this energy transitions from the valence band to empty impurity states become possible, and the absorption increases. Sample 4 would also be expected to show this behaviour. The relatively flat spectrum in this case may show that other losses are dominating the

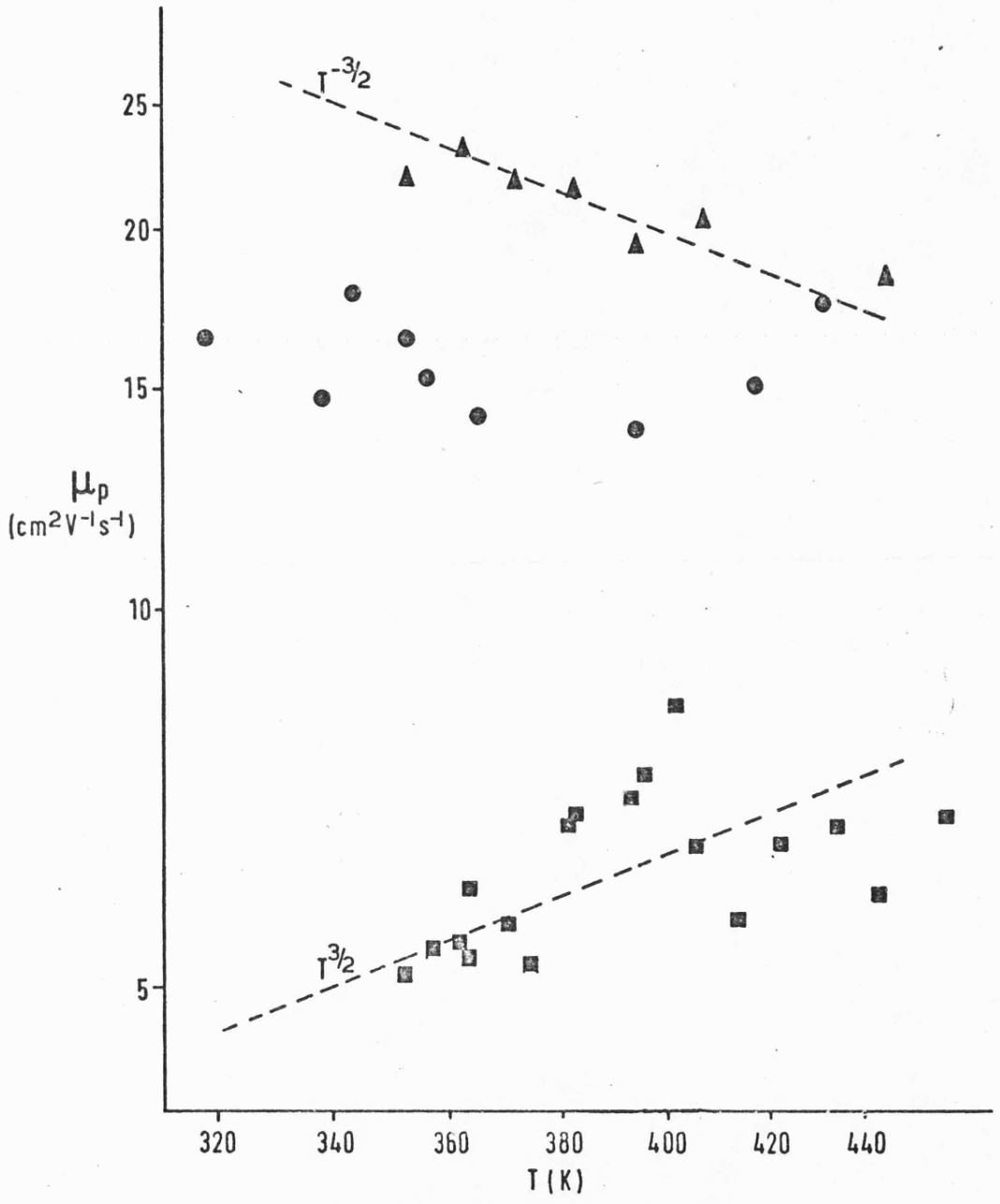

Fig. 4.7 Log-log plot of the Hall mobility of holes as a function of temperature ● sample 1, undoped; ▲ sample 3, Ga doped; ■ sample 4, Se doped. The dotted lines are for comparison only.

measured transmission. The crystal was also considerably thinner than sample 1.

4.7 Conclusions

1. Se is a donor in $ZnSiP_2$ with an activation energy at .042 eV.

2. The ACRT used in crystal growth yields crystals at least as good as those grown in static systems, and the high donor activation energy of sample 1 and the high p-type mobilities indicate that they may be better.

3. The maximum room temperature mobilities in $ZnSiP_2$ are at least 160 cm^2/Vs (electrons) and 22 cm^2/Vs (holes).

4. While Zn solution grown material is sometimes low resistivity n-type and sometimes high resistivity p-type even within the same growth run, the interpretation of electrical measurements and hence the manufacture of material with specific type and carrier concentration is impossible. Some identification of the mechanism responsible for this fluctuation is necessary before much more progress can be made.

CHAPTER 5

Photoeffects in $ZnSiP_2$

5.1 Previous work

In this chapter the results of measurements of photoconductivity and the photovoltaic effect at a rectifying contact are described.

Photoeffects have been observed in $ZnSiP_2$ by several workers, and their results are summarised in Figure 5.1, normalised to the same peak response. Only one of the curves published by Zlatkin and Novikov (1967) (that corresponding to relatively low carrier concentrations) is reproduced here.

The early photoconductivity results show a response extending far below the band gap, presumably reflecting the low quality of the crystals then available. Two curves (a, b) show subsidiary maxima near 1.6 eV, suggesting the presence of an acceptor level some .5 eV above the valence band. Zlatkin and Novikov (1967) also found a maximum near 1.0 eV in heavily doped material, and Belle et al (1965) found maxima at both .84 eV and 1.04 eV.

Zlatkin and Novikov (1967) observed bolometric effects (i.e. due to sample heating) in the infra-red photoconductivity of $ZnSiP_2$ containing Sn.

None of the early results showed a particularly well marked increase in response at the band gap. Kruse and Schulze (1974) found that the photoconductive response increased by about an order of magnitude within .1 eV above 2 eV. They also measured the photovoltaic effect. At high energies this fell to a minimum value and then rose again, which they ascribed to a transition from the photovoltage excited by light reflected from the back surface of the sample onto the contact to the photovoltage due to light absorbed directly near the circumference of the contact. They also suggested that both the photovoltaic

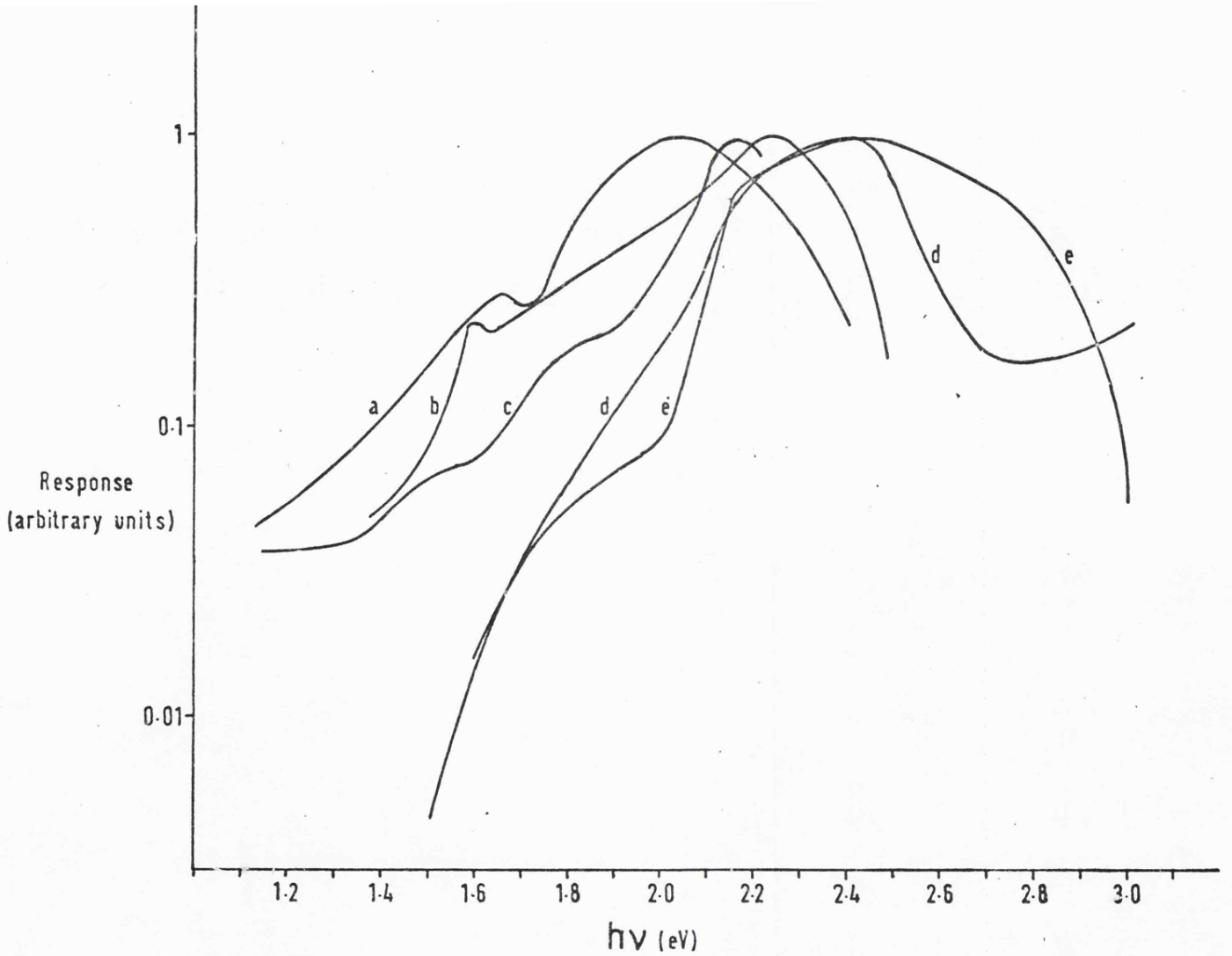

Fig. 5.1 Spectral response curves for photoconductivity (a,b,c,e) and photovoltaic effect (d) in $ZnSiP_2$.
(a) Zlatkin and Novikov (1967); (b) Goryunova et al. (1965), Bychkov et al. (1965); (c) Belle et al. (1965)
(d,e) Kruse and Schulze (1974)

and photoconductive responses below the absorption edge were due to a band tail.

5.2 Origins of photoeffects in semiconductors

The effects of light on the electrical properties of a semiconductor are rather complicated, as they involve both electrical and optical properties under non-equilibrium conditions. In this section the principles behind the effects are described, but it is impossible to give anything like a complete review of the theory. The reader is referred to Bube (1960) and Moss et al. (1973) for a full discussion. The effects are discussed with reference to n-type semiconductors, though of course the situation is similar for p-type. Most of the quantities characterising the processes taking place in the material are averages over statistical distributions, but the situation will be discussed for the sake of simplicity as though all the carriers of a particular type had, for example, the same diffusion length or free lifetime.

It is necessary to distinguish between the free carrier lifetime (the lifetime of a carrier after excitation and before recombination, excluding time spent in traps), the carrier relaxation time, which determines mobility, and is the time spent by a carrier between scattering processes, and the photoconductive decay time, which is the time for photoconductivity to decay including trapping effects.

Two other terms will be used which merit definition. The carrier diffusion length is the distance travelled by carriers before recombining, and the surface recombination velocity is the rate at which carriers recombine at the surface for unit excess carrier concentration.

The diffusion length (L) is given by:

$$L = (D \tau)^{\frac{1}{2}}$$

where the diffusion coefficient D is:

$$D = \frac{kT}{e} \mu$$

and τ is the free electron lifetime. If μ = 100 cm^2/Vs and τ = 10^{-5} s then L is of the order of ·05 mm at room temperature.

5.2.1 Photoconductivity

Photoconductivity takes place when carriers in a semiconductor are excited from bound to free states. Minority carriers are generally quickly trapped, so that photoconduction is chiefly a majority carrier effect. These can be generated by excitation of electrons from the valence band or from impurity states below the Fermi level to the conduction band.

Above the band gap, band to band transitions dominate. The magnitude of the photoconductivity is determined by the number of free carriers generated and the time they spend in the conduction band. At low absorption coefficients, therefore, the photoconductive response is expected to be proportional to the amount of light absorbed. It rises sharply at the band gap and flattens off when virtually all the light incident on the sample is absorbed. At high absorption coefficients, all the incident light is absorbed near the surface and surface recombination causes a decrease in the free carrier lifetime, which reduces the photoconductivity. The response continues to fall as the absorption rises until the excess carrier concentration at the surface is limited by the rate at which carriers diffuse away from it due to the concentration gradient, rather than by the rate of surface absorption, and the response becomes independent of absorption coefficient.

This qualitative description of the expected photoconductive response has been put in more quantitative form by De Vore (1956). The processes involved are so complex, however, that there is rarely

good agreement between theory and experiment.

5.2.2 Photovoltaic effect

The photovoltage which is observed at a metal-semiconductor junction is caused by the local electric field in the depletion region near the contact. Minority carriers generated by photoexcitation within a diffusion length of the contact can on average diffuse to the depletion region where they are swept to the contact and produce a voltage. Minority carriers are usually only generated when light is absorbed whose energy is greater than the separation between the valence band and the Fermi level (in n-type material), since states below the Fermi level are essentially full. Neglecting absorption within the depletion region, where the bands are not at their bulk position relative to the Fermi level, the photovoltaic response should be almost entirely intrinsic. It is therefore expected to rise fairly sharply near the band gap to a maximum value at rather higher energy than that of photoconductivity. So far no adequate theory of the spectral dependence of the photovoltaic effect has been published due to the difficulty of taking into account the effects of trapping by surface states and changes in the barrier height caused by illumination. Since these effects are expected to be most significant at high absorption coefficients where there is a high density of photoexcited carriers, it is difficult to suggest what the expected spectral dependence of the photovoltage will be at high energies.

The situation can be confused by three other voltages which are not directly associated with the rectifying nature of the barrier. When a carrier concentration gradient is generated by non-uniform absorption (i.e. at reasonably high absorption coefficients) electrons and holes diffuse at different rates down the concentration gradient, so that a voltage results. This effect is analogous to the thermoelectric voltage in a semiconductor in a temperature gradient, and is

called the Dember effect. Another photovoltage which is often observed is due to photoemission of electrons from the contact. Light incident on the junction can excite electrons over the barrier into the semiconductor and give rise to a photovoltage. The threshold for this effect is at photon energies equal to the barrier height, and the voltage should depend on $(h\nu - E_o)^2$, where E_o is the barrier height (Cromwell et al (1962)). Mead and Spitzer (1964) have observed that $E_o \sim \frac{2}{3} E_g$ for several III V compounds.

The third effect which can complicate photovoltaic measurements is sample heating which can cause thermoelectric voltages. This problem is common to most photoeffects, and its elimination is difficult, although the response time for such bolometric effects is slow.

5.3 Experimental

The experimental arrangement was relatively simple. Light from a 150 W Xenon arc was mechanically chopped and passed through a P.E. model 98 single prism monochromator, and the output light was focussed on the sample. The spectral response of the system was measured using an RCA C 31025C photomultiplier with a GaAs photocathode. This had been previously calibrated (Kruse and Schulze (1974)) to give an estimate of the absolute intensity of the light. Signals were detected using an Ithaco phase sensitive detector, using a light and photocell combination on the chopper to provide the reference.

Samples were mounted on black painted transistor headers which enabled connections to be made conveniently. For measurements of photovoltaic effect the input to the phase sensitive detector was connected directly to a Ga dot and an ohmic contact on the sample, and the Ga contact was illuminated. For photoconductivity measurements a 6V dry battery maintained a voltage across the sample and a resistance in series with it. The sample (but not its contacts) was illumin-

ated, and the signal taken across the series resistance.

Some samples were cut and polished as plane parallel rectangles. Where as-grown surfaces were required, it was sometimes necessary to use samples of less well-defined shape. All the polished samples were etched with $5HNO_3$:1 HCl and a few drops HF.

Rise and decay characteristics were obtained using a camera shutter and recording the signal on an oscilloscope which stored the signal until it was photographed. The camera shutter itself was not very fast, and time constants less than 1 ms could not be reliably observed. However, in most cases the time constants involved seemed to be longer than this.

The intensity dependence of the photo-response was measured using neutral density filters made and calibrated by Oriel Optics Corp. inserted in the light beam. Similarly a sheet of polaroid was used where required to observe the polarisation dependance of the signal. In most cases unpolarised measurements were made to save time, which was rather limited for these measurements.

Spectra were taken point by point and corrected to constant incident photon density by dividing the signal by the light intensity. Implicit in this is the assumption that the response is linear in intensity, which is not necessarily true. However, curves measured by introducing neutral density filters to eliminate the gross variations in spectral dependence of the source showed basically similar characteristics to those obtained in a more straightforward way, and it is expected that the major features of the spectra will not be greatly affected by the non-uniform spectral output of the source.

5.4 Results

Some of the spectral response curves obtained are shown in Figs 5.2 - 5.7. Only one polarised measurement is shown, for a Cu

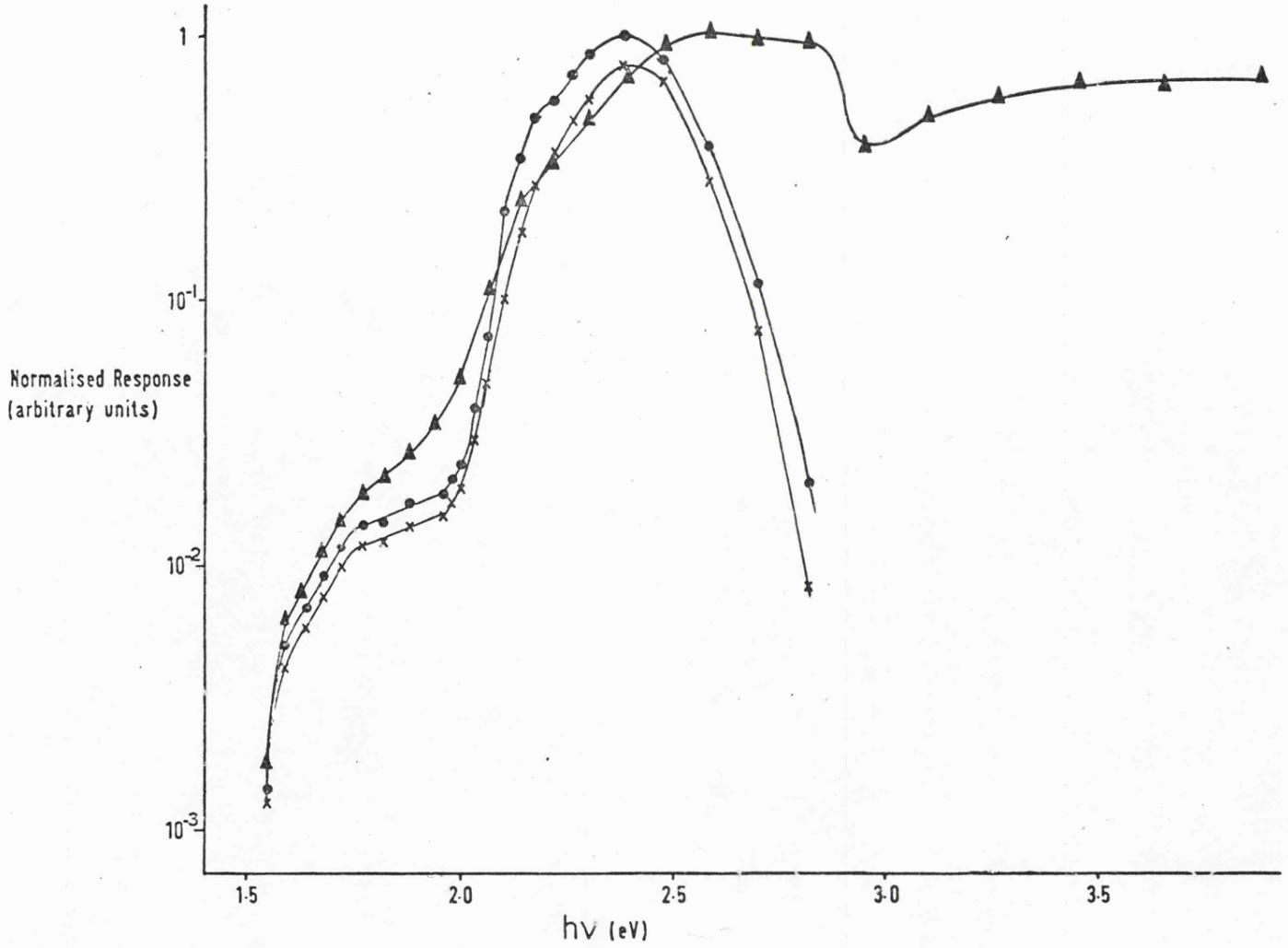

Fig. 5.2 Spectral response curves for a Cu doped sample of $ZnSiP_2$ (~100Ω cm)
Photoconductivity: •E⊥c, ×E//c ; photovoltage: ▲.

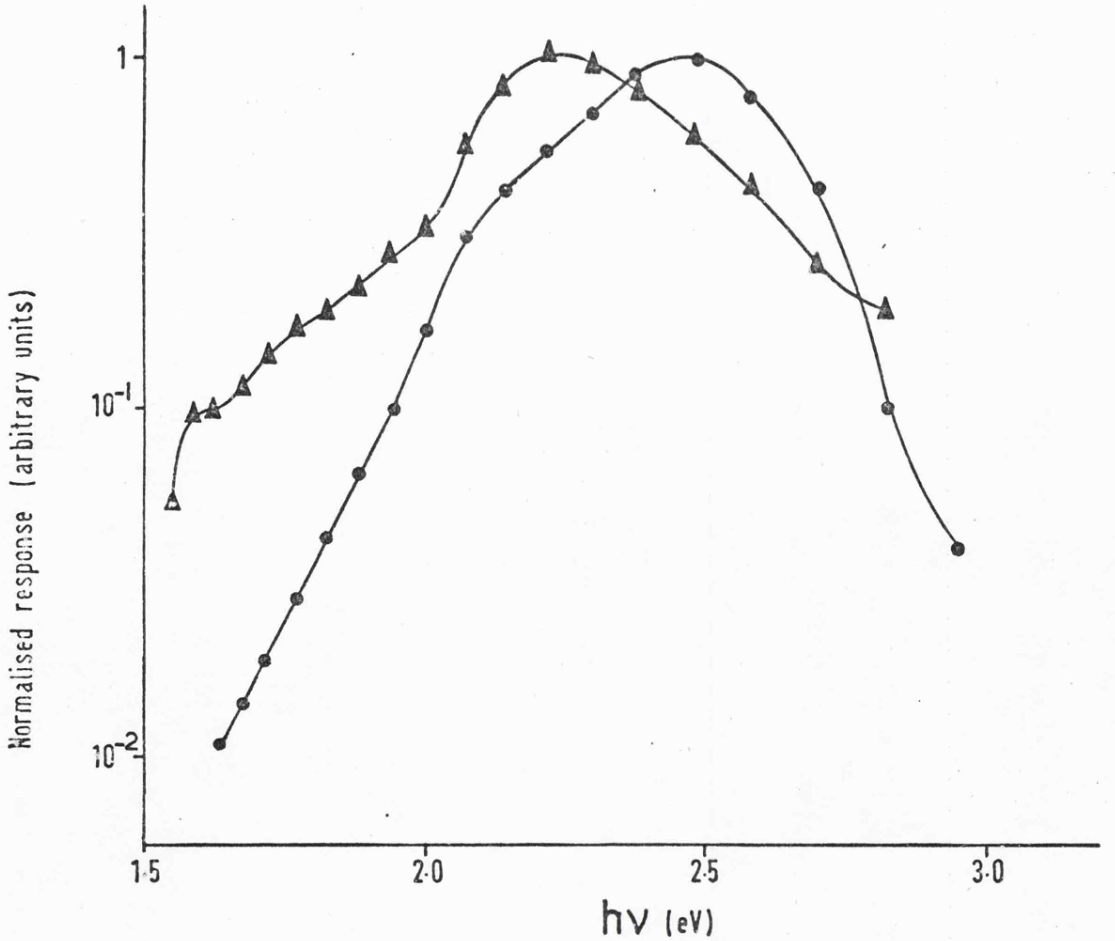

Fig. 5.3 Photoconductivity (▲) and photovoltaic effect (●) of $ZnSiP_2$ grown from Sn solution (~7Ω cm)

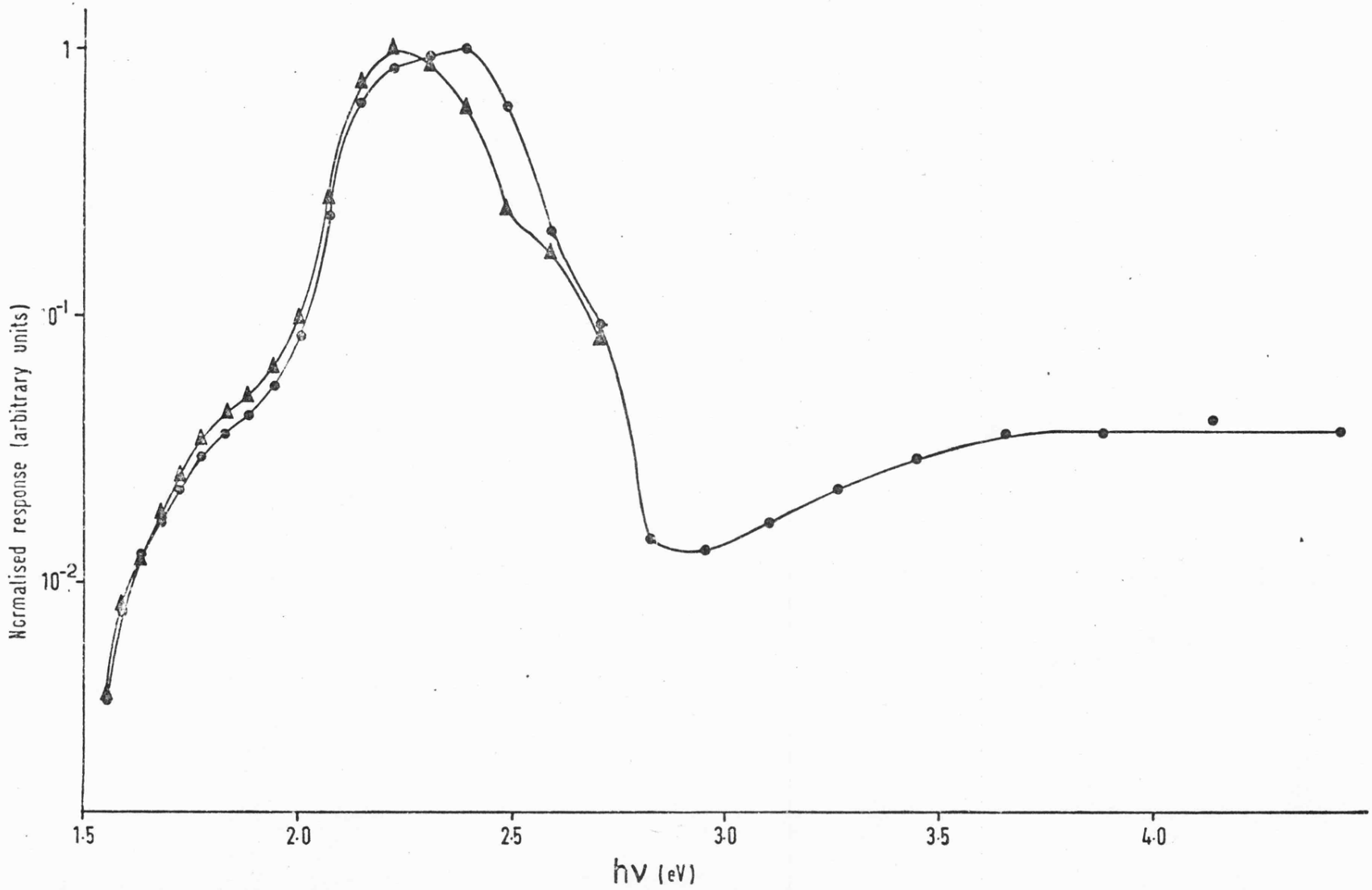

Fig. 5.4 Photoconductivity (▲) and photovoltaic effect (●) of Ga doped $ZnSiP_2$ (~300Ω cm)

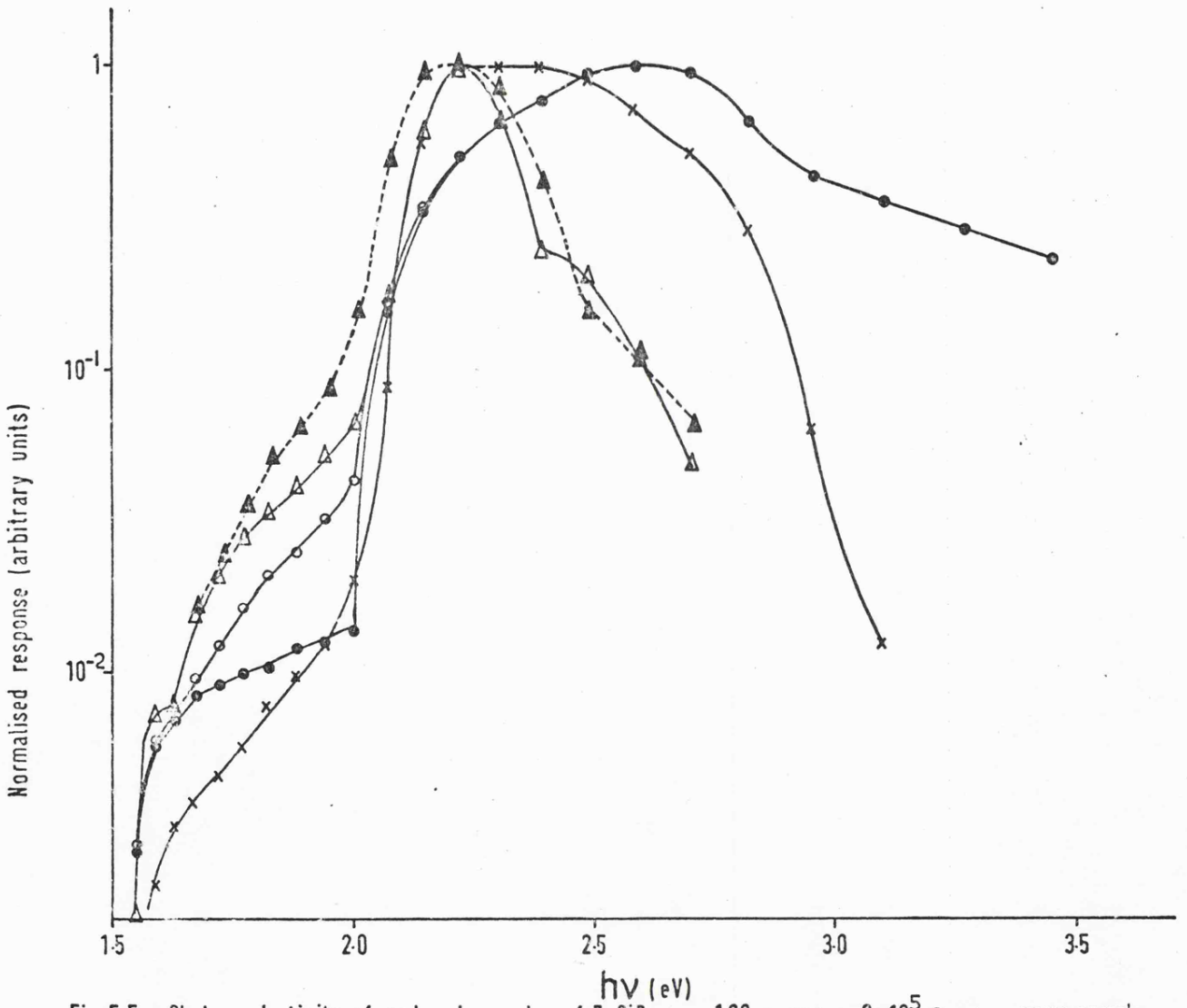

Fig. 5.5 Photoconductivity of undoped samples of $ZnSiP_2$: × 100 Ω cm; • 2. 10^5 Ω cm, o same sample, after exposure to above band gap radiation; Δ 10^8 Ω cm, ▲ same sample, using steady illumination.

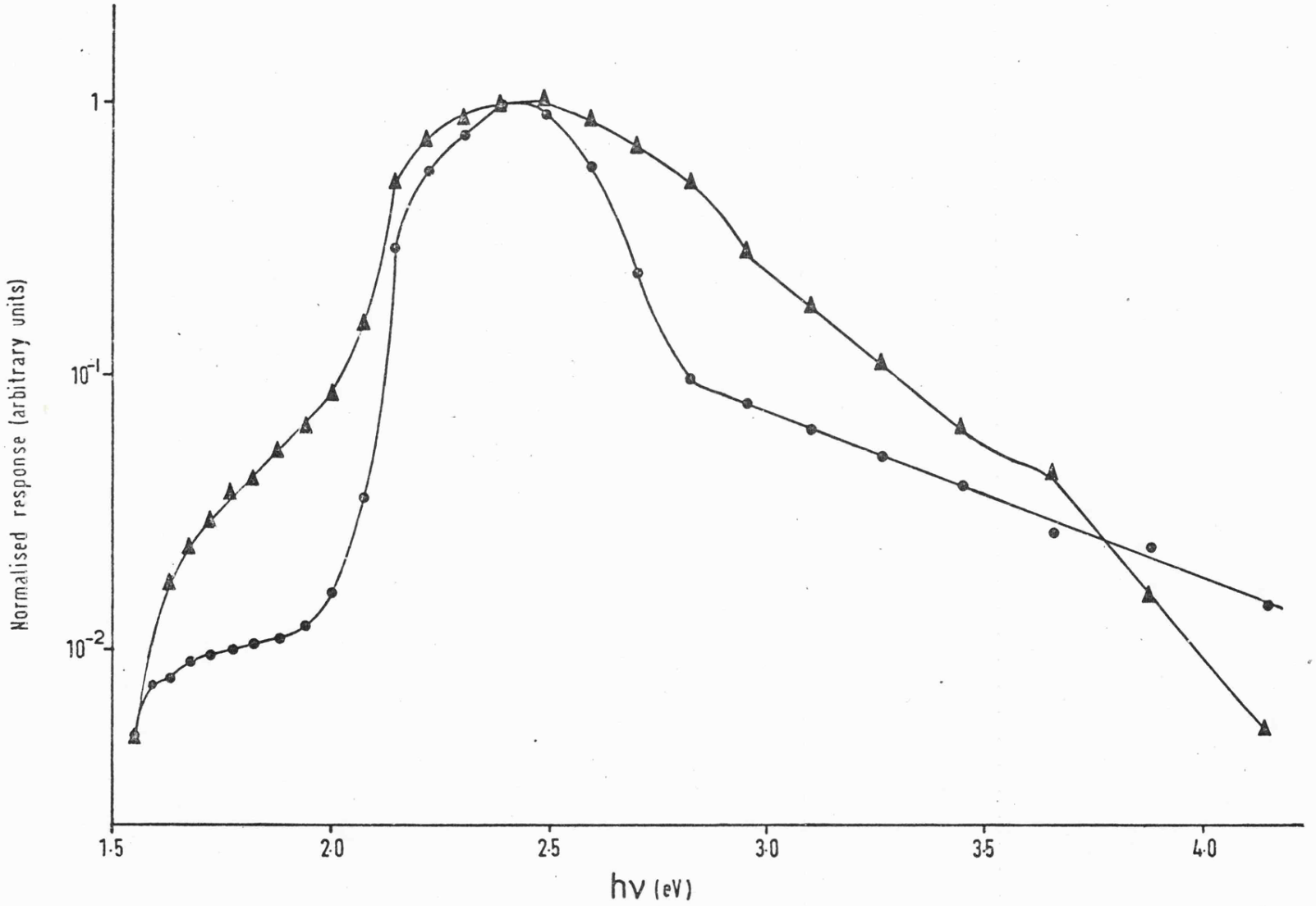

Fig. 5.6 Photoconductivity (●) and photovoltaic effect (▲) of Se doped $ZnSiP_2$ ($\sim 3.10^5 \Omega$ cm)

doped sample (Fig 5.2). This demonstrates that the dependence of photoconductivity on polarisation expected from the absorption measurements of Chapter 3 is qualitatively borne out. There is also a hint of structure near 2.2 eV for $E \perp c$ which could be associated with the structure seen in absorption. The resolution available for these measurements was not very high, and no measurements below room temperature could be made, so that any other structure was obscured.

In almost all cases photoconductivity first became measurable at 1.55 eV, rising rapidly with photon energy. It then flattened off to form a shoulder and rose again sharply at the absorption edge, usually increasing by more than a factor of ten between 2 and 2.2 eV. The onset of the intrinsic response agrees well with the results of absorption. The photoconductive response reached a maximum between 2.2 and 2.4 eV, and then decreased again.

The photovoltaic spectra show very similar behaviour. The photovoltage rose rather less steeply than the photoconductivity near the absorption edge, as might be expected since it depends approximately linearly on α rather than as $(1 - \exp(-\alpha d))$, and the peak values were reached at slightly higher energies. The fall off in the response above this was less sharp than for photoconductivity and in some cases reached a minimum and increased again above about 3 eV.

An exception to this behaviour was observed for crystals grown from Sn solution, which do not show a well marked band edge, and the photoconductivity corresponds very closely with curves of Fig 5.1. There is a suggestion of a peak at about 1.6 eV similar to those seen in curves a and b.

The difficulty of performing reliable measurements on high resistivity material is shown in Fig 5.5 (filled and open triangles). The dashed curve, which is the result of steady illumination, differs

quite considerably from that measured with a phase sensitive detector and chopped illumination. Part of the discrepancy may be due to the difficulty of measuring the dark current through the crystal, which must be subtracted from the current measured under illumination. The problem with chopped radiation and high resistivity crystals is the electrical time constant of the circuit may be long, while steady illumination has the disadvantage that sample heating effects can become significant.

5.5 Discussion

5.5.1 Response in the extrinsic region

There was good agreement between the energy at which the photoeffects increase sharply and the onset of band to band transitions, and the photoeffects above about 2 eV are attributed to intrinsic excitation. At lower energies, the mechanism causing photoeffects is less clear.

The results of photoconductivity alone could be explained as due to extrinsic excitation of electrons from impurity states near the valence band to the conduction band. This interpretation may be valid for the Sn solution grown crystals (Fig 5.3) for which the photoconductive and photovoltaic curves differ considerably. In other cases, however, the similarity between the photovoltaic and photoconductive response curves suggests a similar mechanism for the two effects, and this model should not give rise to a photovoltage since no minority carriers are generated.

Minority carriers could be created by excitation of electrons from the valence band to impurity states near the conduction band, and some photoconductivity would also be observed due to them. However, states below the Fermi level (about .1 eV below the conduction band in low resistivity material) are filled, at least under equilibrium

conditions, and so such a mechanism would not, under normal conditions, give rise to a photovoltage much more than .1 eV below the band gap. Rose (1955) has described how illumination can cause changes in the occupancy of impurity levels, depending on their relative capture cross sections for free carriers, so that it is possible that some of the deep impurity states below the equilibrium Fermi level could be emptied in this way. The long photoconductive decay times observed (seconds, in some cases) and the observation (filled and open circles, Fig 5.5) of photoconductivity in the extrinsic region which depended on whether the sample had been recently illuminated with above band gap radiation both add to the acceptability of this mechanism by indicating that safe traps exist, at least in some samples.

A second possible explanation, suggested by Kruse and Schulze (1974) is that both the photoconductivity and photovoltaic effect could be due to band tail absorption. This is an attractive hypothesis because it requires no involved mechanism such as that described above, and it is probably to be expected that there will be a small band tail at absorption coefficients of the order of a few cm^{-1}.

The spectral dependance of the photovoltage is also not inconsistent with photoemission from the contact. It fits moderately well to a dependence on $(h\nu - E_o)^2$ except close to the band edge, with a value of E_o which extrapolates to about 1.4 eV - close to the $\frac{2}{3} E_g$ value usually found in the III V compounds. The great disadvantage of this interpretation is that it makes the similarity between photoconductive and photovoltaic effects coincidental.

Heating of the sample by the incident light is also a possible explanation for both effects. Observation of the rise time of the photovoltaic effect below the band gap showed a time constant of the order of 20 ms, which is perhaps rather fast for bolometric effects. Above the absorption edge the response was initially much faster,

and then relaxed more slowly to a steady state value. This relaxation of the photovoltage is suggestive of 'trap saturation' effects, or redistribution of carriers amongst impurity states.

The slowness of the response below the absorption edge argues against photoemission from the contact or band tail absorption as explanations for the effect. Sample heating should show up more strongly above the absorption edge than below it, but will not explain the relaxation process described above because its polarity is wrong.

The only explanation which seems to be entirely in agreement with the observed facts is, therefore, that the occupancy of traps is altered by illumination, permitting an extrinsic photovoltaic effect, but the grounds on which the other explanations have been rejected are rather tenuous, and they cannot be conclusively ruled out.

The response of crystals grown from Sn solution does not pose so many problems. The photovoltage falls off much more rapidly than the photoconductivity and could be attributed to any of the effects described above. The photoconductivity shows a rather sharp shoulder at 1.6 eV, where Goryunova (1965b), Bychkov (1965) and Zlatkin and Novikov (1967) observed a peak in the response. In view of the variety of impurities found in Sn solution grown crystals, it is not possible definitely to attribute this to Sn impurities. However, it is interesting to note that a similar singularity occurred in the response of the high resistivity crystals (unfortunately represented by only one point in each case) at the same energy. Sn was detected in one of the high resistivity samples examined by emission spectroscopy (although not in others) and this was the only difference in purity observed between first and last grown crystal. There may be, therefore, a connection between the presence of Sn and high resistivity in crystals grown from Zn solution, although this is only a tentative suggestion, and the mechanism remains unknown.

5.5.2 Intrinsic Response

The photoconductive response above the band gap behaved much as would be expected, rising to a peak and falling off at high energies where surface recombination became important. The photovoltage is similar except that it reached a maximum at rather higher energy than the photoconductivity and fell off less sharply. In some cases the photovoltage increased again at energies above about 2.9 eV, and in others the sign of the signal reversed at this energy.

When such an anomaly was observed, it was also found that the intensity dependence of the response at high energies approached a square root law rather than the approximately linear one below 2.9 eV. The rise and decay characteristics also underwent a considerable change near the mininimum, although it could not be described by a single time constant on either side of it.

It may be significant that the lowest energy direct transition seen in electroreflectance is near 2.96 eV, very close to the anomalies observed. A direct transition of similar oscillator strength to those in the III V compounds might be expected to increase the absorption coefficient from a few thousand cm^{-1} to tens of thousands of cm^{-1}. At such absorption coefficients the absorption length becomes comparable to the depletion layer thickness, the excess carrier concentrations near the surface may be much larger than the equilibrium carrier concentrations and a considerable change could take place in the occupancy of bound states. The carriers will also be generated initially in different valence and conduction band extrema, although whether this will be significant depends on how fast they relax to lower energy states in their bands.

Unfortunately, the only polaroid available began to absorb at 2.9 eV and no measurements of the polarisation dependence of the anomaly could be made. It is tentatively identified as being associated with

a sharp increase in the absorption coefficient due to the onset of direct transitions. A possible mechanism might also be the Dember effect, which was described earlier, caused by the sharp concentration gradient at high absorption coefficients.

5.5.3 Relaxation times and traps

The free electron lifetimes at the peak response were estimated from the photoconductive gain, using (Bube (1960)):

$$G = \frac{\tau \mu V}{L^2} = \frac{\Delta I}{eF}$$

where L is the separation between the contacts on the crystal, V the voltage between them and ΔI the photocurrent caused by F photons being absorbed by the sample per second. Assuming a mobility of 100 cm^2/Vs the free electron lifetimes were estimated as $\tau = 10^{-7}s$ in high resistivity material, in low resistivity samples $\tau = 10^{-5}s$, and in Cu doped material $\tau = 10^{-4}s$. It is not clear whether the lifetime measured in the high resistivity samples is the electron or hole lifetime. The carrier relaxation times calculated from $\mu = 100\ cm^2 V^{-1}s^{-1}$ assuming $m_e = .3m_o$ in equation 4.6 is $1.7\ 10^{-14}s$, so even in the high resistivity material each carrier is scattered very many times before recombining. The free carrier lifetimes are much shorter than the photoconductive decay times, which varied from milliseconds to tens of seconds. This difference is due to trapping, and is almost always observed.

The longer electron lifetime in Cu doped material was associated with long photoconductive decay times. Cu is well known as a deep trap in other semiconductors (eg Burton et al. (1953)) which is why it is so undesirable in junction devices. It would appear that it acts similarly in $ZnSiP_2$, acting as a safe trap for holes and so extending the lifetime of electrons. In other words, Cu is a sensitising impurity in $ZnSiP_2$.

The importance of trapping was also shown by the intensity dependence of the photoconductivity. The response varied superlinearly, with powers up to 1.8, in the region near the peak response, while at lower and higher energies the dependence was sublinear, down to powers of .25. At high intensities near the peak response the intensity dependence fell off to a sublinear dependence. Rose (1955) has shown how different arrangements of traps can lead to different intensity dependences.

5.6 Summary

The photoeffects described agree well with the absorption results of Chapter 3. The predominance of trapping in determining the photoeffects in $ZnSiP_2$ has been demonstrated, and it is suggested that Cu is a sensitising impurity in $ZnSiP_2$. The possibility that high resistivity material contains Sn, which might be the reason for its low carrier concentration, has also been suggested, but the evidence at present is somewhat tenuous. Even the crystals which show sharp structure in absorption have been shown to contain high trap concentrations, and there is clearly considerable room for improvement in the crystal quality of $ZnSiP_2$. An anomaly in the photovoltaic effect at high energies is tentatively associated with the onset of direct transitions.

CHAPTER 6

CONCLUSION

When this work was undertaken, knowledge of $ZnSiP_2$ was rather limited. Its lattice parameters and x-parameter had been measured by Abrahams and Bernstein (1971) but this was almost the only precise information about the compound. Experimental investigations of the band structure were limited to absorption and photoconductivity measurements which yielded only very approximate limits to the magnitude of the lowest band gap. The situation was not clarified by the publication of electroreflectance measurements by Shay et al. (1973) and the luminescence measurements of Shah (1972) appeared to indicate an indirect band gap.

6.1 Discussion of results

In the present work crystals of sufficiently high optical quality have been grown for the absorption due to pseudodirect transitions to be measured. The absorption due to $V_2 - C$ and $V_3 - C$ pseudodirect transitions can be fitted well using the simplest approximation of two Wannier excitons, and the good agreement obtained suggests in particular that the matrix element does not vary much away from the zone centre.

The magnitude of the exciton binding energy has been estimated at 22 meV and found to be in good agreement with that expected using reasonable effective masses.

The matrix element for pseudodirect transitions has been estimated for the first time, and found to be very small. Weaire and Williams (1975) have suggested that this is because the states at X and those at Γ in zinc blende do not mix to first order under a perturbation of the chalcopyrite symmetry, so that pseudodirect matrix elements for direct transitions between such states are second order. A similar

observation has been made by Cohen et al. (1975).

The valence bands are split by the spin-orbit interaction and by the crystal field and can be interpreted in terms of Hopfield's (1960) quasicubic model. The magnitudes of the splittings agree well with those predicted from theory, and the relative intensities of the transitions also show the adequacy of the model.

A peak in the infra-red absorption of n-type material has been tentatively identified with transitions between the Γ_3 and Γ_2 conduction bands, and their splitting is estimated as $\sim$.7 eV. The work of Gallay et al. (1975) suggests that the Γ_1 minimum is 3.42 eV above the top of the valence band, so that the basic band structure near the gap of $ZnSiP_2$ is now known, with the exception of the origin of the lowest transition seen in electroreflectance, and an experimental value for the energy for the $T_1 + T_2$ minimum. The band structure of $ZnSiP_2$ is summarised in Fig 6.1, including such effective mass values as are available from k.p theory (Γ_1, Γ_4, Γ_5) and pseudopotential calculations (Γ_3). The energies of the bands at k = 0 are experimental.

The results of the electrical measurements in many ways parallel the data published by Ziegler et al (1973) and Siegel and Ziegler (1974). The hole mobilities found here are significantly higher, although the maximum value has probably not yet been reached. The electron mobilities are comparable with those obtained by other workers. Both the results of measurements of photoeffects and the temperature dependence of mobility suggest that there is considerably room for improvement in the control of impurities and intrinsic defects, despite the high optical quality of the crystals. The free carrier lifetimes measured by Kruse and Schulze (1974) suggest that lower trap densities may be obtained by halogen vapour transport than by solution growth. Their growth technique has the serious disadvantage, however, that

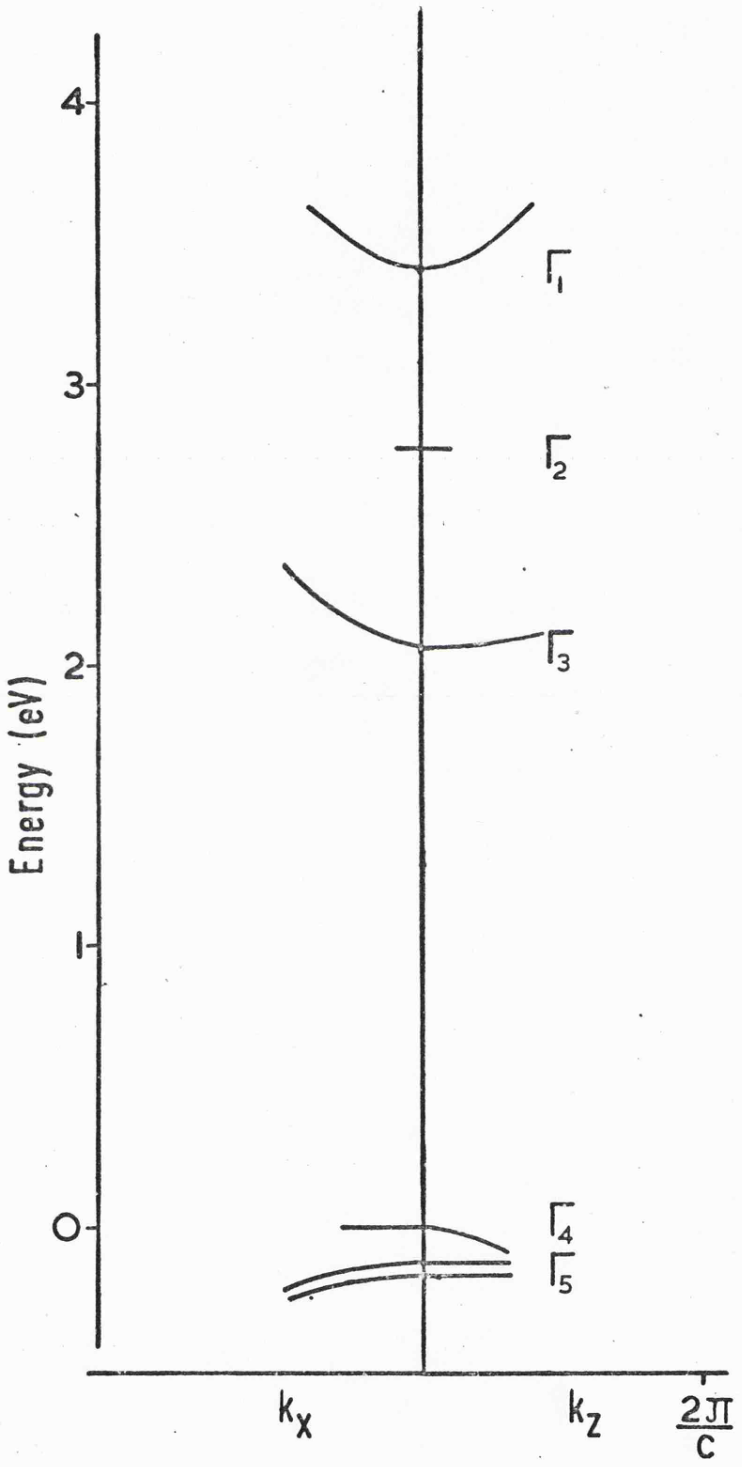

Fig. 6.1 Band structure of $ZnSiP_2$ near k=0 using energies determined in this work (except Γ_1) and effective masses from k.p theory (except Γ_3).

crystals large enough for most measurements were not grown. Solution growth by ACRT certainly yields the largest crystals of $ZnSiP_2$ at present available, although the problem of eliminating inclusions is yet to be solved.

The measurements of thermal expansion fit in well with the bonding picture, suggested by the way in which the compounds are derived, and with Levine's (1973) more quantitative formulation of this. The observation of increasing tetragonal compression with increasing temperature is nevertheless intuitively slightly surprising. The thermal expansion coefficients are sufficiently small that the crystal field splitting is not expected to be significantly affected by changes in temperature.

6.2 Possible applications and suggestions for further work

The most important single characteristic of $ZnSiP_2$ in terms of applications is its pseudodirect band gap. The weakness of transitions associated with this gap makes it unsuitable for light emitting applications. The only possible advantage of this weakness might lie in laser applications, since the population should be easier to invert than in direct gap materials, while retaining the advantage of the well defined gap energy. The problem of eliminating non-radiative transitions to an extent where such a device would be viable, however, may well be insuperable.

Both conduction and valence band are expected to be anisotropic, which is another property unique to the pseudodirect gap II IV V_2 compounds amongst high band gap semiconductors, although it is difficult to see any applications which make use of this characteristic.

The subsidiary conduction band minimum at T, expected to about .23 eV above the lowest conduction band minimum, suggests the possibility of transferred electron effects. Whether $ZnSiP_2$ has any advantages

over GaAs in this respect requires further experimental work.

Some of the chalcopyrite compounds are favoured as potential non-linear optical materials (eg. Boyd et al. (1971), (1972)) which would make use of their birefringence and high non-linear coefficients rather than semiconducting properties. No measurements of such effects in $ZnSiP_2$ have been published, perhaps because of the difficulty of obtaining large crystals of high optical quality. Theoretical considerations (Chemla (1971)) suggest that $ZnSiP_2$ would be inferior to $ZnGeP_2$ and $CdGeAs_2$ in this application, and the onset of lattice absorption near 10μ in $ZnSiP_2$ makes the transparency range in the near infra red rather narrow.

The properties of $ZnSiP_2$ are nevertheless interesting from the scientific point of view. Of the four pseudodirect gap II IV V_2 compounds ($ZnSiP_2$, $ZnSiAs_2$, $ZnGeP_2$ and $CdSiP_2$), $ZnSiP_2$ offers the best chance to study these unusual transitions because the direct gap is well separated in energy from the pseudodirect. At present there is an obvious lack of information on the theoretical side, particularly estimates of the effective masses and some of the band splittings. No theoretical estimate of the magnitude of the pseudodirect matrix element has been published for comparison with that found in the present work. Experimentally, measurements of the effects of large magnetic fields on the II IV V_2 compounds are needed to obtain a detailed knowledge of the conduction and valence bands.

Above all, however, the nature of impurity and native defects in these materials is still not known and the need is still for better quality crystals. Until some systematic work is done on this aspect of the ternary compounds, it will not be possible for their full potential to be assessed, particularly as far as their electrical properties are concerned. The problems are considerable, particularly in isolating cause and effect, but must be solved if these materials

are to be fully understood.

References

S. A. Abagyan (1971) Sov. Phys. Semicond. 4, 1334

S. C. Abrahams and J. L. Bernstein (1970) J. Chem. Phys. 52, 5607

S. C. Abrahams and J. L. Bernstein (1971) J. Chem. Phys. 55, 796

S. C. Abrahams and J. L. Bernstein (1973) J. Chem. Phys. 59, 5415

S. C. Abrahams and J. L. Bernstein (1974) J. Chem. Phys. 61, 1140

I. K. Akopyan, S. S. Grigoryan, A. S. Yakovlev (1966)
Sov. Phys. Solid State 8, 2910

I. K. Akopyan and L. B. Zlatkin (1966) Dokl. Ak. Nauk. SSSR 168, 547

E. E. Alekperova, Yu. A. Valov, E. A. Valova, T. N. Ushakova (1969a)
Izv. Ak. Nauk. SSSR Neorg. Mat. 5, 175

E. E. Alekperova, Yu. A. Valov, N. A. Goryunova, S. M. Ryvkin,
G. P. Shpenkov (1969b) Phys. Stat. Sol. 32, 49

E. E. Alekperova, Yu. A. Valov, A. A. Cheremisina (1970)
Prib. I. Tekh. Eksp. 3, 246

J. W. Allen and J. W. Hodby (1963) Proc. Phys. Soc. 82, 315

I. G. Austin, C. H. L. Goodman, A. E. S. Pengelly (1956)
J. Electrochem. Soc. 103, 609

G. K. Averkieva, N. A. Goryunova, V. D. Prochukhan, M. Serginov (1970)
Dokl. Ak. Nauk. SSSR 191, 811

G. K. Averkieva, N. A. Goryunova, V. D. Prochukhan, Yu. V. Rud', M. Serginov
(1971) Phys. Stat. Sol. a 5, 571

G. K. Averkieva, V. D. Prochukhan, M. Tashtanova (1972)
Dokl. Ak. Nauk. SSSR 206, 638

G. K. Averkieva, V. D. Prochukhan, M. Tashtanova (1973)
Izv. Ak. Nauk. SSSR Neorg. Mat. 9, 487

G. Babonas, G. Abrazevicius, V. S. Grigoreva, V. Neveira, A. Sileika
(1974a) Phys. Stat. Sol. b 62, 327

G. Babonas, R. Bendorius, A. Sileika (1974b) Phys. Stat. Sol b 62, K 13

I. Balslev (1966) J. Phys. Soc. Japan Suppl. 21, 101

M. L. Belle, Yu. A. Valov, N. A. Goryunova, L. B. Zlatkin, A. N. Imenkov,
M. M. Kozlov, B. V. Tsarenkov (1965) Dokl. Ak. Nauk. SSSR 163, 605

R. Bendorius, V. D. Prochukhan, A. Sileika (1972) Phys. Stat. Sol. b
53, 745

L. Bernstein and R. J. Beals (1961) J. App. Phys. 32, 122

I. Bertoti and K. Somogyi (1971) Phys. Stat. Sol. a 6, 439

A. S. Borshchevskii, N. A. Goryunova, F. P. Kesamanly, D. N. Nasledov (1967) Phys. Stat. Sol. 21, 9

G. D. Boyd, H. Kasper, J. H. McFee (1971) I.E.E.E. J. Quantum Electron. Q. E. 7, 567

G. D. Boyd, E. Buehler, F. G. Storz, J. H. Wernick (1972) I.E.E.E. J. Quantum Electron. Q. E. 8, 419

R. H. Bube (1960) 'Photoconductivity of Solids' Wiley

E. Buehler and J. H. Wernick (1971) J. Cryst. Growth 8, 324

J. A. Burton, G. W. Hull, F. J. Morin, J. C. Severiens (1953), J. Phys. Chem. 57, 853

A. G. Bychkov, N. A. Goryunova, F. P. Kesamanly, V. K. Mityurev, Yu. V. Rud, S. V. Slobodchikov (1965) Ukr. Fiz. Zh. 10, 867

L. Cervinka and J. Kaspar (1970) Czech J. Phys. B20, 101

V. A. Chaldyshev and V. N. Pokrovskii (1960) Izv. VUZ Fiz. 2, 173

V. A. Chaldyshev and V. N. Pokrovskii (1963) Izv. VUZ Fiz. 5, 103

D. S. Chemla (1971) Phys. Rev. Lett. 26, 1441

M. L. Cohen et al (1975) to be published

C. R. Cromwell, W. G. Spitzer, L. E. Howarth, E. E. Labate (1962) Phys. Rev. 127, 2006

B. J. Curtis and P. Wild (1970) Mat. Res. Bull. 5, 69

R. C. J. Draper, A. Miller, R. G. Humphreys (1973) 'Bibliography of II IV V_2 compounds' 1st Int. Conf. Ternary Semiconductors, Bath

H. B. De Vore (1956) Phys. Rev. 102, 86

H. Ehrenreich (1961) J. App. Phys.(Suppl) 32, 2155

F. D. Enck and J. G. Dommel (1965) J. App. Phys. 36, 839

R. S. Fiegelson, R. K. Route, H. W. Swarts (1975) J. Cryst. Growth 28, 138

O. G. Folberth and H. Pfister (1958) 'Semiconductors and Phosphors' Vieweg and Son, Braunschweig

J. Gallay, A. Deschanvres, S. Gaillard, C. Alibert (1975) 2nd Int. Conf. Ternary Semiconductors, Strasbourg

F. M. Gashimzade (1963) Sov. Phys. Sol. State 5, 875

C. H. L. Goodman (1957) Nature 179, 828

I. S. Gorban, V. A. Gorynya, V. V. Lugovskii, I. I. Tychina (1974) Sov. Phys. Solid State 16, 1029

N. A. Goryunova (1965a) 'The Chemistry of Diamond-like Semiconductors' ed. J. C. Anderson, M. I. T. Press, Cambridge, Mass. p 142

N. A. Goryunova, F. P. Kesamanly, D. N. Nasledov, V. V. Negreskul, Yu. V. Rud', S. V. Slobodchikov (1965b) Sov. Phys. Solid State 7, 1060

N. A. Goryunova, S. S. Grigoryan, L. B. Zlatkin (1966) Izv. Ak. Nauk. SSSR Neorg. Mat. 2, 2125

N. A. Goryunova, M. L. Belle, L. B. Zlatkin, G. V. Loshakova, A. S. Poplavnoi, V. A. Chaldyshev (1969) Sov. Phys. Semicond. 2, 1126

N. A. Goryunova, A. S. Poplavnoi, Yu I. Polygalov, V. A. Chaldyshev (1970) Phys. Stat. Sol. 39, 9

H. G. Grimm and A. Sommerfeld (1926) Z. Physik 36, 36

H. Hahn, G. Frank, W. Kingler, A. Meyer, G. Storger (1953) Z. Anorg. Allg. Chem. 271, 153

P. G. Harper and J. A. Hilder (1968) Phys. Stat. Sol. 26, 69

N. F. M. Henry and K. Lonsdale (ed) (1965) 'International Tables for X-Ray Crystallography, Vol. 1' Kynoch Press, Birmingham

F. Herman, C. D. Kuglin, K. F. Cuff, R. L. Kortum (1963) Phys. Rev. Lett. 11, 541

M. V. Hobden (1968) Acta. Cryst. A24, 676

G. D. Holah (1972) J. Phys. C 5, 1893

J. J. Hopfield (1960) J. Phys. Chem. Solids 15, 97

K. Hübner (1970) Ann. Phys. 25, 106

K. Hübner and K. Unger (1972) Phys. Stat. Sol. b 50, K105

R. G. Humphreys (1973) MSc Thesis, Bath University

A. Kahan (1963) Tech. Rept. AFCRL - 63 - 325

U. Kauffman and J. Schneider (1974) Festkörperprobleme XIV, 229

H. Kildal (1972) PhD Thesis, Stanford University

C. Kittel (1963) 'Quantum Theory of Solids', Wiley

S. Knight, E. Buehler, I. Calimbel (1972) J. App. Phys. 43, 3422

I. I. Kozhina and A. S. Borshchevskii (1971) Vesknik Leningrad Skogo Univ. Fiz. & Khim. 4 Ser. 87

G. Z. Krivaite, L. V. Kradinova, A. Yu. Sileika (1973) Sov. Phys. Semicond. 6, 1945

P. Kruse and R. G. Schulze (1974) J. Electron. Mater. 3, 431

W. Y. Law (1971) MSc Project Report, Bath University

P. Lawaetz (1975) S. S. Commun. 16, 65

Y. L. Lee (1970) PhD Thesis, Bath University

B. F. Levine (1973) J. Chem. Phys. 59, 1463

M. D. Lind and R. W. Grant (1973) J. Chem. Phys. 58, 357

O. Madelung (1964) 'Physics of III V Compounds', Wiley

C. A. Mead and W. G. Spitzer (1964) Phys. Rev. 134, A713

A. Miller (1974) PhD Thesis, Bath University

A. Miller and W. C. Clark (1975) 2nd Int. Conf. Ternary Semiconductors, Strasbourg

Y. Montfort, J. Vizot, G. Allais (1975) 2nd Int. Conf. Ternary Semiconductors, Strasbourg

D. J. Morgan (1971) Phys. Stat. Sol. b 48, 771

T. S. Moss, G. J. Burrell, B. Ellis (1973) 'Semiconductor Opto-Electronics', Butterworths, London

S. A. Mughal, A. J. Payne, B. Ray (1969) J. Mat. Sci. 4, 895

S. A. Mughal (1971) PhD Thesis, St Andrews University

S. A. Mughal and B. Ray (1973) J. Mat. Sci. 8, 1523

R. E. Nahory, J. Shah, R. C. C. Leite, E. Buehler, J. H. Wernick (1970) Phys. Rev. B 1, 4677

D. F. Nelson, L. F. Johnson, M. Gershenzon (1964) Phys. Rev. 135, A 1399

J. Noolandi (1974) Phys. Rev. B 10, 2490

S. I. Novikova (1966) in 'Semiconductors and Semimetals', ed. Willardson and Beer, Vol. 2, p. 33, Academic Press

J. F. Nye (1957) 'Physical Properties of Crystals', O.U.P.

A. Onton and R. J. Chicotka (1970) J. App. Phys 41, 4205

B. R. Pamplin (1964) J. Phys. Chem. Solids 25, 675

B. R. Pamplin (1965) 1st Annual Rept. CVD Project RU33-1

B. R. Pamplin (1974) J. Crystal Growth 26, 239

M. B. Panish and H. C. Casey (1969) J. App. Phys. 40, 163

L. Pauling and M. L. Huggins (1934) Z. Krist. 87, 205

L. J. Van der Pauw (1958) Phillips Res. Repts. 13, 1

W. B. Pearson (1967) 'Handbook of Lattice Spacings and Structures of Metals and Alloys' Vol. 2, Pergamon, Oxford

H. Pfister (1963) Acta Cryst. 16, 153

J. C. Phillips (1973) 'Bonds and Bands in Semiconductors', Academic Press, New York

J. C. Phillips, (1974) J. Phys. Chem. Solids 35, 1205

F. H. Pollack, C. W. Higginbotham, M. Cardona (1966), J. Phys. Soc. Japan Suppl. 21, 20

A. S. Poplavnoi and G. F. Karavaev (1968) Izv. Ak. Nauk. SSSR Neorg. Mat. 4, 196

A. S. Poplavnoi, Yu. I. Polygalov, V. A. Chaldyshev (1969) Izv. VUZ Fiz. 11, 58

A. S. Poplavnoi, Yu. I. Polygalov, V. A. Chaldyshev (1970a) Izv. VUZ Fiz. 6. 91

A. S. Poplavnoi, Yu. I. Polygalov, V. A. Chaldyshev (1970b) Izv. VUZ Fiz. 7, 17

B. Ray (1967) J. Mat. Sci. 2, 284

B. Ray (1971) Proc. Int. Conf. Semiconductor Heterojunctions, Budapest Vol. 5, p. 339

A. Rose (1955) Phys. Rev. 97, 322

J. E. Rowe and J. L. Shay (1971) Phys. Rev. B3, 451

R. Sandrock and J. Treusch (1964) Z. Naturforschg. 19, 844

H. J. Scheel and E. O. Schulz-Dubois (1971) J. Crystal Growth 8, 304

H. J. Scheel and D. Elwell (1972a) J. Crystal Growth 12, 153

H. J. Scheel (1972b) J. Crystal Growth 13, 14, 560

D. D. Sell and P. Lawaetz (1971) Phys. Rev. Lett. 26, 311

J. Shah and E. Buehler (1971) Phys. Rev. B 4, 2827

J. Shah (1972) Phys. Rev. B 6, 4592

J. L. Shay, E. Buehler, J. H. Wernick (1970a), Phys. Rev. B2, 4104

J. L. Shay, R. F. Leheny, E. Buehler, J. H. Wernick (1970b) J. Luminescence 1, 2, 851

J. L. Shay, E. Buehler, J. H. Wernick (1971) Phys. Rev. B3, 2004

J. L. Shay, B. Tell, E. Buehler, J. H. Wernick (1973) Phys. Rev. Lett. 30, 983

J. L. Shay, B. Tell, L. M. Schiavone, H. M. Kasper, F. Thiel (1974) Phys. Rev. B9, 1719

J. L. Shay and J. H. Wernick (1975) 'Ternary Chalcopyrite Semiconductors' Pergamon

A. V. Shubnikov (1960) 'Principles of Optical Crystallography', Consultants' Bureau, New York

W. Siegel and E. Ziegler (1974) Phys. Stat. Sol. a 21, 639

A. Sileika (1973) Surface Science 37, 730

R. A. Smith (1959) 'Semiconductors' C.U.P.

H. W. Spiess, U. Haeberlen, G. Brandt, A. Räuber, J. Schneider (1974) Phys. Stat. Sol. b 62, 183

W. G. Spitzer, M. Gershenzon, C. J. Frosch, D. F. Gibbs (1959) J. Phys. Chem. Solids 11, 339

A. J. Springthorpe and B. R. Pamplin (1968) J. Crystal Growth 3, 4, 313

A. J. Springthorpe and R. W. Monk (1970) Phys. Stat. Sol. a 1 K9

R. J. Stirn (1972) 'Semiconductors and Semimetals' ed. Willardson and Beer, Vol. 8, p. 59

R. F. Stroud (1970) PhD Thesis, Bath University

B. Tell, J. L. Shay, H. M. Kasper (1972) J. App. Phys. 43, 2469

M. Toyama, M. Naito, A. Kasami (1969) Jap. J. App. Phys. 8, 358

A. A. Vaipolin, N. A. Goryunova, E. O. Osmanov, D. N. Tretyakov (1964a) Dokl. Ak. Nauk. SSSR 154, 1116

A. A. Vaipolin, F. M. Gashimzade, N. A. Goryunova, F. P. Kesamanly, D. N. Nasledov, E. O. Osmanov, Yu. V. Rud' (1964b) Izv. Ak. Nauk. SSSR Ser. Fiz. 28, 1085

A. A. Vaipolin, E. O. Osmanov, D. N. Tretyakov (1965) Rep XXth Int. Congr. Theoretical and Applied Chemistry, Yupak, Moscow

A. A. Vaipolin, E. O. Osmanov, D. N. Tretyakov (1967) Izv. Ak. Nauk. SSSR Neorg. Mat. 3, 260

A. A. Vaipolin, N. A. Goryunova, L. I. Kleschchinski, G. V. Loshakova, E. O. Osmanov (1968) Phys. Stat. Sol. 29, 435

A. A. Vaipolin (1972) in 'Ternary Semiconductors $A^{II}B^{IV}C_2^V$ and $A^{II}B_2^{III}C_4^{VI}$ (in Russian)

Yu. A. Valov and T. N. Ushakova (1968) Izv. Ak. Nauk. SSSR Neorg. Mat. 4, 1054

Yu. A. Valov (1969) Izv. Ak. Nauk. SSSR Neorg. Mat. 5, 2115

J. A. van Vechten (1969) Phys. Rev. 187, 1007

J. A. van Vechten and J. C. Phillips (1970) Phys. Rev. B2, 2160

W. Wardzynski, A. Wojakowski, W. Zdanowicz (1967) Phys. Lett. 29A, 547

D. Weaire (1975) 2nd Int. Conf. Ternary Semiconductors, Strasbourg

L. R. Weisberg (1962) J. App. Phys. 33, 1817

L. B. Zlatkin and B. V. Novikov (1967) Izv. Ak. Nauk. SSSR Neorg. Mat. 3, 78

E. Ziegler, W. Siegel, G. Kühnel (1973) Phys. Stat. Sol. a 18, 483